CARBON DIOXIDE ADSORPTION ON FLAT Pt_3Sn SURFACES

by

Duygu Başaran

B.S. in Chemical Engineering, Boğaziçi University, 2004

Submitted to the Institute for Graduate Studies in
Science and Engineering in partial fulfillment of
the requirements for the degree of
Master of Science

Graduate Program in Chemical Engineering

Boğaziçi University

2007

ACKNOWLEDGEMENTS

This thesis is the product of many months that I used to think that it was never going to end. But now, when I finally completed the "improbable", I would like to express my gratitude for several people who believed in me.

First, I would like to express my gratitude to my thesis supervisor Prof. Ahmet Erhan Aksoylu. He gave me the confidence and support to begin my Master's program in Chemical Engineering. His advices helped me improve my work and his guidance was invaluable throughout my thesis. Besides, I should thank Asst. Prof. Nihat Baysal and Assoc. Ramazan Yıldırım for reading and commenting on my thesis.

I would like to thank my former colleagues at Yeditepe University. Their friendship had made my first business experience tolerable and their moral support had encouraged me through the hard times. I also want to thank my friends in CATREL; Tuğba Davran, Feyza Gökaliler, Şeyma Özkara, Ilgaz Soykal, Aslıhan Sümer, Burcu Selen Çağlayan. Moreover, I want to thank Mine Ayşe Gülmen; though I hardly know her, her work has helped me a lot.

I am grateful to my friends Berk Berksoy, Pınar Ak, Ayşegül Özen, Şebnem Koyunluoğlu Aynur, Gülçin Ergül, Rana Kıdak and Uğur Emekli for their moral support and their help in keeping myself sane.

I feel a deep sense of gratitude for my family, who taught me life and brought me up to stand the difficulties I would face. Nothing I would say to thank them would explain how much gratitude I feel towards them.

This study is supported by State Planning Organization of Turkey, DPT, through projects DPT-01K120300 and DPT-03K120250.

ABSTRACT

CARBON DIOXIDE ADSORPTION ON FLAT Pt_3Sn SURFACES

The experimental studies have shown that the PROX activity of the Pt–Sn/AC catalyst is either unaffected or positively affected from the presence of carbon dioxide in the feed mixture. The catalyst characterization studies revealed that Pt–Sn/AC system has Pt_3Sn alloy as one of the active metallic phases and the alloy plays a dominant role in the PROX activity. Thus, the unaffected or enhanced PROX activity levels by the presence of carbon dioxide can be explained by either the stabilization of carbon dioxide on AC surface or limited interaction between carbon dioxide and Pt_3Sn alloy surface. In this computational work, the proposed mechanism on the alloy surface was investigated by reproducing the periodic vacuum slabs of the Pt_3Sn alloy. Thus, carbon dioxide adsorption on the Pt_3Sn (111), (110), and (001) surfaces was studied at atomic level by utilizing semi ab-initio quantum mechanical code, CASTEP. The surfaces of Pt_3Sn alloy were generated with all possible bulk terminations, and all types of active sites on these terminations were tested for carbon dioxide adsorption. The adsorption energies of carbon dioxide molecule at all adsorption sites were calculated. The Local Density of States (LDOS) analysis was used for understanding the electronic interaction between the atoms of the adsorption sites and carbon dioxide molecule. In order to identify whether the carbon dioxide adsorption is stable, geometries of the carbon dioxide molecule as well as LDOS of both the carbon dioxide molecule and binding atom of the surface, Pt and/or Sn, were analyzed for all of the sites on each termination. The LDOS profiles for each active site were compared with those of the corresponding bare surfaces and free carbon dioxide to determine the new mixed orbitals. The study showed that (i) carbon dioxide adsorption on Pt_3Sn surfaces is not thermodynamically favorable, (ii) the adsorbed carbon dioxide assumes two different geometries dependent on the presence of a Sn atom at the site of adsorption, (iii) the

adsorbed carbon dioxide molecule does not dissociatively adsorb on Pt_3Sn surfaces, and (iv) the adsorbed carbon dioxide molecule resembles the structure of the carbon dioxide anion (CO_2^-).

ÖZET

DÜZ Pt_3Sn YÜZEYLERİNDE KARBONDİOKSİT ADSORPSİYONU

Deneysel çalışmalar besleme karışımında karbondioksit varlığının Pt–Sn/AC katalizörünün seçimli karbonmonoksit oksidasyon aktifliğini etkilemediğini ya da pozitif yönde etkilediğini göstermiştir. Katalizör karakterizasyon çalışmaları Pt–Sn/AC sisteminde aktif metalik fazlardan biri olarak Pt_3Sn alaşımının oluştuğunu ve bu alaşımın seçimli karbonmonoksit oksidasyon (PROX) aktifliği üzerinde etkin rol oynadığını ortaya çıkarmıştır. Karbondioksit varlığı ile PROX aktiflik seviyesinin değişmemesi veya artması karbondioksitin aktif karbon yüzeyi üzerinde kararlı hale gelmesi veya karbondioksit molekülü ile Pt_3Sn alaşım yüzeyi arasındaki etkileşimin kısıtlı olması ile açıklanabilir. Bu hesaplamalı çalışmada, Pt_3Sn alaşımının periodik vakum dilimlerinin oluşturulması yoluyla alaşım yüzeyi için önerilen mekanizma incelendi. Bunun için karbondioksitin Pt_3Sn alaşımının(111), (110) ve (001) yüzeylerindeki adsorpsiyonu atom düzeyinde yarı ab-initio kuantum mekaniksel kod, CASTEP, kullanılarak araştırıldı. Pt_3Sn alaşımının yüzeylerinin olası tüm sonlanma yüzleri belirlenerek bu yüzler üzerindeki tüm aktif merkez tipleri karbondioksit adsorpsiyonu için denendi. Karbondioksitin bu merkezlerdeki adsorpsiyon enerjileri hesaplandı. Adsorpsiyon merkezlerinin atomlarının karbondioksit molekülü ile elektronik etkileşimini anlamak için enerji düzeyleri lokal yoğunluk (LDOS) analizi kullanıldı. Adsorpsiyonun gerçekleşip gerçekleşmediği, karbondioksit molekülünün geometrisi ile birlikte LDOS profilleri incelenerek karar verildi. LDOS profilleri karbondioksit molekülü ve yüzeyde bağlandığı atom, Pt ve/veya Sn, için tüm yüzeylerdeki merkezlerde hesaplandı. Aynı aktif merkezdeki LDOS profilleri yeni orbitallerin oluşup oluşmadığını gözlemlemek amacıyla uygun yalın yüzeyler ve CO_2 molekülü ile karşılaştırıldı. Çalışma sonucunda (i) Pt_3Sn yüzeylerinde karbondioksit adsorpsiyonunun termodinamik olarak kararlı olmadığı, (ii) adsorbe edilen karbondioksit molekülünün, aktif merkezde Sn atomu bu-

lunup bulunmadığına bağlı olarak iki farklı geometri gösterdiği, (iii) Pt_3Sn yüzeylerinde adsorbe edilen karbondioksitin karbonmonoksit ve oksijene ayrışmadığı, ve (iv) adsorbe edilen karbondioksitin yapısının karbondioksit anyonuna (CO_2^-) benzediği belirlendi.

TABLE OF CONTENTS

LIST OF FIGURES

LIST OF TABLES

1. INTRODUCTION

Major improvement in energy efficiency of electric power plants and transportation vehicles is needed to enable the world to meet the energy demands at a lower rate of energy consumption with corresponding reduction in pollutant and CO_2 emissions. Fuel cells are intrinsically much more energy-efficient, and could achieve as high as 70–80 per cent system efficiency (including heat utilization) in electric power plants using solid oxide fuel cells (SOFC, versus the current efficiency of 30–37 per cent via combustion), and 40–50 per cent efficiency for transportation using proton-exchange membrane fuel cells (PEMFC) or solid oxide fuel cells (versus the current efficiency of 20–35 per cent with internal combustion (IC) engines) [1]. The most promising fuel-cell technology for transport applications appears to be the polymer electrolyte membrane fuel-cell (PEMFC) fueled by hydrogen. In order to avoid storing high pressure H_2 on a vehicle, it has been proposed that hydrogen for PEMFC can be produced in an onboard fuel processor [2]. It is now agreed that such a H_2 production system will involve a combination of three different reaction steps in series: partial oxidation (POX), water-gas shift (WGS) and preferential oxidation (PROX) [3]. The last reaction, which eliminates CO impurity in the produced hydrogen system, is a crucial reaction since the Pt-anode of the fuel cell can operate only at CO levels below 4 ppm [4].

PROX has been studied on a wide variety of catalysts having different metal(s), promoters and supports. These studies indicate that noble metals such as Pt [3,5–10], Rh [3], Ru [3] and Au [7, 9, 11, 12] provide high CO conversion and high oxygen selectivity for CO. Pt is the most studied catalyst for PROX. The major focus is on bimetallic Pt systems, i.e. Pt either alloyed or modified with other elements such Ru, Sn, Mo, Re, and Rh.

Experimental studies showed that (i) the active site properties of a catalyst determine its performance and (ii) the structure of the support as well as of the active site can be tailored, when a support that has a modifiable surface chemistry, like activated carbon (AC), is used [13–15]. Recent studies on AC supported Pt–Sn showed

that the presence of Pt–Sn alloys, especially Pt_3Sn, drastically changes the activity and stability characteristics of the catalyst in CO oxidation for both H_2-free and H_2-rich streams. Those studies also indicated that the formation and abundance of the Pt_3Sn alloy as well as the ratio of the Pt sites to that of the alloy sites can be tailored via changing the type and amount of oxygen bearing surface groups of the AC support used. The modification of carbon support may also be optimized in order to obtain a Pt_3Sn surface that has both superior electrochemical properties as well as long term stability.

Catalytic steam reforming of methanol or partial oxidation of gasoline followed by water gas shift reaction will produce a gas stream with 40–75 per cent H_2, 15–20 per cent CO_2, ∼10 per cent H_2O, 0–25 per cent N_2 and 0.5–1 per cent CO [6]. Since this stream will be the feed to the preferential oxidation reaction, it is important to study selective CO oxidation under these realistic gas mixture conditions. It is reported that the presence of CO_2 leads to a decrease on the CO oxidation rate over Au/α–Fe_2O_3 [7, 12], Pt/γ–Al_2O_3, and CuO–CeO_2 [7]. It is also reported that CO_2 inhibits the rate of reaction over Pt/alumina catalysts, alumina-supported Pd/CeO_2/ZrO_2 catalysts [16] and decreases the performance of Au/MnO_x and Pt/SnO_x catalysts [9]. In contrast to the results reported on the effect of CO_2 on CO oxidation activity of the catalysts, the detrimental effect of presence of CO_2 on CO oxidation was not seen on AC supported Pt–SnO_x and Pt–CeO_x catalysts studied [17].

The PROX activity enhancement of Pt–Sn/AC and Pt–Ce/AC catalysts, in the presence of CO_2, which was observed by Şimsek may stem from two alternative interactions; (i) the interaction between CO_2 and the free surface carbon atoms on the AC surface which had lost their surface oxygen bearing groups during the pretreatment of the catalyst leading stabilized CO_2 on the support, or (ii) the very limited interaction between CO_2 and the active sites, which leads to no hindrance of O_2 adsorption on the active sites and, as a consequence, negligible r-WGS activity. The latter possibility can be investigated theoretically by quantum mechanical calculations; in those studies, the interaction strength between possible adsorption sites of the active Pt_3Sn faces and CO_2 can be investigated.

In CO_2 adsorption at metal surfaces, a partial charge from the metal is transferred to the CO_2 molecule. For platinum group metals, this process has a high energy barrier. Thus, the CO_2 adsorption in these surfaces is weak and non-dissociative [18]. In a theoretical study of CO_2 activation on Pt (111), it has been stated that CO_2 was undistorted and weakly bound on the clean surface; and, on the contrary, the presence of a coadsorbed K atom on the surface had resulted in the formation of a highly distorted CO_2 molecule interacting strongly with the surface [18]. There is no study published in literature about CO_2 adsorption on flat Pt_3Sn surfaces.

In this study, the adsorption properties of CO_2 on Pt_3Sn were investigated via quantum mechanical calculations. The procedure can be summarized in a stepwise manner:

- The structures of the stable Pt_3Sn surfaces (alloy surfaces) and their reconstructions (surface alloys) were found from the literature.

- 3D models of the stable low-index Pt_3Sn surfaces (111), (110) and (001) were generated with all possible bulk terminations and CO_2 adsorption sites were determined under the light of the previous CO adsorption QM simulation studies.

- The adsorption energies and the geometries of the CO_2 molecule at all adsorption sites were calculated, aiming to determine the relative strengths of CO_2 adsorption at the sites.

- Aiming to understand the details of the interactions between CO_2 and the metal adsorption sites, the local density of states (LDOS) were evaluated for adsorption on Pt_3Sn(111), (110) and (001) surfaces. They were compared with the LDOS at CO_2 and the binding Pt or Sn in the isolated states of CO_2 and of the corresponding alloy surface, aiming to understand the energetic and mechanistic details of CO_2 adsorption.

2. LITERATURE SURVEY

2.1. PEMFC

Polymer electrolyte membrane fuel-cell (PEMFCs) is widely considered to be a most promising fuel cell system that has widespread applications. The technology is primarily suited for residential/commercial (business) and transportation applications. PEMFC offers an order of magnitude higher power density than any other fuel cell system [1].

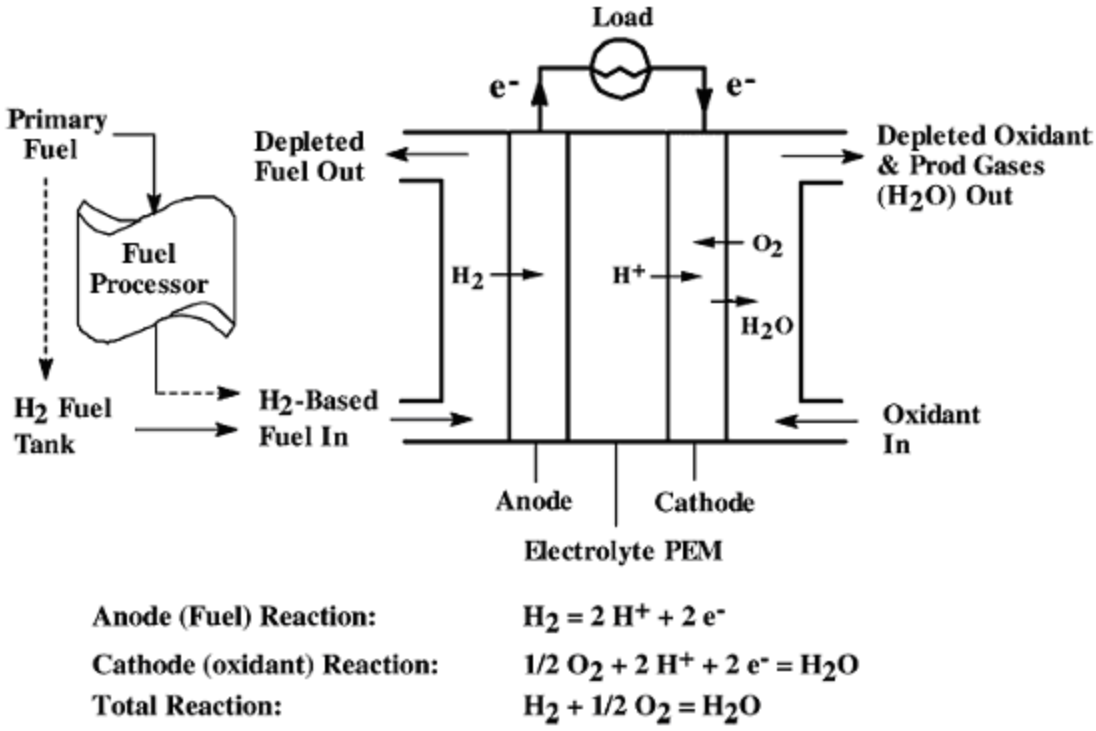

Figure 2.1. Concept of PEMFC system using on-board or on-site fuel processor, or on-board H_2 fuel tank [1]

The PEMFC uses a solid polymer membrane as its electrolyte (Figure 2.1). This membrane is an electronic insulator, but an excellent conductor of protons (hydrogen cations). Because of the limitation on the temperature imposed by the polymer and water balance, the operating temperature of PEMFC is less than 120 °C, usually between

70 and 90 °C. The PEMFC technology is primarily suited for residential/commercial (business) and transportation applications. In addition to pure hydrogen, the PEMFC can also operate on reformed hydrocarbon fuels without removal of the by-product CO_2. However, the Pt-anode of the PEMFC is sensitive to CO impurity at these low operation temperatures [1].

2.2. CO Oxidation

2.2.1. Importance of CO Oxidation

The main disadvantage of PEMFC is that CO, which is the product of a reforming reaction occur in the fuel processor, is a poison for the anode catalyst; it strongly chemisorbs onto Pt and deactivates the catalyst for the anode reaction (H_2 oxidation). The Pt-based anode catalyst can tolerate a maximum of 4 ppm CO concentration [4] and for a combined fuel processor-fuel cell system, a single WGS (water-gas shift) converter in the fuel processor is not enough to reach that low CO concentration levels. Hence, the traces of CO produced during the reforming process must be converted to CO_2 by a catalytic process. This operation should be conducted efficiently at temperatures between the operation temperatures of the WGS unit and the fuel cell, ie. 353–453 K range. Several methods such as preferential oxidation of CO to CO_2, methanation of CO and the use of hydrogen diffusion membranes are proposed to meet the above-mentioned criteria [19, 20]. Since during methanation, CO_2 may be converted along with CO, resulting in considerable H_2 loss, and the use of Pd-based H_2-membranes requires high-pressure differentials and high temperatures, both of which can significantly reduce the overall efficiency, the preferential oxidation method is the optimal option for CO removal [2]. However, hydrogen oxidation competes with CO oxidation leading to the loss of fuel efficiency. In order to reduce CO to the desired level and to minimize H_2 consumption, selective and active catalysts are needed.

The crucial requirement for the catalyst used for preferential CO oxidation (PROX) is to provide appropriate active sites for the two reactants; if both CO and O_2 compete for the same type of active site, the sites are completely occupied by CO,

leaving no opportunity for the fixation of O_2 on the surface [13, 14]. Thus, the key to high and stable conversion levels is to maintain two different kinds of active sites, one for the adsorption of CO and the other for the adsorption of O_2.

In the presence of H_2, a PROX catalyst must be active in CO oxidation, but, at the same time, its selectivity to the other possible oxidation reaction, H_2 oxidation, must be suppressed.

$$CO + O_2 \rightarrow CO_2 \tag{2.1}$$

$$H_2 + O_2 \rightarrow H_2O \tag{2.2}$$

The desired and undesired reactions are given in Equations (2.1) and (2.2), respectively. Thus, the selectivity of the catalyst is another important concern.

2.2.2. Systems Used in CO Oxidation

Various monometallic and bimetallic systems have been investigated for this reaction, aiming to:

- Lowering the reaction temperature to room temperature (necessary for complete CO oxidation) and even to cryogenic temperatures for space applications,

- Performing selective CO removal at low temperatures where there is a presence of excess hydrogen (crucial for supplying pure hydrogen feed to PEM fuel cells).

The catalysts that have been proposed in the literature for CO oxidation in H_2-free or H_2-rich streams are noble metals and their alloys with several metals; supported on metal oxides, silica, carbon or activated carbon [2]. If the low temperature oxidation involves reaction between CO adsorbed on one component and oxygen species adsorbed on or originating from a second component, then the interface between the components

is critical. As a result, preparation techniques are vital to the preparation of active catalysts.

Noble metal reducible oxide (NMRO) catalysts consist of a noble metal and one or more reducible oxides. These catalysts have significantly higher catalytic activities than noble metal or reducible oxide catalysts alone. The catalysts consist of a zero-valent noble metal intermixed with a metal oxide that has variable valency states and can easily be reduced under reaction conditions. Neither the noble metal nor the reducible oxide alone is able to catalyze CO oxidation at temperatures below 150 °C under practical conditions; hence, a synergetic interaction is present in the two-component material. Pt/SnO_2, Au/MnO_2, Au/Fe_2O_3, and Pd/SnO_2 are among the NMRO catalysts that have been developed for low-temperature oxidation of CO. The noble metal activates the CO molecules whereas the metal-metal oxide support perimeter interface acts as a site for activating O_2. Since CO and O_2 do not compete for the same adsorption sites; the inhibition of low-temperature CO oxidation by CO is eliminated.

Oh and Sinkevitch [21] reported that Ru/Al_2O_3 and Rh/Al_2O_3 were highly active and selective at 100 °C in a diluted mixture of H_2 and CO in N_2; while Pt/Al_2O_3 catalyst was similarly active and selective at around 200 °C. Kahlich *et al.* [22] also reported that the optimum temperature with Pt/Al_2O_3 was around 200 °C and proposed a power-law kinetic model for the selective CO oxidation on Pt/Al_2O_3. A Pt–Ru alloy catalyst and a promoted Pt catalyst were used in temperatures lower than 150 °C. On the other hand, Haruta and his coworkers have shown that Au supported on metal oxides exhibited high catalytic activity for the oxidation at much low temperatures (≤ 0°C). A comparison of an Au catalyst with a Pt/Al_2O_3 showed that yet known to be an inert material, the Au catalyst at 80 °C offered comparable activity and selectivity to those of the Pt catalyst at 200 °C [23].

Gold supported on ferrous oxide have been studied by both Schubert *et al.* [12] and Avgouropoulos *et al.* [7]. Both studies agree that the selectivity of CO oxidation to H_2 oxidation on Au/α–Fe_2O_3 is high. At 80 °C, the selectivity is around 70 per cent, increases as temperature decreases, and no change is observed in long-term

measurement. Avgouropoulos *et al.* stated that the activity of Au/α–Fe_2O_3 was the highest among the three catalysts tested, which were Pt/γ–Al_2O_3, CuO–CeO_2 and Au/α–Fe_2O_3. But the most selective sample in the conditions of that study was CuO–CeO_2. Although they claimed that the Au/α–Fe_2O_3 catalyst is superior to the other two for the selective CO oxidation, this catalyst lost a considerable portion of its activity during the first 80 h under reaction conditions [7]. The activity lost can not be considered for all Au catalysts since the activity of Au/MnO_x catalyst increases over 300 h [9]. The stability of Au/MnO_x catalysts in H_2 atmospheres was attributed to the reversible transformation between three Mn oxides, MnO, MnO_2, Mn_2O_3 and Mn_3O_4, depending on the O_2 concentration and temperature [2].

Pt supported on tin oxide(IV), with or without additional promoters, is amongst the most promising catalysts investigated for the oxidation of CO at low temperatures. They require a reductive pretreatment [24] and traces of H_2 or H_2O in the reaction mixture, in order to exhibit maximum activity. Pt/SnO_x has much higher catalytic activity than either Pt or SnO_x alone [2].

2.2.3. Effect of Alloying on CO Oxidation

Alloys of noble metals on carbon and activated carbon supports form another important class of catalysts for low temperature CO oxidation. These studies have mainly focused on bimetallic Pt systems, i.e. Pt either alloyed or modified with other elements such as Ru, Sn, Mo, Cu, Re, Pd, Rh, etc. The system that has been studied in the greatest detail is Pt–Ru, as this is still one of the most stable and active CO tolerant catalysts under practical conditions. Recently, well defined PtSn surfaces have been reported to have even better CO tolerance compared to those of PtRu surfaces. When alloys of zero-valent Pt with Sn, especially the Pt-rich Pt_3Sn are involved, high and stable CO conversion levels have been reported [13, 14].

It is generally believed that the mechanism by which CO is removed from the PtRu surface is the so-called "bifunctional mechanism". In this mechanism, CO adsorbed on Pt is oxidized preferentially by an oxygen containing species, OH as most

scientists propose, on Ru. However, this mechanism does not take into account a possible change in the CO binding energy on Pt induced by Ru, so-called "electronic effect" [25].

With this information on mind, Pt_3Sn alloy can be investigated in terms of bifunctional and electronic (ligand) effects. The enhanced catalytic activity of Pt_3Sn is usually ascribed to a combination of both effects [26]. The bifunctional effect means that alloying component Sn adsorbs oxygenated species (multiple oxygenated ligands or simply adsorbed OH, OH_{ad}), which can then react in the Langmuir-Hinshelwood (L-H) type reaction with the adsorbed CO on Pt atoms [26],

$$\mathrm{Pt} - \mathrm{CO}_{ad} + \ \mathrm{Sn} - \mathrm{OH}_{ad} = \mathrm{CO}_2 + \mathrm{H}^+ + \mathrm{e}^- \tag{2.3}$$

The theoretical study done by Shubina *et al.* [25] is consistent with this interpretation, i.e. from the calculated binding energies of CO_{ad} and OH_{ad} on the Pt_3Sn surface it was found that CO_{ad} does not bind to the Sn, and OH_{ad} clearly shows a preference for the Sn atop coordination site [27].

The electronic (ligand) effect, where the alloying component (Sn atoms) may alter the electronic properties of catalytically active metal (Pt atoms), is a consequence of the strong intermetallic bonding between Pt and Sn. The change in the electronic properties of Pt leads to the formation of the so-called "weakly" adsorbed state of CO_{ad}(low heat of adsorption) on Pt sites [26]. Sn atoms located below outermost Pt sites affects different adsorption properties of Pt atoms. This results in promoted OH adsorption at Pt sites (or at the bridge-sites between Pt and Sn atoms) at a lower electrode potential than on pure Pt surfaces. Therefore Equation (2.3) should be expanded for :

$$\mathrm{Pt} - \mathrm{CO}_{ad} + \quad \begin{array}{c} \mathrm{OH}_{ad} \\ | \\ \mathrm{Pt} \end{array} \ -\mathrm{Sn} = \mathrm{CO}_2 + \mathrm{H}^+ + \mathrm{e}^- \tag{2.4}$$

where Sn atoms could be either from the second atomic layer or adjacent to Pt on the

outermost layer [27].

Experimental studies showed that (i) the active site properties of a catalyst determine its performance and (ii) the structure of the support as well as of the active site can be tailored, when a support that has a modifiable surface chemistry, like activated carbon (AC), is used [13, 14, 15]. Recent studies on AC supported Pt–Sn showed that the presence of Pt–Sn alloys, especially Pt_3Sn, drastically changes the activity and stability characteristics of the catalyst in CO oxidation for both H_2-free and H_2-rich streams. Those studies also indicated that the formation and abundance of the Pt_3Sn alloy as well as the ratio of the Pt sites to that of the alloy sites can be tailored via changing the type and amount of oxygen bearing surface groups of the AC support used. The modification of carbon support may also be optimized in order to obtain a Pt_3Sn surface that has both superior electrochemical properties as well as long term stability.

2.3. The Effect of CO_2 on Selective CO oxidation

It is reported that CO_2 generally decreases the catalytic activity of Pt/γ–Al_2O_3, Au/α–Fe_2O_3 and CuO–CeO_2 catalysts for the selective CO oxidation. The magnitude of this negative effect depends on the nature of the catalyst. Au/α–Fe_2O_3 was found to be the most sensitive, while the Pt/γ–Al_2O_3 catalyst was the most resistant towards deactivation by CO_2 [7].

It is reported that the addition of CO_2 leads to opposite effects on the CO oxidation over Au/α–Fe_2O_3. At 80 °C it decreases the CO oxidation rate, by about a factor of 2–4, depending on the partial pressure, and also the selectivity, by about 15 per cent. This is explained by coadsorption of CO_2 on the gold particles or at the gold-metal oxide interface. The effect of CO_2 is almost independent of the temperature, reflecting similar activation energies in idealized reformate and in CO_2-containing reformate for both CO oxidation and H_2 oxidation. In addition, the deactivation is enhanced due to faster carbonate formation, and also the selectivity decreases steadily with time, by about 5–7 per cent over 1000 min [12].

The presence of realistic amounts of CO_2 in the feed has a detrimental effect on the activity of Pt/alumina catalysts. This can be either due to the reverse water gas shift reaction, formation of carbonates on the support or an increase in the effective surface concentration of CO by dissociative adsorption of CO_2 [6].

CO_2 inhibits the rate of reaction over alumina-supported $Pd/CeO_2/ZrO_2$ catalyst. The inhibiting effect of CO_2 on the reaction may be explained by the adsorption of CO_2 on ceria, leading to the formation of carboxylate and carbonate species and decreasing the ceria surface available for oxygen adsorption. This in turn decreases the concentration of adsorbed oxygen on ceria and hinders the interface reaction [16].

The CO conversion in the presence of CO_2 on Pt promoted catalyst deposited on a monolith remained essentially constant throughout an experiment conducted at 90 °C. The selectivity also remained constant [10].

The presence of 15 vol. per cent CO_2 in the reactant feed has a negative effect on the performance of CuO–CeO_2 catalysts via the urea-nitrate combustion method and it lowers their catalytic activity by approximately one order of magnitude. This is probably due to competitive adsorption of CO and CO_2 on the catalyst surface [28].

The presence of CO_2 in the feed induces a loss in the catalytic performance of Cu–CeO_2 catalyst. The decrease in the activity and the selectivity of the catalyst observed experimentally in the presence of CO_2 would probably be attributed to the competitive adsorption of CO_2 on the copper sites and to the inhibition of the oxygen mobility on the ceria support in the presence of adsorbed CO_2, as carbonates [29].

CO_2 negatively affects the activity of both calcined and uncalcined Fe_2O_3-supported gold catalysts. CO conversion linearly decreases as the CO_2 concentration increases. However, for CO_2 concentration higher than 12 per cent, where CO conversion is lower than 20 per cent, CO_2 slightly affects the CO conversion. Likewise, selectivity to CO_2 decreases as the CO_2 concentration in the feed increases [30].

It is reported that CO_2 (10 vol. per cent) also caused a detrimental effect over both Au/MnO_x and Au/FeO_x catalysts. The negative effect CO_2 was more with the Au/MnO_x but became negligible with Au/FeO_x. In addition, the absence of CO_2 for Au/MnO_x catalyst shifts the maximum conversion temperature to 80 °C instead of 130 °C. The detrimental effect of CO_2 on catalyst activity can be due to two reasons: the formation of carbonates or adsorbed carboxylate which will prevent oxygen adsorption and splitting on the support and/or the reverse water gas shift reaction [31].

The Au-catalyst loses activity in the presence of CO_2, while the CO conversion of the $Pt_{0.5}Al_1Mn_{6.7}Co$ increases significantly in the presence of CO_2. This is also reflected in the CO selectivity, where the CoMn-catalyst in the presence of CO_2 shows the highest CO oxidation selectivity. Apparently on this catalyst, CO_2 preferentially blocks the sites responsible for H_2 oxidation [32].

Opposed to all these studies putting forward the negative effect of CO_2 on CO oxidation, a study conducted by Şimşek [17] proposed that 15 per cent CO_2 present in the feed has a highly positive influence on CO oxidation activity for the AC supported Pt–SnO_x and Pt–CeO_x catalysts. Three types of activated carbon, namely (i) grinded and HCl washed activated carbon (AC1), (ii) air-oxidized form of AC1 (AC2), and (iii) HNO_3 oxidized form of AC1 (AC3), were prepared and used. 91–95 per cent CO conversion was obtained on the sequentially impregnated 1% Pt–0.25% SnO_x/AC1 catalyst, with addition of CO_2; while in the absence of CO_2 the conversion was about 66–74 per cent. The best catalyst performance obtained in the dry gas feed was over air oxidized 1% Pt–0.25% SnO_x/AC2 catalyst and the conversion was found to be 74–81 per cent [4]. The addition of CO_2 increased catalyst performance by 7–17 per cent in CO conversion. The AC3 supported 1% Pt–0.25% SnO_x, which showed about 36–41 per cent catalytic activity in the dry gas feed, on the other hand, gave complete conversion (100 per cent) for selective CO oxidation in the presence of CO_2. The reason for complete conversion was described by the acidic CO_2 molecules being agreeable to the HNO_3-oxidized support surface of Pt–SnO_x/AC3; it is very well known that fresh AC3 support has a very carboxylic acid rich surface chemistry. The carboxylic acid groups, which are attached to carbon atoms at the edges of the randomly oriented

carbane layers, are decomposed during high temperature treatments, like calcination and reduction. Considering the fact that carboxylic acid groups decompose into CO_2, the AC support surface prior to reaction becomes rich in free/bare carbons which are prone to strongly interact with CO_2 and stabilize CO_2 on the support reversibly. The addition of CO_2 to the feed stream increased the activity of the coimpregnated 1% Pt–1% CeO_x/AC1 catalyst for CO oxidation. The coimpregnated 1% Pt–1% CeO_x/AC2 catalyst exhibited the best performance when CO_2 was added to the feed, and the conversion level reached almost 80 per cent. The AC3 supported 1% Pt–1% CeO_x catalyst showed similar performance to that of the AC2 supported catalyst in the presence of CO_2 with only 2–3 per cent lower CO conversion.

2.4. Theoretical Works on Pt and Alloyed Pt Surfaces

Experimental works, which have pointed out the superior performance of Pt and Pt-alloys in many different catalytic reactions, are the main reason why this class of catalysts is the subject of interest in many theoretical works. Results of the theoretical works are mostly used in the detailed molecular level understanding of how Pt-based active sites participate in the reaction mechanism, and, as a consequence, in the validation of models proposed by experimentalists.

2.4.1. CO Adsorption on Pt Surfaces

CO adsorption on various Pt surfaces has been investigated in literature. Gajdoš *et al.* studied on the trends in CO adsorption on close-packed metal surfaces: Co, Ni, Cu from the 3d row, Ru, Rh, Pd, Ag from the 4d row and Ir, Pt, Au from the 5d row using density functional theory [33]. At a coverage 0.3 ML, the normal distance between carbon and the Pt surface on the top site and the C–O bond length was calculated as 2.00 and 1.157 Å, respectively. The experimental results obtained from low energy electron diffraction (LEED) study for those two distances were 1.85±0.10 and 1.15±0.1 Å, respectively [34].

A DFT study on CO and atomic oxygen adsorption on Pt(111) revealed that

the CO adsorption energies of the high-symmetry sites on this surface are quite close; unlike for the oxygen [35]. The most favorable site for oxygen was found as the face centered cubic (fcc) hollow site. The coadsorption of CO and O was also investigated by the adsorption of CO on a precovered surface by fcc oxygen; and the result was that the most favorable site for CO is the top site on the next nearest neighbor Pt atom of the oxygen-adsorbing site.

The study by Hammer *et al.* is one of the few theoretical studies on CO adsorption on defect surfaces [36]. The structure sensitivity of CO adsorption on different flat, stepped, kinked and reconstructed Pt surfaces is studied using large-scale DFT calculations. CO adsorption energies on (111), (100)-hexagonal-constructed, (211)-step and (11 8 5)-kink surfaces were calculated. The extremely strong structure sensitivity of the adsorption energy with variations up to 100 percent is explained by the proposed model on the d band center of Pt.

An *ab initio* density functional theory study on CO oxidation on Pt(111) investigated the transition state in the reaction and the physical origin of the reaction barrier [37]. In the transition state, CO molecule was bonded atop Pt and O atom was bonded over the bridge site. This result reflects the findings of other studies [38, 39]. The reaction barrier was calculated as 1.01 eV in the LDA and 1.05 eV in the GGA. Zhang *et al.* [38] proposed this barrier as 0.85 and Ji and Li [39] as 1.20 eV. From the remarkably long C and O adsorbed atom distance in the transition state compared with C–O bond in CO_2 molecules, it is deduced that the direct repulsion between chemisorbed CO and chemisorbed O atom may not be so important in generating the reaction barrier. The key role of the weakening and breaking of an O–Pt bond suggests that the predominant barrier to the reaction is the strength of this bond. It was also observed that the reaction pathway has the feature of least bond breaking. The initial motion of CO molecule did not weaken any chemical bond and at the transition state only one O–Pt bond was broken whereas in alternative pathways both competition for bonding and more broken bonds were present.

2.4.2. CO Adsorption on Alloyed Pt Surfaces

Zhang *et al.* carried out a comparative study on CO oxidation on $Cu_3Pt(111)$, Pt(111) and Cu(111) surfaces [38]. Alloying effects on the bonding sites and CO bonding energies are investigated from the LDOS graphs, along with the CO oxidation pathways. It has been found that CO preferentially adsorbs on an atop site of Pt and O preferentially adsorbs on a fcc hollow site of three Cu atoms on $Cu_3Pt(111)$. Moreover, the adsorption energies of CO and O were found to be less on their favorable sites of the alloy surface than are on the pure metals. The reaction barrier on $Cu_3Pt(111)$ is found to have an intermediate value between those on the pure metals.

Koper *et al.* carried out periodic DFT calculations for CO and OH adsorption on Pt, Ru and Pt–Ru alloys [40]. The mixing of Pt by Ru led to weaker bonds with the Pt sites, whereas mixing of Ru by Pt caused stronger bonds with the Ru sites. Differences in the binding energies have been explained by electronic alloying effect proposed in d band shift model of Hammer *et al.* Finally it is concluded that for a good CO oxidation fuel cell catalyst, it is important to have both Pt (which bind CO relatively weak due to alloying effect) and Ru (which bind OH strongly) sites on the surface.

Shubina and Koper carried out periodic DFT calculations for CO and OH interacting with bimetallic surfaces of Pt–Ru, Pt–Mo, Pt-Sn alloys and several transition metals modified with a Pt overlayer [25]. The mixing of Pt by Ru leads to a weaker bond on both CO and OH to the Pt sites but both adsorbates are also strongly adsorbed on Ru sites. The mixing of Pt by Mo, on the other hand, leads to weakly adsorbed CO on both Pt and Mo sites, and OH strongly adsorbed only on Mo sites. Comparison with the result from the above study suggests that Pt–Mo could be a better bifunctional catalyst for CO oxidation then Pt–Ru.

Same adsorption study has been carried out on the $Pt_3Sn(111)$ surface, and it was found that CO binds only to Pt and not to Sn, whereas OH has an energetic preference for the Sn sites. This also implies that Pt–Sn should be a good oxidation catalyst.

Ji and Li carried out periodic DFT calculations to investigate the oxidation of CO on the PtMo(111) surface [39]. The surface was approximated by a Pt surface slab, with one Mo atom per layer, yielding a Mo concentration of 25 per cent. The alloying of Pt by Mo reduces the reaction barrier. To examine the electronic effect and the geometric effect on the barrier, the electronic structure information is used to find which effect plays a major role in reducing the barrier. The geometric effect of PtMo is that the transition state is achieved without a significant O movement, and the electronic effect is that CO chemisorption energy is lower than on pure Pt. From partial density of states (PDOS), it is seen that the electronic effect of PtMo plays a minor role while the geometric effect is the major responsible for the reduced barrier.

Gülmen *et al.* investigated the adsorption properties of CO on Pt_3Sn by utilizing quantum mechanical calculations [41]. The adsorption energies and the geometries of the CO molecule at all types of active sites on all possible bulk terminations of the (111), (110) and (001) surfaces of Pt_3Sn were found and the results were compared with the results obtained from the adsorption of CO on similar sites of Pt(111), Pt(110) and Pt(001) surfaces. The term "stable adsorption" was used to indicate an adsorbed CO molecule staying at the adsorption site whereas "unstable adsorption" was used when a CO molecule moves from an adsorption site to the closest neighboring site. The differences in binding energies of CO at different sites of $Pt_3Sn(111)$ were small, suggesting a relatively flat potential energy surface (PES) and easy diffusion across the $Pt_3Sn(111)$ surface. The most stable site on this surface was found to be the the hcp hollow site with three Pt atoms; the second layer atom at the hollow being an Sn, and the secondly preferred one to be the bridge site with two Pt atoms and Sn at the bottom; both of them suggesting that the presence of a Sn atom beneath has a strengthening effect on CO adsorption. The sites which Sn was present turned out to be unstable: the CO placed at a fcc hollow site with two Pt's and one Sn moved away from the Sn atom and reached stability at the most stable site, and the one placed at a hcp hollow site with two Pt's and one Sn moved and reached stability at the fcc hollow site with three Pt's. The CO orientation was perpendicular in all cases except one, the stable CO adsorption on the bridge site, two Pt atoms and a Pt at the bottom, resulted in a bent position toward another site owing to the neighboring Sn atom. From the two possible

terminations of $Pt_3Sn(110)$ surface, the mixed atom termination is the thermodynamic equilibrium structure but the pure Pt-termination was found to be much more favorable for CO adsorption, having the lowest CO adsorption energy values among all Pt_3Sn surfaces studied. Two stable structures were obtained on Pt–Sn termination, the most favorable one being the atop site, followed by the long Pt–Pt bridge site. The atop site on pure-Pt termination was the energetically the most favorable site of all. The short bridge site was the preferred structure over the long bridge site and this was explained by the larger hollow volume at short bridge site due to the 90 ° difference in site orientations. The presence of unstable sites on pure Pt surface was dedicated to the destabilizing effect of highly strong adsorption sites. The strengthening effect of Sn beneath on CO adsorption was also proved on this surface. The mixed termination of $Pt_3Sn(001)$ surface had a single stable site, atop, and this site was also the most favorable of $Pt_3Sn(001)$. The pure-Pt termination had five stable sites, the most stable being the short Pt–Pt bridge. It was also noted that the Pt–C and C–O bond lengths do not follow the expected decreasing pattern with decreasing adsorption energy values and the Pt–C–O angle is kept nearly at 180 ° in all stable sites.

Same study used LDOS profiles to investigate the electronic mechanism of CO adsorption. The electronic structure was examined using the Orbital Mixing Model, which envisages the overall quantum states of a chemisorption system as being formed by the mixing of discrete CO molecular orbitals with the continuum of metal d states [42]. It was observed from LDOS profiles of C end of CO that 4σ molecular orbitals of CO was involved in some mixing with metal d-states, but there is a strong contribution to bonding from $1\pi/5\sigma$ orbitals, the strongest contribution of the two from the 5σ molecular orbital. Also the 2π derived orbitals above the Fermi level contribute strongly to the bonding. From the LDOS profiles of Pt adsorption site, it is observed that the peaks decrease and shift approximately 2 eV downwards in the region that contain strong metal character indicating the contribution of metal d-states to bonding. Also the existence of 3σ- and 4σ-like states are represented by their corresponding peaks in the profiles. Effect of alloying was also investigated in terms of electronic structure. The interaction between Pt of Pt(110) and adsorbed CO dominantly showed characteristics of $5\sigma/1\pi$ derived states of CO while for Pt of Pt_3Sn(110-mixed termination) showed

mostly the 5σ derived states of CO. For both cases 4σ-derived state plays a role in adsorption. In the examination of LDOS profiles for bridge type adsorption, it was seen that 3σ-derived states contribution was negligible for the alloy surface whereas it was important on Pt(111) surface and the 4σ-derived state contributed higher for the alloy surface.

The adsorption properties of stepped surfaces are known to be better relative to flat surfaces. Recently, Sümer *et al.* studied CO adsorption on $Pt_3Sn(102)$ surface via quantum mechanical calculations [43]. The $Pt_3Sn(102)$ surface has two possible row ending terminations, pure-Pt-ending termination and mixed-atom-ending termination. Since $Pt_3Sn(102)$ surface geometry has $Pt_3Sn(110)$ terraces, the adsorption energies and bond lengths obtained for that flat surface were used to analyze the effect of steps. On the surface with pure-Pt-ending termination, the most stable site was the atop site at the step-edge (SE) of pure-Pt row. This was an expected result since the SE atom's coordination number is low. Energy of atop site at the SE of the mixed row was approximately 25 per cent weaker than in the pure-Pt row. This result was also expected as Gülmen *et al.* has already stated that the neighboring Sn destabilizes the adsorption. There was a bond energy difference between the mixed row SE atop adsorption and mixed termination atop adsorption of the flat surface that arised from the low coordination number of atop SE site, due to a missed Sn neighbor at the surface or, the Sn atom present beneath the adsorption site. The second energetically preferred site is the bridge site between the SE of mixed row and the terrace atom next to the step edge (TA) of pure-Pt row; the strength of which is denoted to the presence of Sn atom beneath. The adsorption energy of the threefold adsorption site which consists of two Pt mixed row SE atoms and a pure-Pt row TA atom was found to be very close to the formerly mentioned one. The reason of closeness was explained by the similarity between the geometries of those sites, such as the C-Pt bond lengths and bond angles of CO adsorbed. The instability of CO adsorption on sites with a neighboring Sn atom was further proved by the examination of the CO's tendency to diffuse away from Sn. Another important concern is that the adsorption strength at pure-Pt row was decreased from atop-SE to atop-TA site, and it became unstable for atop adsorption site next to TA (TB). The reason was proposed to be a combination of electronic

modification of the adsorption sites by neighboring Sn atoms present at the upper row (indirect effect), direct effects to adsorbed CO, and the change in coordination number of Pt atoms, which increases as it moves from SE to TB. The most favorable site on $Pt_3Sn(102)$ surface with mixed-atom-ending termination was the bridge site of a SE and a TA atom of pure-Pt row. The reason for strong adsorption was propounded as the result of the presence of Sn atoms beneath the Pt atoms of the site and positioned orthogonal to the CO adsorption axis. It was also found out that if Sn atoms were common neighbors of the Pt atoms, the adsorption was stronger, though the presence of Sn atoms above. The second most favorable site was the atop adsorption at the SE atom of the pure row, which was expected from the low coordination number of that atom. The CO molecule adsorbed on the stable atop adsorption site at the TA atom on the mixed row was tilted towards TB on the pure row, and the movement was thought to be induced by Pt atoms at the SE of the upper pure-Pt rows and the adsorbed CO tried to escape from the Sn neighbor at SE position. The atop TB adsorption site on the pure row was highly unstable, being neighbor to two Sn atoms from the upper row.

The effect of different coverages was also examined in this study. The effect of CO–CO interaction on $Pt_3Sn(102)$ surface was rather limited at low surface concentrations such as those used. On the other hand, the calculations made for different surface concentrations indicated that when a surface Pt atom was shared by more than one CO molecule adsorbed in bridge form, the strength and stability of CO adsorption decreases.

Same study also used LDOS profiles the explain the CO-surface metal atom interaction. From the LDOS analysis of atop sites it was concluded that, for the stable sites, reduced electron density immediately below E_f and the increased density at lower energies were indicative of the orbital mixing between CO molecular orbitals and Pt d-states. The increased electron density of Pt at ca. -10 eV is the indication of participation of 4σ orbitals during adsorption. For unstable sites, on the other hand, the shift of the peaks was very small indicating that the contribution of metal d states to bonding was very small. The comparison of clean Pt atop adsorption sites were also made to investigate the effect of stepped structure. The formation of a stronger bond

came mostly from the higher electron density around −2 eV, and a weaker Pt–CO bond from the lower electron density around the Fermi level but very similar electron density with that of the flat surface site for the rest of the energy spectrum. Diffusion process in the light of electronic structure was also investigated by means of a threefold unstable site and a twofold stable site. It was seen that the atom which was present in only the unstable site had no contribution to the adsorption. About the decrease of adsorption energy in the higher surface concentrations, the LDOS profiles suggested that the sharing of Pt by two CO's for (1×1) case limits electron transfer process and extend of molecular orbital/metal orbital overlap, leading to a weaker adsorption. In this study, it was proposed that a new methodology, one that combines LDOS analysis with a screening methodology, can be used to find out the possible active surfaces by screening of possible metal/alloy surfaces without performing any adsorption study.

It is concluded that, in general, Sn atoms present beneath an adsorption site strengthens the adsorption whereas a neighboring Sn at the same plane or present above either weakens the adsorption or destabilizes the adsorbed CO.

2.5. Theoretical Works on CO_2 Adsorption

The considerable amount of experimental work concerning the interaction of CO_2 on single crystal metal surfaces evidences the importance of this process and shows the experimental effort towards understanding the finer details of CO_2 chemisorption on different metal surfaces [44, 45]. However, there are few theoretical works devoted to this problem. This problem partly arises from the difficulty of properly describing the interaction energy. Recently, by using density functional theory (DFT) approach, various works have been published on different metal surfaces.

Habas *et al.* used the cluster model approach within a DFT based program to investigate the coordination modes and adsorption sites involved in the interaction of CO_2 on Pd(111) [46]. Pd_{10} and Pd_{15} clusters were chosen to represent mono-coordinated and bi-coordinated adsorption modes, respectively. Three different surface species corresponding to only two coordination modes, C atom of the CO_2 molecule and both

C and O atoms of the CO_2 molecule bonded to the metal surface, were predicted. The first species involved a stable physisorbed CO_2 interacting with the Pd_{10} cluster, bonded at the C atom. Physisorption was assumed for the first species as its geometry was that of the gas-phase CO_2 and its long distance from the surface. The second stable species was also found for CO_2 on Pd_{10}, bonded at the C atom. This second structure was different from the first by its highly bent, thus resembling CO_2^- anion, geometry and its proximity to the surface. The third stable species involves a bi-coordinated bent species above Pd_{15} with one CO bond parallel to the surface, a rather bent OCO angle, and with the C and one O atom interacting directly with different surface metal atoms.

Same adsorption study has compared its results with those obtained previously. The bonding for alkali or early transition metal atoms was ionic, due to their low ionization potentials, whereas late transition metals have higher ionization potentials and thus, the bonding for these systems is not as ionic as for the alkali or early transition metals.

In another theoretical study, Ricart *et al.* worked on the adsorption of CO_2 on the clean and potassium-precovered Pt(111) surface by the cluster model approach within a DFT based program [18]. The chemisorption of a CO_2 molecule on clean Pt(111) was simulated by two different cluster models, Pt_{10} and Pt_{16}. The larger Pt_{16} cluster was used to simulate the interaction of CO_2 with a potassium-precovered surface. In both clusters, all geometry optimizations starting with the C atom near an on-top site of the surface, the optimum geometry reached corresponded to a linear CO_2 molecule that lies parallel to surface and with a C–Pt distance of 3.75 Å for Pt_{10} and 3.70 Å for Pt_{16}. For both clusters, the C–O distance was exactly the same for the free molecule. From these calculations, it is concluded that CO_2 does not chemisorb on the clean, ideal, Pt(111) surface. To model the effect of a coadsorbed alkali metal, a potassium atom was located in a threefold, hcp, position and the geometry of the molecule was optimized together with the vertical position of the K atom. Two resulting structures involved a highly bent molecule with the C atom above a Pt surface atom and elongated C–O distances. The only difference was the positioning of O atoms towards the K atom. When K

atom was also allowed to relax, another stable structure with K on a bridge site was obtained, and it was found to be the most stable one. This chemisorbed species was CO_2^-, characterized by its electronic structure.

Another important conclusion that can be drawn from that study is that the presence of a K atom does not enhance the adsorption of the molecule but its proximity to the molecule does. In other words, the decrease in the surface function is not responsible for the CO_2 activation, and a direct interaction with the coadsorbate is required.

Wang *et al.* investigated the adsorption behavior and thermal activation of carbon dioxide on the Cu(111), Cu(100), and Cu(110) surfaces by means of density functional theory calculations and cluster models and periodic slabs [47]. According to the cluster models, the optimized results indicated that the basis set of C and O atoms has a distinct effect on the adsorption energy, but an indistinct one on the equilibrium geometry. For the CO_2/Cu(*hkl*) adsorption systems studied, the final structure of adsorbed CO_2 was near linear and the preferred modes for the adsorption of CO_2 onto the Cu(111), Cu(100), and Cu(110) surfaces are the side-on adsorption at the cross bridge site, the side-on adsorption at the short bridge site, and the end-on adsorption on the on-top site with CO bonds located along the short bridge site, respectively. However, the calculated adsorption energies from periodic slabs were lower as compared to the experimental data as well as the cluster model data, indicating that the periodic slab approach of generalized gradient approximation in the DFT may be not suitable to obtain quantitative information on the interaction of CO_2 with Cu(*hkl*) surfaces.

Density functional theory calculations was also employed for CO_2 chemisorption on Ni surfaces [48]. Ni(111),(100) and (110) facets were used to describe nickel catalysts. At 1/4 ML coverage; four, three and six stable structures were obtained for all possible orientations on Ni(111), (100), and (110) surfaces respectively. On Ni(111) surface, the chemisorption energies were endothermic, with the most stable structure being the 2-fold bridge site, C bonded with two Ni atoms. On Ni(100) surface, both exothermic and endothermic energies were calculated but all of them were very low,

indicating the rather thermally neutral chemisorption. The most stable site was the 3-fold hollow site, all atoms bound to different Ni atoms. On Ni(110) surface, all of the structures had negative (exothermic) chemisorption energies, with the most stable 3-fold hollow up site, all atoms bound to three different Ni atoms. The chemisorbed CO_2 moiety has a bent structure with an OCO angle of about $123 - 143\,^\circ$. The net charge of the chemisorbed CO_2 on all Ni facets was found to be partially negative, indicating electron transfer from the nickel surface into CO_2. Therefore, the best and most appropriated description of CO_2 on the surface should be $CO_2^{-\delta}$. Higher coverages, 1/2 ML, were also tested to investigate the possibility of further CO_2 chemisorption. On the Ni(111) surface, no stable structures were obtained, indicating the impossibility of CO_2 chemisorption on coverages higher than 1/4. On Ni(100) surface, one stable structure was obtained, but the C–O bonds were shorter indicating that the high coverage decreased the degree of activation of the chemisorbed $CO_2^{-\delta}$. From the thermodynamic data, it is seen that the adsorption of a second molecule cost energy, indicating that it is not favorable to get higher coverages. On Ni(110), the possibility of further CO_2 adsorption was important because of the exothermicity; three stable structures were obtained, but with a weaker energy which indicated the repulsive interaction between the adsorbed CO_2 molecules. Possible lateral interaction was also tested with a surface model of 1/6 ML coverage. The results from all surfaces showed that the chemisorption energies were slightly stronger, suggesting no lateral repulsion exists at 1/4 ML.

3. CALCULATIONS

3.1. Computational Details of CASTEP Calculations

Density-functional theory calculations were carried out in a repeated slab geometry, using the program package CASTEP in Materials Studio of Accelrys Inc. (version 2.2.1). The Pt_3Sn surfaces were modeled as five-layer slabs, with the uppermost three layers relaxed together with the adsorbate, while the two bottom layers were fixed in their bulk positions. The vacuum thickness between slabs was 10 Å. The electron-ion interaction was included through the use of ultrasoft pseudopotentials and the electronic wave functions involved were expanded in a basis set of plane waves, up to a kinetic energy cutoff of 340 eV. Sampling of the (1×1) and (1×2) Brillouin zones were achieved by summation over Monkhorst-Pack meshes of dimensions $3 \times 6 \times 1$.

Exchange and correlation were included through the use of generalized gradient approximation (GGA) along with the PBE (Perdew-Burke-Ernzerhof) functional. No spin-polarization effects were included in the exchange-correlation functional, thus the calculation uses the same orbitals for alpha and beta spins.

Pulay's density mixing scheme was used for the SCF electronic minimization. A smearing range of 0.1 eV was applied at the Fermi level and four or eight empty bands were introduced in order to speed up the convergence. The energy was corrected by extrapolation to zero temperature.

3.2. Building and Optimizing the Pt_3Sn Crystal

The Pt_3Sn alloy crystallizes in the $L1_2$ structure with tin atoms on the corners of the face-centered cubic unit cell and platinum atoms on the center of faces. The bulk lattice constant has been determined as 4.00 Å. The unit cell was drawn with MS visualizer supported by this information. The ball-and-stick model of the unit cell is given in Figure 3.1.

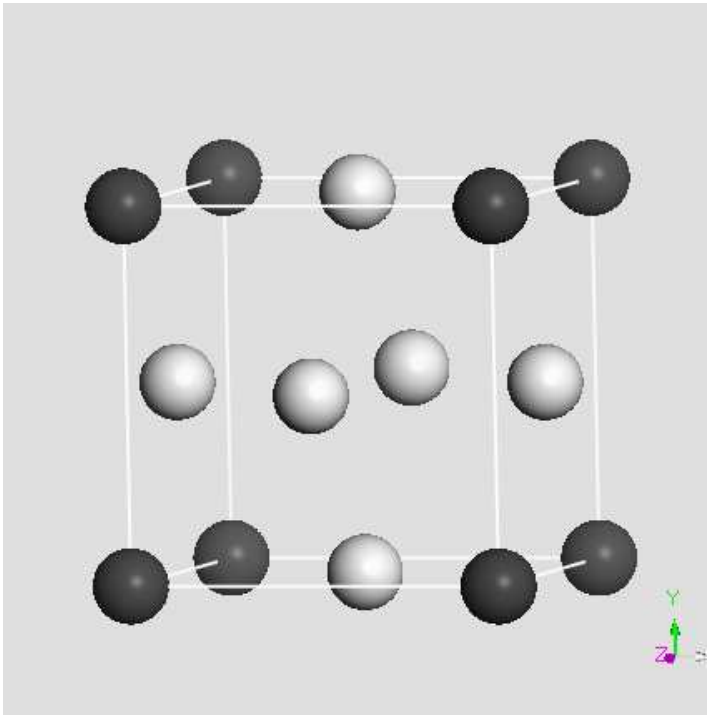

Figure 3.1. The Pt_3Sn crystal (○: Pt ●:Sn)

The geometry of the bulk Pt_3Sn alloy was, then, optimized by CASTEP using the parameters that are specified in Section 3.1.

3.3. Building the Pt_3Sn surfaces

Creating the surface is a two step process. The first step is to cleave the surface and the second is to create a vacuum slab containing the surface.

In the first step, the cell was cut in the direction of the surface specified by the Miller indices. This is called "cleaving the crystal". Determination of the cleave plane was carried out by entering the Miller indices of the surface, the top position and the depth of the cleave slab. The top position helps choose the surface characteristics (i.e. Pt-rich, Sn-rich, etc.) and the depth determines the number of the atom layers in the 3D model to be created. In this study 5-layer surfaces are simulated to provide sufficiently accurate results within a reasonable computational time.

Figure 3.2 gives the cleaved structure for the $Pt_3Sn(111)$ surface. A cleaved crystal contains a 2D periodic surface. However, CASTEP requires a 3D periodic system as input. This was obtained by building a slab including the surface.

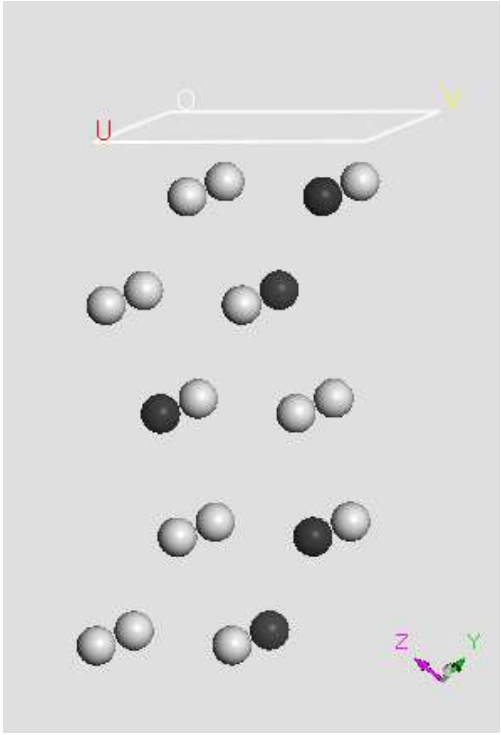

Figure 3.2. The cleaved $Pt_3Sn(111)$ crystal (○: Pt ●:Sn)

In the second step, where a vacuum slab was created, a crystal was built from a surface. The crystal was constructed by repeating the surface in a given direction using a repeat distance which is greater than the surface thickness. This introduces a region of vacuum or a vacuum slab between the surface units. The important thing in determining the size is to be sure that the cell is wide enough so that the adsorbant molecule does not interact with the ones in the neighboring cells and the slab includes sufficiently thick vacuum layer above the adsorbent and the surface, so that the adsorbate molecule is not attracted by both the topside and the underside of the surface. The vacuum thickness selection is in fact an optimization problem as the computational time increases as the layer gets thicker and the basis functions included in the formulations gets more. In this study, 10 Å of vacuum thickness was sufficient to obtain accurate results.

Vacuum thickness is added to the thickness of the surface to give the so-called repeat distance, or the crystal thickness. The (1 × 1) slabs are given in Figures 3.3, 3.4 and 3.5. All slabs were realigned into the standard orientation specified by the software to observe the surface structure easily. For sites of high coordination number, larger supercells were reproduced from the unit cells.

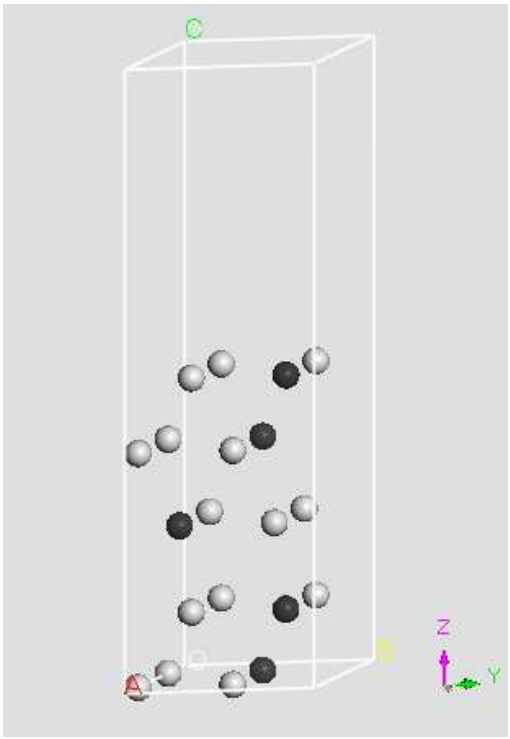

Figure 3.3. The (1 × 1) vacuum slab for the $Pt_3Sn(111)$ surface (○: Pt ●:Sn)

The slab of 10 atoms in Figure 3.4(a) represents the model for the 2D-infinite $Pt_3Sn(110)$ mixed surface, the CPK style of which is displayed in Figure 3.6. (In CPK style display, atoms are rendered as spheres with radii related to the van der Waals (VDW) radii scaled by the CPK scale factor.)

Finally, the top three layers of the slabs in each surface were relaxed using the parameters that are specified in Section 3.1, while the lower two layers were fixed at their fractional positions.

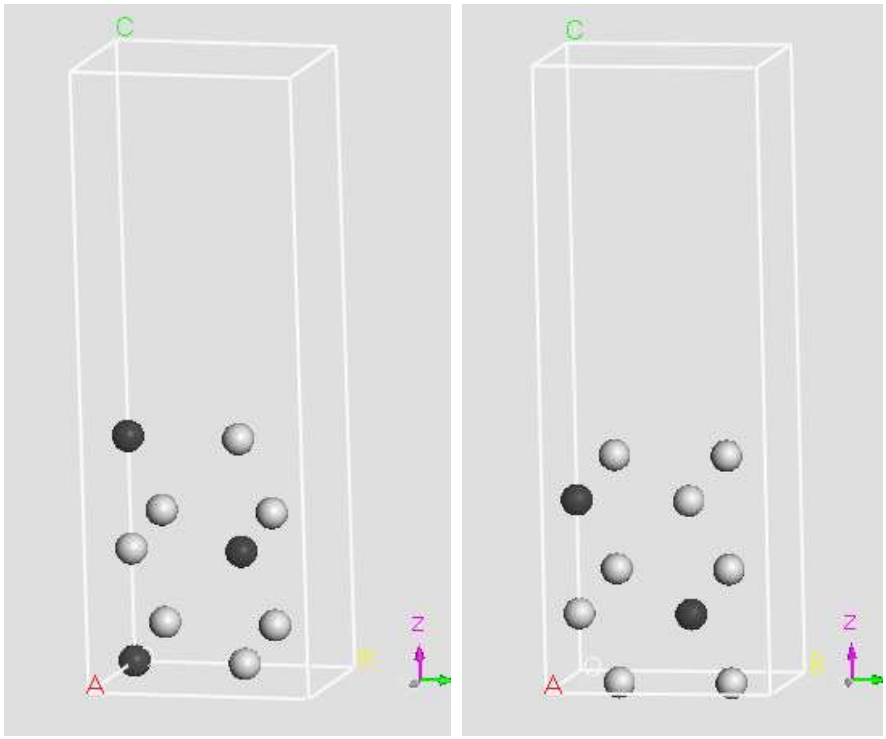

(a) (b)

Figure 3.4. The (1×1) vacuum slab for the $Pt_3Sn(110)$ surface (○: Pt ●:Sn)
(a) mixed termination (b) pure-Pt termination

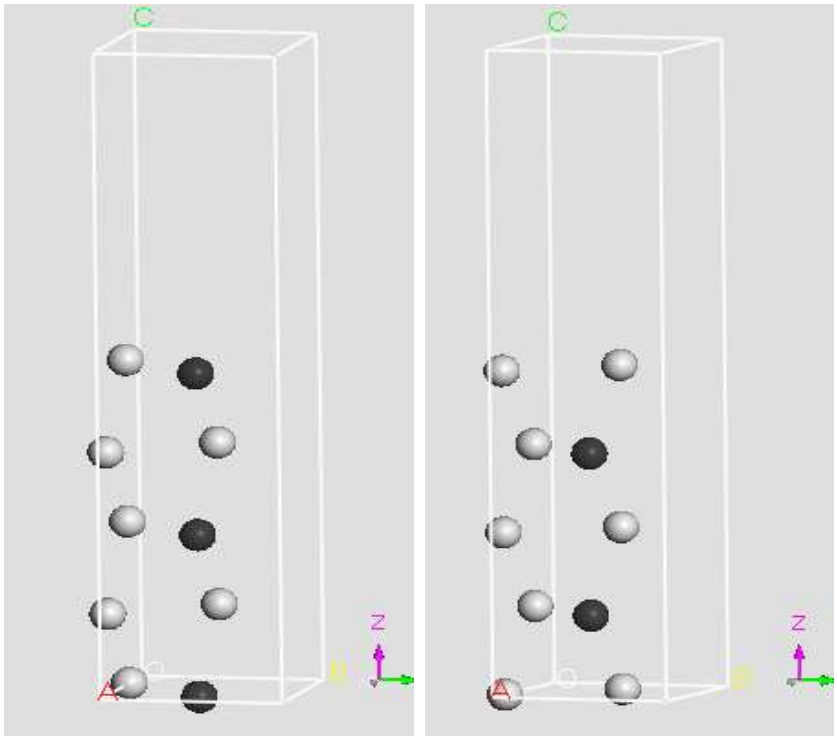

(a) (b)

Figure 3.5. The (1×1) vacuum slab for the $Pt_3Sn(001)$ surface (○: Pt ●:Sn) (a) mixed termination (b) pure-Pt termination

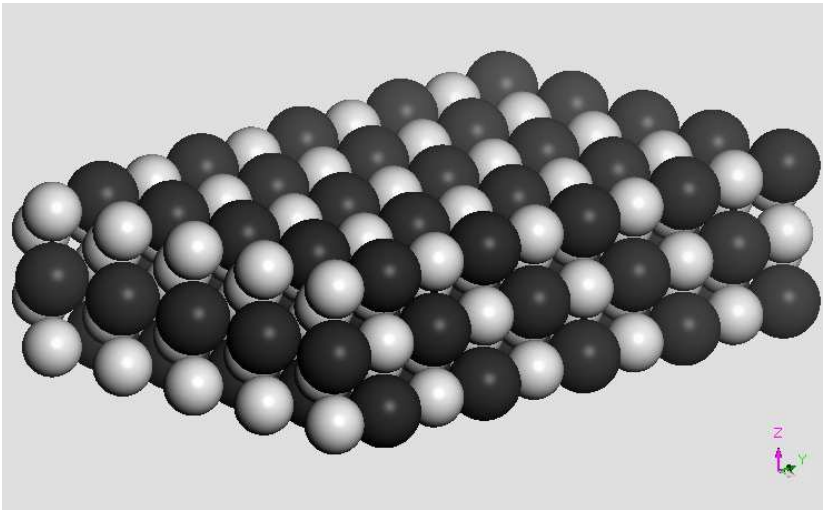

Figure 3.6. The $Pt_3Sn(110)$ mixed surface (○: Pt ●:Sn)

3.4. Determination of the Active Sites for CO_2

Several types of twofold, threefold and fourfold sites exist on the Pt_3Sn surfaces, depending on the positions of atoms in the second layer, e.g. threefold site with fcc or hcp configuration. In this study, the active sites are determined by taking into account the sites suitable for CO adsorption in the study of Gülmen [41]. However, there is an important difference between the sites determined for CO adsorption and the sites determined for CO_2 adsorption. Since CO molecule is known to be adsorbed on platinum sites and O_2 on tin sites, no tin atoms were included directly in the previous study. Since there is no general agreement on CO_2 adsorption on Pt_3Sn, all possible sites are investigated.

Figures 3.7, 3.8 and 3.9 show the sites for each surface and termination. The tables given for each surface summarizes the names given to the active sites, and also for each site the width of the supercell involved in its simulation.

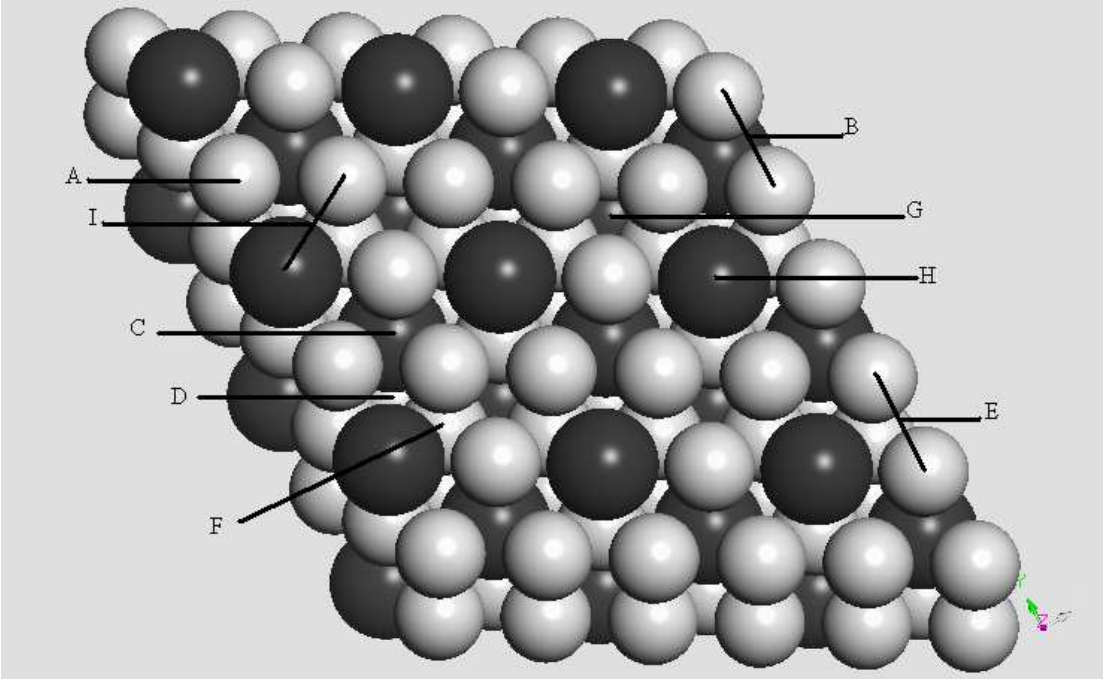

Figure 3.7. Schematic representation for the active sites on the $Pt_3Sn(111)$ surface (○: Pt ●:Sn)

Table 3.1. List of active sites on the $Pt_3Sn(111)$ surface

Surface	Site	Name	Supercell	Coverage
(111)	A	atop Pt	(1×1)	0.25
	B	bridge Pt–Pt on Sn		
	C	hollow hcp Pt_3 on Sn		
	D	hollow fcc Pt_2Sn		
	E	bridge Pt–Pt on Pt		
	F	hollow hcp Pt_2Sn on Pt		
	G	hollow fcc Pt_3		
	H	atop Sn		
	I	bridge Pt–Sn		

Table 3.2. List of active sites on the $Pt_3Sn(110)$ surface

Surface	Site	Name	Supercell	Coverage
(110) mixed	A	atop Pt	(1×1)	0.5
	B	bridge Pt–Sn		
	C	atop Sn		
	D	long bridge Pt–Pt	(2×1)	0.25
	E	long bridge Sn-Sn		
(110) pure	F	atop Pt	(1×1)	0.5
	G	bridge Pt–Pt		
	H	long bridge Pt–Pt	(2×1)	0.25
	I	ffh, Pt @ bottom		
	J	ffh, Sn @ bottom		

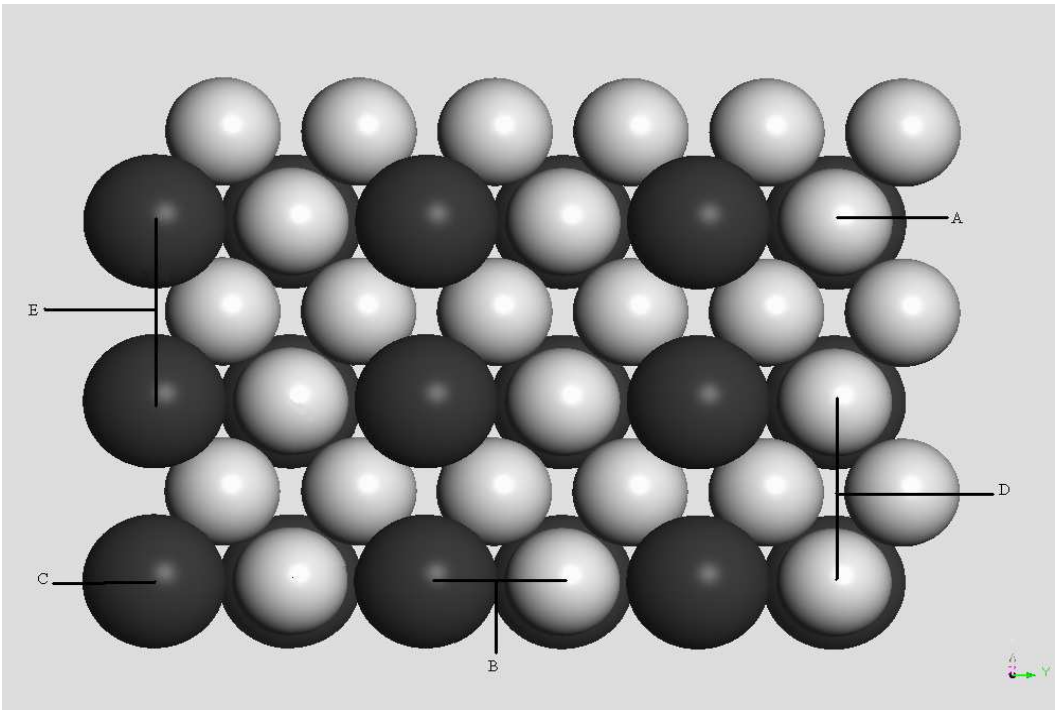

(a)

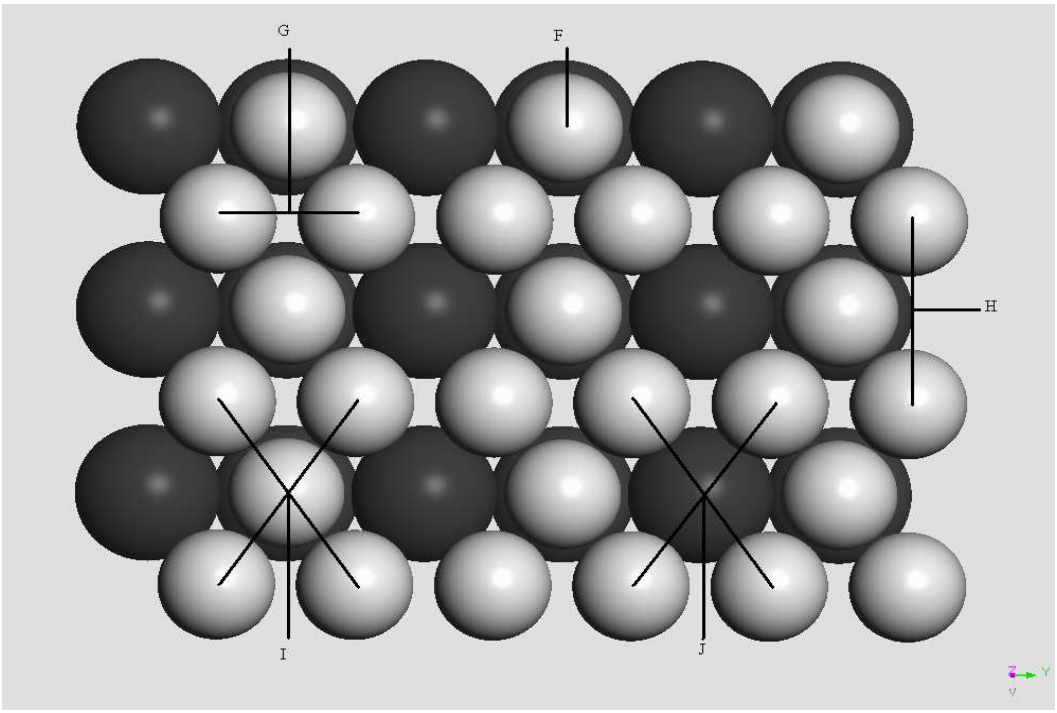

(b)

Figure 3.8. Schematic representation for the active sites on the $Pt_3Sn(110)$ surface (a) mixed termination (b) pure-Pt termination (○: Pt ●:Sn)

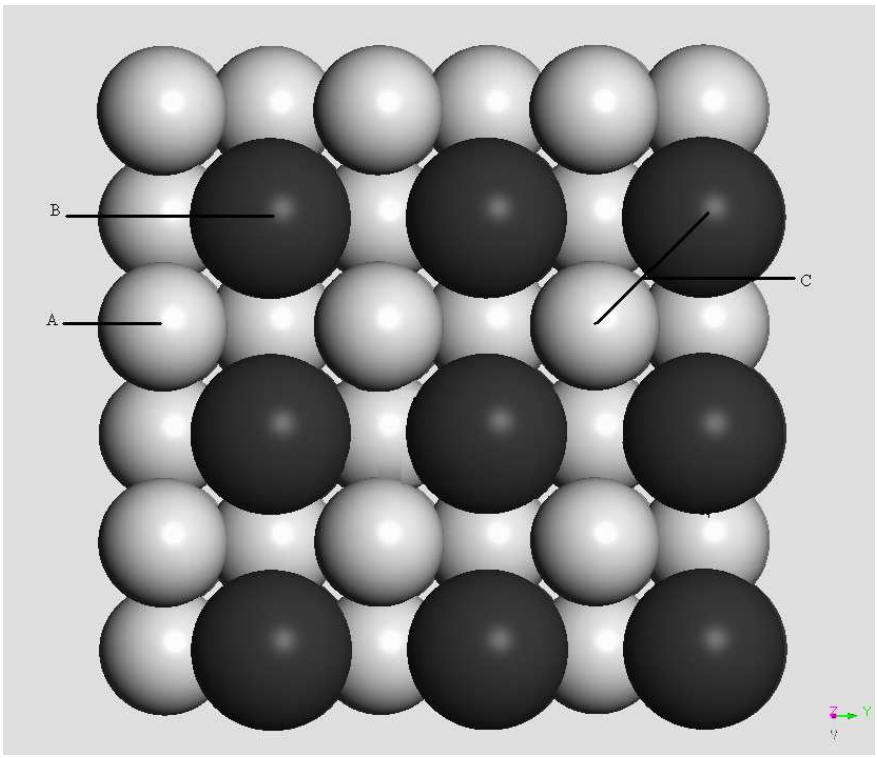

(a)

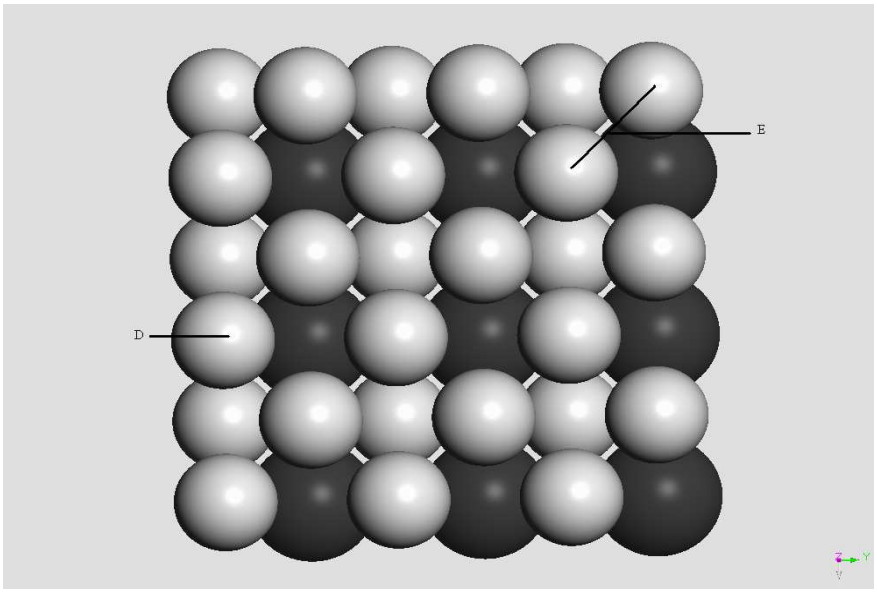

(b)

Figure 3.9. Schematic representation for the active sites on the $Pt_3Sn(001)$ surface (a) mixed termination (b) pure-Pt termination (○: Pt ●:Sn)

Table 3.3. List of active sites on the $Pt_3Sn(001)$ surface

Surface	Site	Name	Supercell	Coverage
(001) mixed	A	atop Pt	(1×1)	0.5
	B	atop Sn		
	C	bridge Pt–Sn		
(001) pure	D	atop Pt	(1×1)	0.5
	E	bridge Pt–Pt		

3.5. Optimization of the Adsorption System

The CO_2 molecule was bound to surface sites determined in Section 3.4 by its carbon end while oxygen atoms were bound to the carbon by a bond distance of free CO_2 molecule. The bond length of CO_2 molecule was calculated by building the molecule and optimizing by CASTEP. The adsorption energy and geometry of each site was calculated by geometry optimization using CASTEP. During the optimization, the adsorbate was allowed to relax with the top three layers of the slab.

As an example, Figure 3.10 shows a hollow hcp Pt_3 on Sn bound CO_2 on $Pt_3Sn(111)$ prior to optimization .

The adsorption energies per CO_2 molecule was obtained as:

$$\mathrm{E}_{ads} = \mathrm{E}_{CO_2/slab} - (\mathrm{E}_{CO_2} + \mathrm{E}_{slab}) \tag{3.1}$$

where E_{ads} is the adsorption energy of CO_2 at that site, $\mathrm{E}_{CO_2/slab}$ is the total energy for the slab with the adsorbed CO_2 on the surface, E_{CO_2} is the total energy of the optimized free CO_2 molecule, which is taken as -1031.8221 eV and E_{slab} is the total energy of the optimized bare slab of the surface.

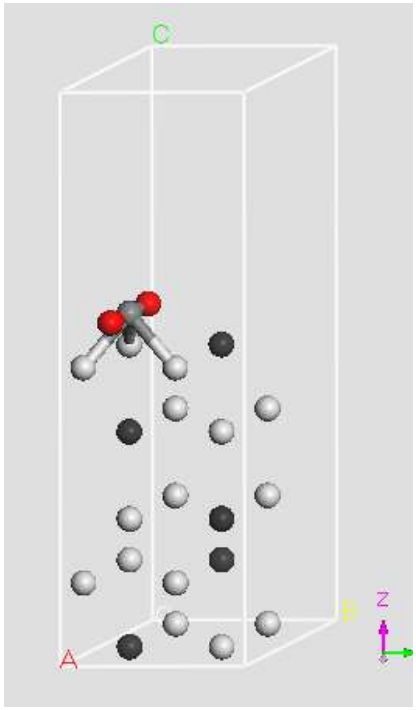

Figure 3.10. Hcp Pt_3 on Sn bonded CO_2 on $Pt_3Sn(111)$ (○: Pt ●:Sn)

3.6. Plotting the LDOS Charts

To gain more insight into the electronic mechanism of CO_2 adsorption, the key should be a comparison-based evaluation of the electronic states. Essential qualitative information is provided by the LDOS (local density of states) charts of the bonding atoms.

The LDOS of an atom in a system shows the atom's contribution to the electronic states of the system in various parts of the energy spectrum, without resolving these contributions according to the angular momenta of the states (i.e. identifying the s, p, d and f characters). Materials Studio can produce several types of DOS (density of states) plots based on the results of a geometry optimization by CASTEP. Each program can produce DOS graphs only if results data are available in the same medium. Therefore CASTEP Analysis was used to generate the LDOS charts.

CASTEP uses a simplified linear interpolation scheme developed by Ackland

(1998). This method is based on linear interpolation in paralelopipeds formed by the points of the Monkhorst-Pack set, followed by the histogram sampling of the resultant set of band energies. Smearing method is employed with a width of 0.1 eV. Charts are produced by plotting the LDOS data (electrons/eV) versus energy (eV) [49].

The LDOS of adsorbent atom was determined for both bare surface and for CO_2 adsorbed state at the binding Pt atom. The LDOS of adsorbate was determined for both free state and adsorbed state of CO_2. The LDOS figure of each atom was compared on the same chart with the LDOS figure of the same atom in the isolated or bare state; for CO_2, the CO_2 molecule; and for Pt and Sn, Pt and Sn atoms on the adsorbing site of the corresponding bare alloy surface. The isolated state of CO_2 was created by approximating it to an empty slab of the same size as the adsorption system, and placing the CO_2 in that slab. Keeping the C–O bond at 1.17 Å, the exact value for the relaxed molecule, a Single-Point-Energy (SPE) calculation was carried out by CASTEP to obtain the LDOS data. The isolated state of an alloy surface was, on the other hand, represented by the optimized geometry of the corresponding bare slab. The LDOS data was extracted from the bare slab optimization that was carried out for calculation of the site's adsorption energy, named as E_{slab} in Equation 3.1.

LDOS profiles were used to analyze (i) the electronic properties of Pt atoms on bare Pt_3Sn, and (ii) the changes occurred in the electronic properties of the binding atom end of the CO_2 adsorbed on Pt_3Sn surfaces.

4. RESULTS AND DISCUSSION

Carbon is considered as an inert material in comparison with other catalyst supports though its surface is not as inert as expected due to the presence of oxygen bearing surface groups. In terms of catalyst preparation, the presence of oxygen bearing groups is of great interest as they act as nucleation centers for both precursors and reduced metal particles. Most of the chemical properties of activated carbon come from the incorporation of oxygen during its production; the surface oxides formed, i.e. carboxylic, phenolic, lactonic and etheric groups, are responsible both for the acid/base and the redox properties of activated carbons. The main goal of oxidation is to obtain a more hydrophilic surface; the extent of hydrophilic properties of AC is directly related with amount and type of oxygen containing surface groups. In order to create more oxygen bearing surface groups, AC can be modified with different oxidation procedures. In one of the studies, bimetallic Pt–Sn catalysts supported on non-oxidized or oxidized (by air or by HNO_3 oxidation) activated carbon was investigated [13]. Less acidic groups increase the interaction of the metal precursor or the metal particle with the support and thus minimizing the sintering propensity of Pt/AC catalysts while the acidic groups decrease the hydrophobicity of activated carbon, thus making the surface more accessible to the aqueous solutions of metal precursors. Aksoylu *et al.* has stated that excess in oxygen bearing groups that produce CO_2 in their decomposition, ie. mostly carboxylic acid groups, favors the formation of Pt_3Sn [13]. Thus, the formation of all kinds of this group is favorable, but carboxylic acid groups are preferred as they decompose during pretreatment of catalyst, for example calcination under inert atmosphere. It was observed in the same study that the sample prepared by HNO_3 oxidation had a very high concentration of carboxylic acid groups whereas the small amount of carboxylic acid groups that formed on non-oxidized sample was decomposed during air oxidation at 723 K. In another work, Aksoylu *et al.* studied the activity of Pt–Sn/AC catalysts in CO oxidation and found out that it was stable and it showed strong activity in reaction [14]. In those studies, the results of the PROX tests conducted on Pt–Sn bimetallic system supported on HNO_3-oxidized AC clearly showed that the Pt_3Sn alloy present on the catalysts plays a dominant role in enhanced

activity, selectivity and stability characteristics of the catalysts. They pointed out that if a catalyst has optimum Pt:Pt_3Sn ratio, it is of highest activity. All of these facts indicate HNO_3 oxidation is more beneficial compared to the other oxidation procedures as it decreases the hydrophobicity of the activated carbon by forming acidic groups and led to the formation of only the Pt-rich alloy, Pt_3Sn, during the catalyst preparation.

Most of the catalysts used in CO oxidation reaction have stability as one of the main problems. The reason for the activity loss can be studied through investigating the mechanism of the CO oxidation reaction. At low temperatures, the reaction mechanism between O_2 and CO is according to Langmuir-Hinshelwood model, where both reactants are adsorbed on the surface. Oxygen, which is adsorbed on the surface dissociatively, needs two adjacent sites for adsorption, whereas CO needs only a single site. As Nijhuis *et al.* pointed out that at low temperatures the limiting factor is the absence of sites for O adsorption led by the slow desorption of CO as it adsorbs strongly to the active sites [50]. Additionally, the CO_2 production rate, which is higher than its desorption rate, also inhibits the rate of reaction. Parallel to those findings, the study conducted by Aksoylu *et al.* has also shown that the monometallic Pt showed no activity in CO oxidation, due to inhibition of O adsorption led by strong CO adsorption on the active sites leaving very limited number of sites for oxygen adsorption and, as a consequence, results in deactivated sites occupied by irreversibly adsorbed CO. On the other hand, bimetallic Pt–Sn samples did not lose their activity as they provide sites for oxygen adsorption [14].

The necessity of considering the selective oxidation of CO in the presence of H_2 widened the scope of previous study by Aksoylu *et al.* [14]; Özkara and Aksoylu studied Pt–SnO_x and Pt–CeO_x catalysts supported on untreated and oxidized (air and HNO_3 oxidization) activated carbons (AC) to determine one or more catalysts that had sufficient low temperature activity in dry H_2 rich streams [4]. The HNO_3 oxidized sample is known to be more active in CO oxidation due to Pt_3Sn presence in its surface, but, on the other hand, Pt_3Sn presence under H_2-rich reactant stream turns to a disadvantage as Pt_3Sn alloys have H_2 adsorption capacity, which may prevent oxygen adsorption. The HNO_3 oxidized sample showed low activity and selectivity

to CO oxidation, as surface hydrogen fixed on the active sites was used for water production. The air oxidized support has the highest activity and selectivity level, so having thermally stable surface oxygen groups is more beneficial in CO oxidation when the test is conducted with H_2-rich reactant stream.

The activity loss seen in many catalysts used for CO oxidation was not the case for the catalysts having Pt_3Sn alloy, as mentioned above [4, 14]. The possible explanations for this stability can be made based on atomic scale studies conducted via reproducing the periodic vacuum slabs of the alloy, for the flat surfaces [41] and terraced surfaces [43] and studying CO adsorption on those surfaces through using quantum mechanical codes, like CASTEP or DMOL3 by Accelrys. The CO adsorption strength on those surfaces and its interaction model at atomic scale would give an idea on the reasons of high activity of the catalysts having Pt_3Sn alloy phase. The density functional theory calculations were performed on experimentally verified flat surfaces of Pt_3Sn (111), Pt_3Sn (110), Pt_3Sn (001) surfaces and compared with the results obtained from the adsorption of CO on similar sites of Pt (111), Pt (110) and Pt (001) surfaces [41]. Results of quantum mechanical study showed that inclusion of an Sn atom at the adsorption site causes dramatic decrease in stability; CO molecules that was bound to those unstable sites diffuses toward the neighboring stable sites. In addition to unstable sites formed by the presence of Sn, the comparison between bimetallic and monometallic surfaces revealed that adsorption strength of CO on Pt sites of the Pt_3Sn surface, whether it is an atop, bridge, or a threefold site, is lower; this is the highly probable reason why catalysts with Pt_3Sn phase do not suffer from CO poisoning as encountered in experimental works. Parallel to the findings of CO–Pt_3Sn studies for flat faces of Pt_3Sn, CO adsorption studies conducted on terraced Pt_3Sn, Pt_3Sn (102), clearly showed that (i) Sn presence decreases the CO adsorption strength on the active sites, (ii) the active sites that include Sn can not adsorb CO stably. The results obtained for the sites on this surface can be compared with those similar sites on Pt_3Sn (110) surface considering that the terraces of Pt_3Sn (102) are in (110) orientation. The comparison reveals that the adsorption strength is found to be, in general, stronger on (102) surface than on (110) surface. Both studies, [41] and [43], showed that the catalysts that have Pt_3Sn are not affected from CO poisoning due to the fact that

presence of Sn decreases the number of sites that have ability to adsorb CO and, at the same time, decreases the adsorption strength of CO for all sites, which adsorb CO stably. Additionally, almost all the studies in literature show that presence of Sn offers suitable adsorption sites to O_2, which partially offsets the CO competition effect limiting O_2 adsorption if only one type of adsorption site present on the surface.

In selective CO oxidation, i.e. PROX, the presence of CO_2 in the stream is an important parameter since it is present in exhaust gas mixture in high concentrations. The combustion reaction proceeds on the surface of the catalyst, according to LH mechanism for which the two reactants are adsorbed on the surface. The resulting state is therefore a molecule, CO_2, on the surface, and how this molecule behaves at the end of surface reaction when it is already present in the stream is a factor that determines the apparent rate. Most of the catalysts that are active in selective CO oxidation reaction loose their activities in the presence of CO_2. The possible reasons of this activity loss include dissociatively adsorbed CO_2, reverse water gas shift reaction [6], and hindrance of surface mobility of CO oxidation reactants, especially O_2, on both metal and the support by mobile CO_2 on the catalyst surface [6, 9, 16]. From these possibilities, hindrance seems to be the most effective. As Avgoroupolous *et al.* has stated, CO_2 effect is strongly dependent on the nature of the catalyst [7].

Since Pt_3Sn/AC is such a beneficial catalyst for CO oxidation in both H_2-free and H_2-rich streams, the activity and stability of it must be tested in streams containing CO_2, since it is present in the feed mixtures encountered in commercial operation. Şimşek *et al.* have studied preferential CO oxidation over AC supported Pt–SnO_x catalysts that have been previously studied for PROX in a dry, H_2-rich streams free from CO_2 [4]. The results of the study showed that CO conversion was increased in all of the samples, prepared on nonoxidized or oxidized AC supports; in these tests, HNO_3 oxidized sample gave 100 per cent conversion. The increase in the activity of this sample was 144 per cent, whereas it was 28 per cent for the sample prepared on nonoxidized AC and 10 per cent for the sample prepared on air-oxidized AC. This high conversion level was explained by stabilization of CO_2 on active carbon surface. The carboxylic acid groups that are present in high concentration on HNO_3 oxidized

sample participate in the reversible adsorption of CO_2 on the bare surface carbon atoms with low coordination; by this way, CO_2 is stabilized on the AC support surface not inhibiting oxygen mobility, and, at the same time, does not adsorb dissociatively on the metallic surface, leaving adsorption sites for oxygen adsorption [17].

The explanations given in the previous studies point out two different sources for the no negative effect of CO_2 present in the reaction mixture on the PROX activity of Pt–Sn/AC system: the stabilizing effect of oxidized activated carbon support and the limited interaction between CO_2 and Pt_3Sn alloy surface. It is well known that the alloy surface can be reproduced and the proposed mechanisms can be tested via quantum mechanical calculations. Thus, in current study, we focused on the CO_2–Pt_3Sn system in order to investigate how CO_2 behaves on the active Pt_3Sn sites of this catalyst. Throughout the study, semi ab-initio DFT code, CASTEP, was utilized. It should be noted that for the previous assumptions to be valid, the CO_2 adsorption on Pt_3Sn surface should be weak and/or dissociation into CO and O should be limited, since this would increase surface CO concentration.

4.1. Construction of Clean Surface Models

The bulk lattice constant of Pt_3Sn is calculated as 4.0145 Å, in good agreement with the experimental value of 4.00 Å [51] and the theoretical value of 4.0148 Å [41].

Ball-and-stick models of the Pt_3Sn(111), (110) and (001) surfaces are given in Figures 3.3, 3.4 and 3.5. The (1×1) slab representing the (111) surface consists of 20 atoms; with a single Sn atom in each layer. The layers being identical lead to a single type of bulk-termination. The other surfaces on the other hand have two possible bulk-terminations, one consisting of only Pt atoms ("pure-Pt ending"), the other including both Pt and Sn ("mixed atom ending"). The (1×1) slabs of both (110) and (001) surfaces consist of 10 atoms, representing the mixed layers by one Pt and one Sn.

4.2. CO_2 Molecule

The bond length of the optimized CO_2 molecule is calculated as 1.171 Å, in agreement with the results from experimental (1.168 Å[52]) and theoretical (1.171 Å[48]) studies. Its energy is recorded as -1031.8221 eV.

4.3. CO_2 Adsorption

The binding site preferences of the CO_2 molecule were investigated for Pt_3Sn (111), (110) and (001) surfaces and their different terminations. For each adsorption site the slabs representing the bare surface and CO_2–Pt_3Sn complex have been optimized, and their energy values (E_{slab} and $E_{CO_2/slab}$, respectively) are given in Table 4.1.

The CO_2 binding energy of each site was determined from Equation 3.1. Table 4.2 lists the active sites, the corresponding CO_2 adsorption energies, Pt–C, Sn–C, Sn–O and C–O bond lengths as well as the O–C–O bond angle.

Table 4.1. Calculation of adsorption energies

Surface	Site	Name	Supercell	E_{slab}	$E_{CO_2/slab}$	E_{ads}
(111)	A	atop Pt	(1×1)	-11325.654	-12357.552	-0.076
	B	bridge Pt–Pt on Sn			-12357.541	-0.065
	C	hollow hcp Pt_3 on Sn		-11325.641	-12356.679	0.785
	D	hollow fcc Pt_2Sn			-12357.282	0.182
	E	bridge Pt–Pt on Pt		-11325.638	-12357.560	-0.099
	F	hollow hcp Pt_2Sn on Pt			-12357.267	0.194
	G	hollow fcc Pt_3			-12357.091	0.370
	H	atop Sn		-11325.641	-12357.512	-0.048
	I	bridge Pt–Sn			-12357.308	0.156
(110) mixed	A	atop Pt	(1×1)	-5349.787	-6381.675	-0.066
	B	bridge Pt–Sn			-6381.582	0.027
	C	atop Sn			-6381.551	0.058
	D	long bridge Pt–Pt	(2×1)	-10699.574	-11731.620	-0.224
	E	bridge Sn-Sn			-11731.592	-0.196
(110) pure	F	atop Pt	(1×1)	-5970.583	-7002.209	0.196
	G	bridge Pt–Pt			-7002.319	0.086
	H	long bridge Pt–Pt	(2×1)	-11941.166	-12973.094	-0.106
	I	ffh, Pt @ bottom			-12973.101	-0.113
	J	ffh, Sn @ bottom			-12973.098	-0.110
(001) mixed	A	atop Pt	(1×1)	-5350.570	-6380.338	2.054
	B	atop Sn			-6379.810	2.581
	C	bridge Pt–Sn			-6382.279	0.112
(001) pure	D	atop Pt	(1×1)	-5972.393	-7001.742	2.473
	E	bridge Pt–Pt			-7004.301	-0.086

Table 4.2: Possible CO_2 adsorption sites, corresponding adsorption energies and data on geometric properties of CO_2–Pt_3Sn system (* Unstable)

Surface	Site	Coverage	E_{ads} (eV)	Pt–C (Å)			Sn–C (Å)		Sn–O (Å)	C–O (Å)		θ (deg)
(111)	A*	0.25	-0.076	3.577						1.171	1.172	179.065
	B*		-0.065	3.733	3.904					1.171	1.171	179.478
	C		0.785	2.584	2.588	2.125				1.253	1.256	130.306
	D		0.182	3.360	2.116		2.793		2.132	1.282	1.203	132.221
	E*		-0.099	3.929	3.865					1.171	1.172	179.601
	F		0.194	2.114	3.331		2.772		2.134	1.279	1.204	132.890
	G*		0.370	2.919	3.396	3.373				1.184	1.163	167.387
	H*		-0.048				3.860			1.171	1.172	179.384
	I		0.156	2.113			2.780		2.128	1.284	1.204	132.086
(110) mixed	A*	0.5	-0.066	3.308						1.172	1.172	179.069
	B		0.027	2.065					2.092	1.290	1.205	130.430
	C*		0.058				3.438			1.171	1.171	179.407
	D*	0.25	-0.224	3.560	3.560					1.172	1.172	178.644
	E*		-0.196				3.768	3.768		1.171	1.171	179.366

Continued on next page

Table 4.2 – continued from previous page

Surface	Site	Coverage	E_{ads} (eV)	Pt–C (Å)			Sn–C (Å)		Sn–O (Å)	C–O (Å)		θ (deg)
(110) pure	F	0.5	0.196	2.167						1.209	1.217	148.083
	G		0.086	2.382	2.382					1.219	1.219	143.960
	H*	0.25	-0.106	3.682	3.680					1.172	1.172	179.662
	I*		-0.113							1.171	1.172	179.365
	J*		-0.110							1.172	1.172	179.899
(001) mixed	A	0.5	2.054	2.049						1.241	1.241	112.293
	B*		2.581				3.694			1.120	1.120	178.086
	C		0.112	2.094			2.854		2.093	1.292	1.209	128.457
(001) pure	D	0.5	2.473	2.017						1.233	1.233	114.635
	E*		-0.086	3.890	3.948					1.170	1.172	179.778

During geometry optimization both the top layer of the metal surface and the adsorbate molecule are relaxed and the simulation is terminates when they reach a minimum energy configuration. At some of the sites the CO_2 molecule deviates significantly from the site region studied. The optimized adsorption system at a threefold hollow site D of the $Pt_3Sn(111)$ surface is given in as an example Figure 4.1. The site is comprised of two Pt's and a Sn atom(top view).

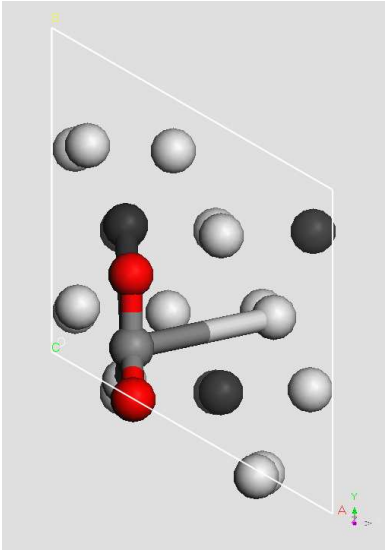

Figure 4.1. The optimized threefold hollow site on the $Pt_3Sn(111)$ surface, as an example of an unstable adsorption site (○: Pt ●:Sn)

As can be seen from the optimized geometry, the adsorbed CO_2 molecule has moved significantly toward the bridge Pt–Sn site; thereby it approaches the nearest stable site. The threefold hollow site is clearly an unstable site for the CO_2 molecule. All the unstable sites are marked with a superscript (*) in Table 4.2. The underlined bond lengths are for the bonds that are not broken or newly formed during adsorption process.

The adsorption energies obtained for all surfaces were both endothermic and exothermic. Their values were close to zero from either way; thus, the E_{ads} values do not indicate the stability of the adsorption significantly. Generally, an adsorption process is called stable if the energy is exothermic, as calculated from Equation 3.1, and unstable if it is endothermic. On the other hand, when the adsorption energy values are

close to zero, the optimized geometry of CO_2 on the surface must be analyzed further. This geometry check can be made by utilizing the bond calculation tool of CASTEP [49] which shows the bonds broken or newly formed or through the analysis of local density of states (LDOS) graphs. The bond calculation tool assumes no bonding to s- and f- shells, takes bond length tolerance from 0.6 to 1.5 Å and converts representation to Kekule type. The resulting bonding properties are evaluated through the lengths and angles. Geometry and/or LDOS analysis were performed on the optimized structures and the sites that adsorb CO_2 stably were determined.

4.3.1. $Pt_3Sn(111)$ surface

Atop CO_2 adsorption at site A is studied firstly. At the end of the optimization process, the resulting structure laid at a distance of 3.58 Å from the surface. The molecule's orientation was perpendicular to the surface at the beginning and this did not change at the end optimization. The C–O bond lengths of the resulting structure were both 1.17 Å, and the O–C–O bond angle was 179.06 °. These values indicate that the geometry of CO_2 molecule did not change during optimization process, thus no adsorption has taken place. LDOS graphs of the free CO_2 and bare surface as well as those of the CO_2 and Pt site at the end of the optimization for atop adsorption are given in Figure 4.2. The peaks present in the free CO_2 below the Fermi level (0 eV) did not shift in energy (or in electrons/energy) upon interacting with the surface. LDOS graph of the surface Pt atom on which CO_2 molecule is adsorbed is also given in Figure 4.2 (b). The Pt LDOS curves of the figure are of the highest intensity just below the Fermi level (0 eV), in the region between -5 and 0 eV. The peaks in the LDOS profile of the Pt atom of the bare Pt_3Sn (111) surface did not shift and the intensity of the peaks did not change as seen from the matching profiles of the free Pt atom and the Pt atom of the CO_2–Pt_3Sn complex upon adsorption. The assumption that CO_2 does not adsorb on site A of the Pt_3Sn (111) surface deduced from geometry analysis is supported by the LDOS profiles, which do not exhibit different characteristics between profiles of the bare and interacted atoms during adsorption simulation.

There are two stable structures on $Pt_3Sn(111)$ surface, both with endothermic

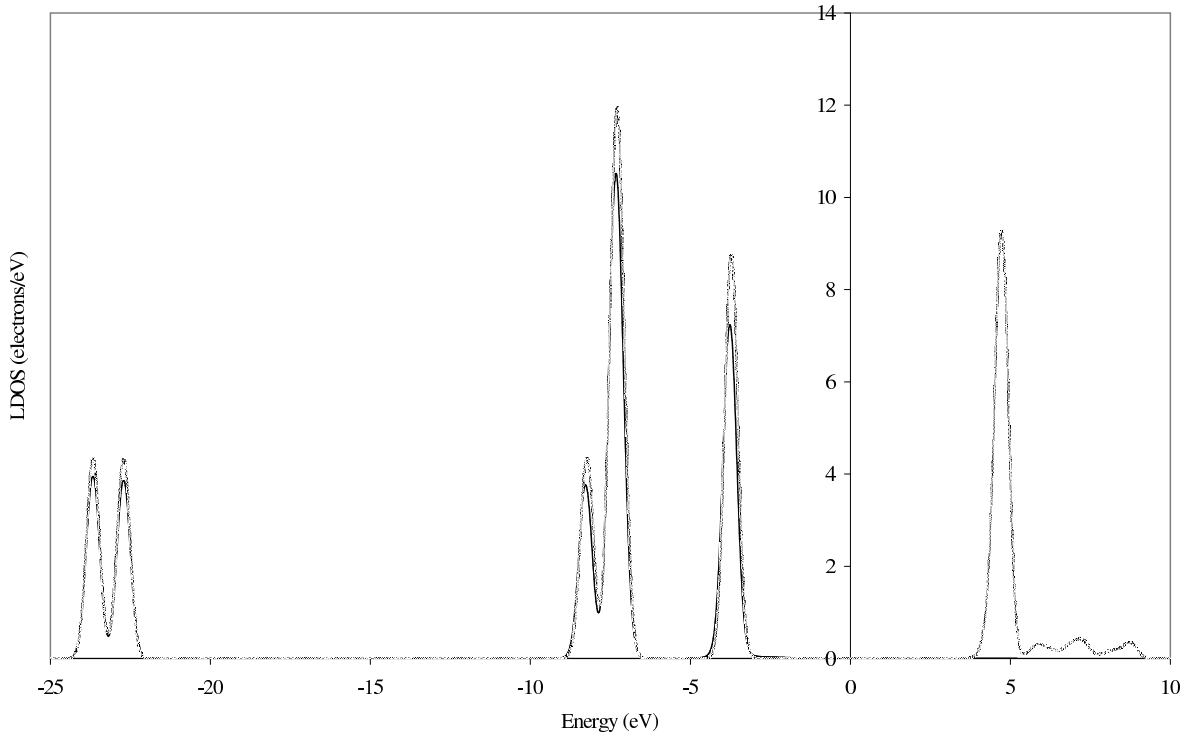

(a)

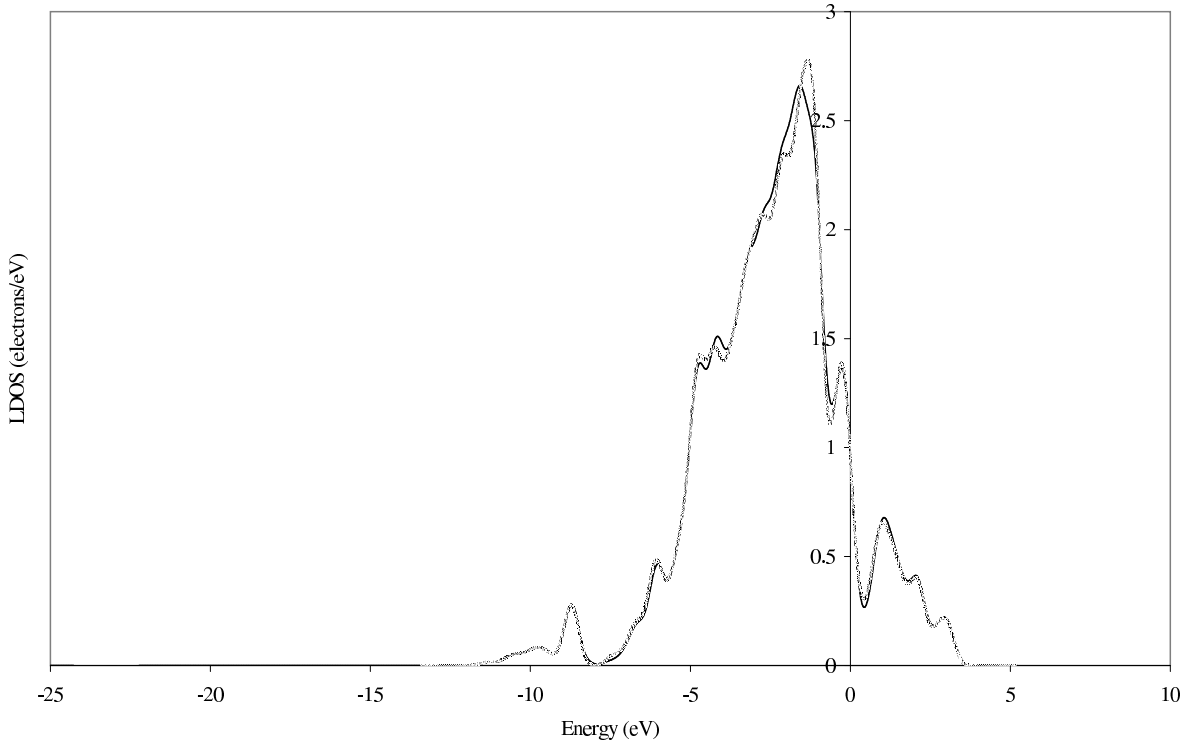

(b)

Figure 4.2. LDOS for site A of $Pt_3Sn(111)$ surface (a) CO_2 molecule (b)surface Pt atom (black: bonded cases, gray: free cases)

adsorption energies. The other structures either turned out to be physically adsorbed or transformed into one of the stable structures. The adsorbed CO_2 showed a bent structure at the sites of stable adsorption.

One of the structures that adsorb CO_2 stably was the hollow hcp Pt_3 on Sn, site C. The adsorption energy of this site was 0.78 eV, showing that it is not thermodynamically favored. The threefold site in the original turned into a structure that is bonded to one of the Pt atoms from C atom. The Pt–C bond length was 2.12 Å. The distance from the surface to the C atom was 1.73 Å. The O atoms were tilted upwards and toward the two unbonded Pt atoms, as seen in Figure 4.3. The C–O bond lengths were elongated, 1.25 and 1.26 Å for adsorbed CO_2 compared to 1.17 Å for gaseous CO_2. The molecule was bent, and the O–C–O angle was 130.31 ° in the final structure. The LDOS profiles of free CO_2 and Pt atoms of the bare Pt_3Sn (111) surface as well as CO_2 and Pt atoms of the CO_2–Pt_3Sn complex upon adsorption are given in Figure 4.4. Figure 4.4 (a) shows the LDOS profile for CO_2, Figure 4.4 (b) shows the LDOS profile of the Pt atom that is bound to CO_2 at the end of the optimization, and Figure 4.4 (c) shows the LDOS profile of one of the unbound Pt atoms, since the profiles of the two unbound Pt atoms on site C are same. LDOS profile of the free CO_2 given with the profile of the CO_2 upon adsorption reveals that the molecular energy levels has changed to a great extent. The highest occupied molecular orbital (HOMO) of free CO_2 is $1\pi_g$, and the lowest unoccupied molecular orbital (LUMO) is $2\pi_\mu$. LUMO is situated at 6.00 eV and HOMO is situated at -2.44 eV in the LDOS profile of free CO_2. Upon chemisorption, the $2\pi_\mu$ and $1\pi_g$ bands shifted downward, to -2.08 eV and -6.51 eV, respectively, and this is the consequence of the binding of the CO_2 to one of the Pt atoms at site C of the Pt_3Sn (111) surface. The antibonding $2\pi_\mu$ orbital fell below the Fermi level. The other bands also shift downward but not as extensively as the HOMO and LUMO bands. The intensities of the bands decrease for the chemisorbed CO_2. Further analysis on bent CO_2 reveal that the more the CO_2 molecule bends, the lower the intensity and the energy level of the LUMO gets. Figure 4.4 (b) is for the Pt atom of the bare Pt_3Sn (111) surface in comparison with the Pt atom that is bound to the C atom of the CO_2 molecule, and Figure 4.4 (c) is for the Pt atom of the bare Pt_3Sn (111) surface in comparison with the Pt atom found not bounded to the C atom

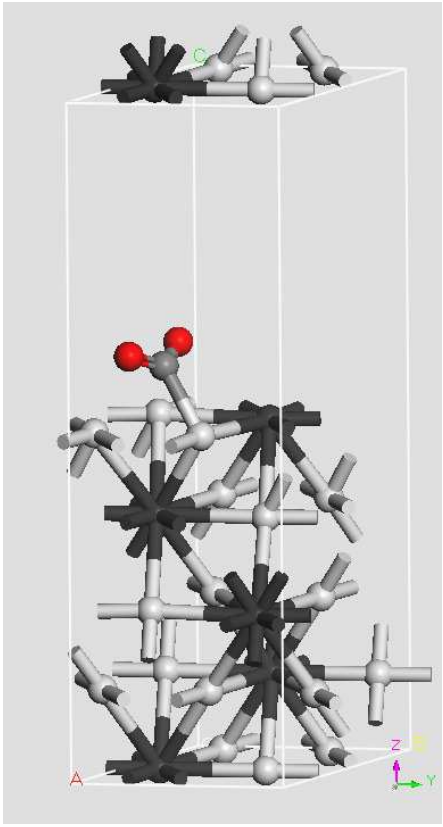

Figure 4.3. The optimized structure of hollow hcp Pt_3 on Sn site on $Pt_3Sn(111)$ surface (○: Pt ●:Sn)

of the CO_2 molecule at the end of the simulation. The shifts in the peaks between −5 eV and 0 eV are striking in Figure 4.4 (b) when compared with the shifts in Figure 4.4 (c). The frontier orbitals of Pt atom are in broad form and the d orbitals herein are responsible for the electron transfer to CO_2 molecule, thus, they are responsible for the bonding. This broadening effect is seen in the LDOS profile of the chemisorbed CO_2 molecule (see Figure 4.4 (a)). The peaks present in the LDOS profile for the free CO_2 have lost their sharpness and has broadened in this region. The electron density at the Fermi level has also decreased in intensity to a great extent, which is also a clue for the bonding of the molecule.

The other stable structure was the bridge Pt–Sn site, site I. The adsorption energy of this site, although still endothermic, was lower than that of the former site, 0.16 eV, which can be considered as a more thermodynamically favorable structure.

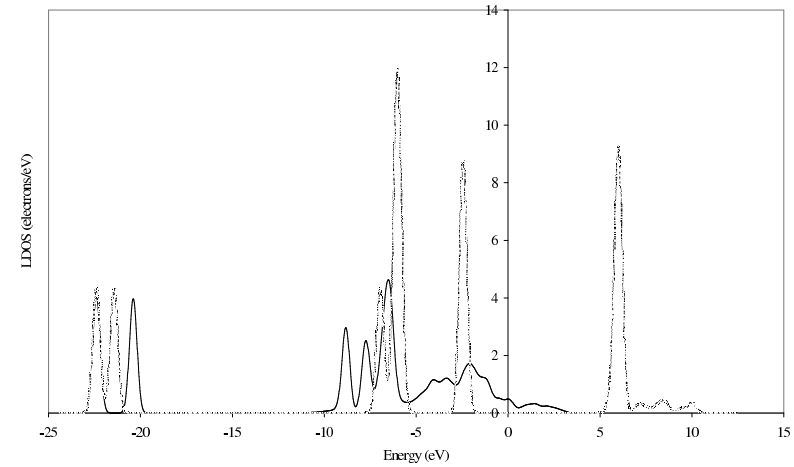

(a)

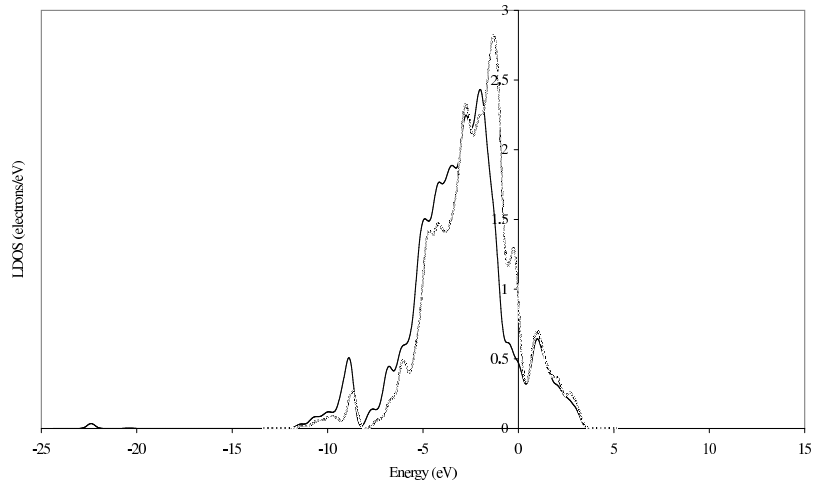

(b)

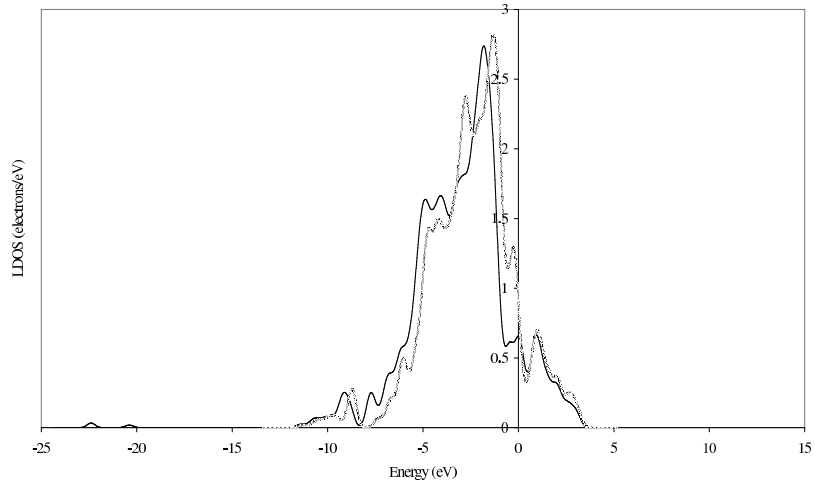

(c)

Figure 4.4. LDOS for site C of $Pt_3Sn(111)$ surface (a)CO_2 molecule (b)surface Pt atom bonded (c)surface Pt atom unbonded(black: bonded cases, gray: free cases)

This argument is also supported by the fact that two other structures, namely hollow fcc Pt_2Sn and hollow hcp Pt_2Sn on Pt, have moved and stabilized on this very site. Originally, C atom was bonded to two Pt atoms; in the final structure ,on the other hand, single Pt atom was bonded to C atom with a bond length of 2.11 Å and the Sn atom was bonded to one of the O atoms with a bond length of 2.13 Å. The C–O bond length was 1.28 Å for the C and O bonded, and 1.20 Å for C and O unbonded. The O–C–O bond angle of the optimized structure was 132.09 °. The resulting slab and CO_2 molecule that is bonded to the surface via Pt and Sn atoms is given in Figure 4.5. In order to analyze the bonding in CO_2 molecule to site I on Pt_3Sn (111) surface, LDOS profiles of free CO_2 is compared with CO_2 at the site upon adsorption (Figure 4.6). In the same figure, LDOS of bare Pt and Sn atoms of the surface are compared with LDOS of Pt and Sn at the site upon adsorption as well. In the LDOS profile for CO_2 molecule, the LUMO band, the band for the antibinding $2\pi_\mu$ orbital, has moved significantly below the Fermi level and its intensity is well below from its value that calculated for free CO_2 molecule. The peaks at region between -5 eV and 0 eV have broadened, in accordance with the broadness of the d-orbitals of the Pt atom at the Pt_3Sn (111) surface. The LDOS profile of the Pt atom given in Figure 4.6 (b) shows the shifts in peaks and decrease of the intensities upon chemisorption. Also, the LDOS profile of the Sn atom on surface Pt_3Sn at site C shows differences from the Sn of the bare Pt_3Sn surface; the intensity is lowered for many peaks, and the peak at -8.07 eV for bare Sn atom has shifted downward to -9.02 eV.

From the two adsorbed CO_2 structures that have moved and stabilized at site I, hollow fcc Pt_2Sn site, site D, had a CO_2 adsorption energy of 0.18 eV. The Pt–C bond was 2.12 Å, and the newly formed Sn–O bond was 2.13 Å. C–O bond lengths were 1.28 Å and 1.20 Å and O–C–O bond angle was 132.22 °. The other adsorbed CO_2 that stabilized at site I, hollow hcp Pt_2Sn on Pt, site F, had an adsorption energy of 0.19 eV. The Pt–C bond was 2.11 Å, and the newly formed Sn–O bond was 2.13 Å. C–O bond lengths were 1.28 Å and 1.20 Å and O–C–O bond angle was 132.89 °. These values are very close to the results obtained for site I, since they all are bridge Pt–Sn sites. The resulting bridge Pt–Sn site can be seen on Figure 4.5.

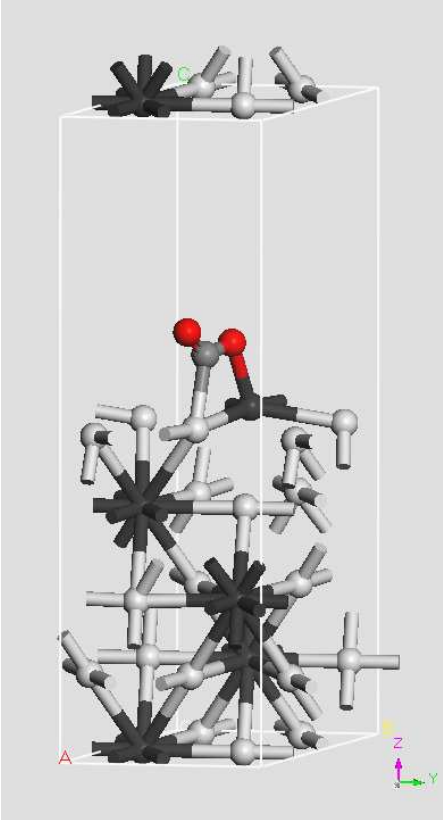

Figure 4.5. The optimized structure of bridge Pt–Sn site on $Pt_3Sn(111)$ surface (○: Pt ●:Sn)

LDOS profiles for the Pt atoms of site D are given in Figure 4.7. Figure 4.7 (a) is the profile of the Pt atom that is bonded to C atom of the CO_2 molecule upon adsorption and Figure 4.7 (b) is the profile of the Pt atom from which the CO_2 molecule has diffused away. It is seen that the electron density curve around Fermi level representing the unbonded Pt atom has the same amplitude as the bare Pt atom of the surface; whereas, for Pt atom bonded to the CO_2 molecule, the electron intensity decreases. While the peaks for the Pt atom unbound follow the trend of bare Pt atom of the surface, the density profile for bound Pt deviates from the profile of the bare atom which has peaks that have shifted downward. The changes occurring in Figure 4.7 are not significant and does not identify any bonding.

The same argument is valid for site F of the Pt_3Sn (111) surface; the CO_2 molecule on this site has also diffused and assumed a position for which it is bonded to one Pt

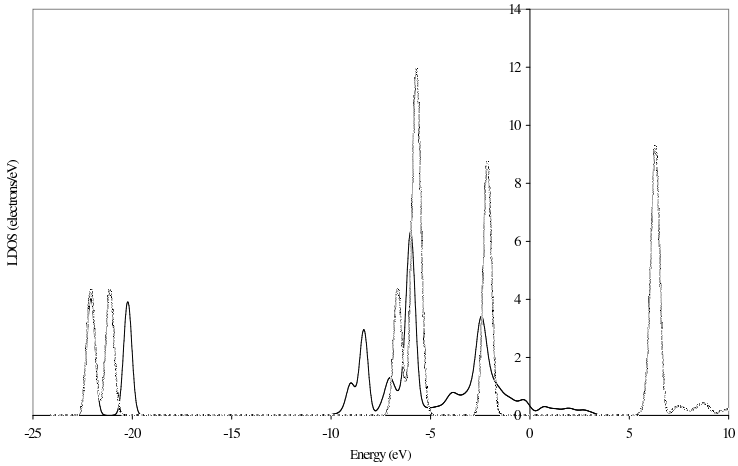

(a)

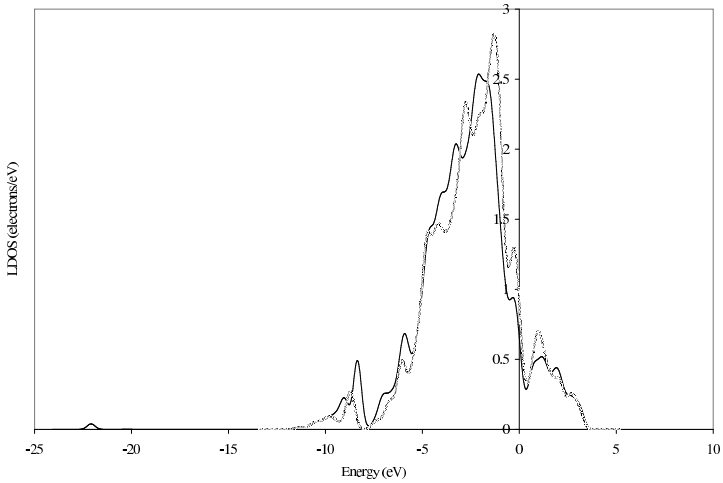

(b)

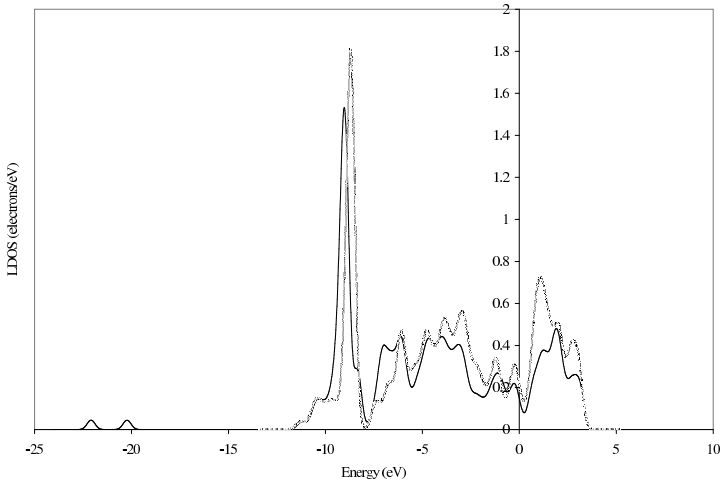

(c)

Figure 4.6. LDOS for site I of $Pt_3Sn(111)$ surface (a)CO_2 molecule (b)surface Pt atom (c)surface Sn atom(black: bonded cases, gray: free cases)

and one Sn. The LDOS profiles clearly show that the other Pt atom's electron density has not changed upon adsorption while the energy levels of the bonded Pt atom of the surface has changed significantly due to electron donation-backdonation with the CO_2 molecule at the end of the optimization.

CO_2 on all the other Pt_3Sn (111) adsorption sites, site B, E, G, and H, assumes a linear form that lies parallel to surface and with a C-surface distance of 2.64 Å–3.92 Å indicating no adsorption. The CO_2 distance was maximum for the one adsorbed on-top of a Sn atom and the minimum for the one adsorbed on hollow fcc Pt_3 site. The O–C–O bond angles were varying between 167.39 °–179.60 °. In all of these optimizations, the C–O distance was exactly the same for the free CO_2 molecule. The LDOS profiles of the sites B, E, G, and H show the trends similar to that of site A; the profiles of CO_2 and surface atoms at the site upon adsorption overlap those of free CO_2 molecules and surface atoms of the bare Pt_3Sn surface, respectively. Therefore, electron density analysis confirms these sites do not adsorb CO_2, as the geometry of the optimized CO_2 has suggested.

Habas *et al.* [46] had found three different surface species for CO_2 adsorption on Pd(111) surface and had classified them as physisorbed CO_2 molecule and chemisorbed CO_2^- anion from the geometry and the proximity to the surface. Table 4.3 lists the structural parameters for neutral and anionic CO_2 molecules. Notation used in this table is as follows: d(C–O) is the C–O distance in (Å) and O–C–O is the CO_2 bond angle in (°). The three species resulted on $Pt_3Sn(111)$ surface can also be classified as physisorbed molecule and chemisorbed anion as the C–O bond lengths and O–C–O bond angles resemble the experimental parameters. Additionally, the proximity of the species to the surface confirm that classification.

CO_2 is bonded to the surface through carbon and oxygen for late transition metals, whereas its interaction with the surface is only through oxygen(s) when the adsorbent is an alkali metal and/or early transition metal. This phenomenon is explained by the ionization potentials of the surfaces [46]. Alkali or early transition metal atoms have low ionization potentials, and hence can easily transfer an electron to CO_2;

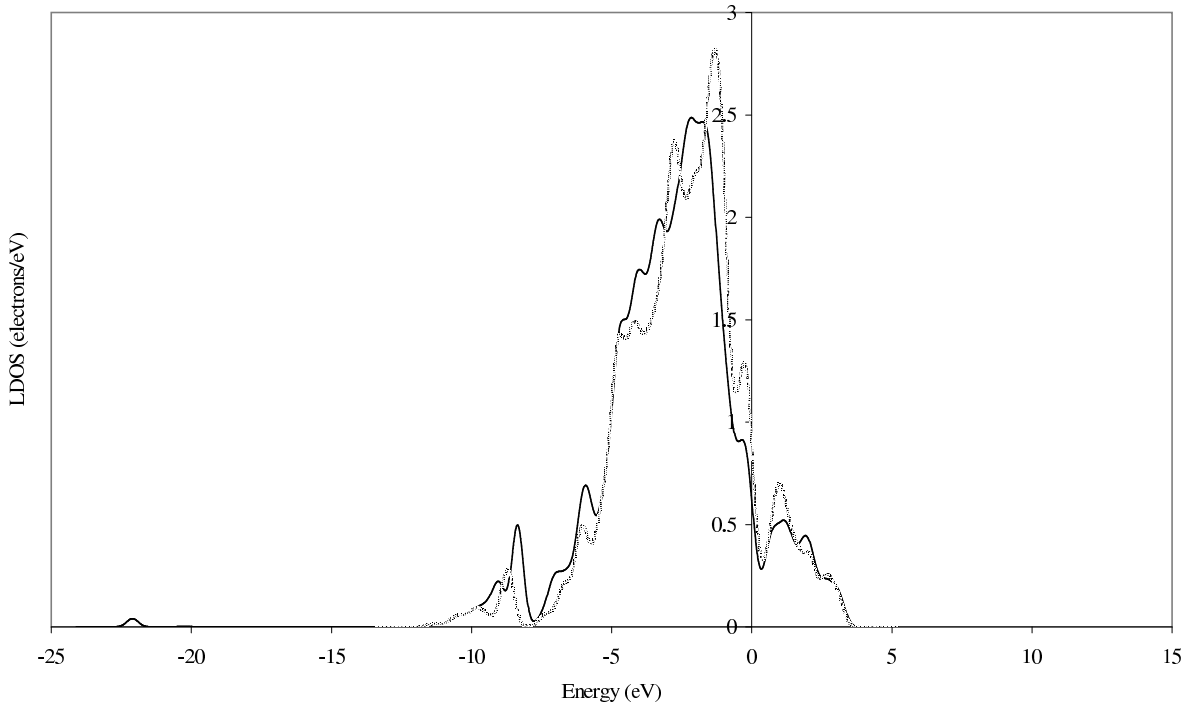

(a)

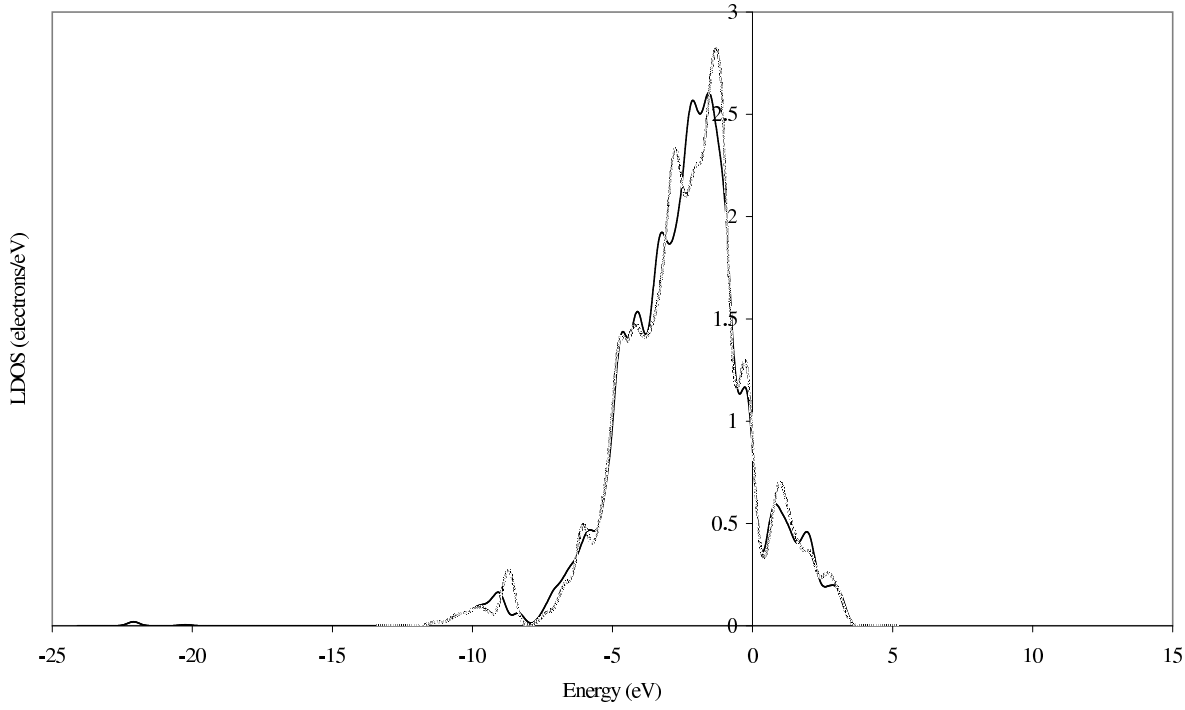

(b)

Figure 4.7. LDOS for site D of $Pt_3Sn(111)$ surface (a)bonded Pt atom (b)unbonded Pt atom (black: bonded cases, gray: free cases)

Table 4.3. Experimental values of structural parameters (Å and °) for neutral and anionic CO_2

	CO_2	CO_2^-
d(C–O)	1.17	1.24
O–C–O	180.0	135.0

the interaction is stabilized through the electrostatic interaction and the bonding has a large ionic character. Therefore, the preferred coordination mode for those cases is mainly determined by the electrostatic stabilization, which favors the interaction of the two negatively charged oxygens of CO_2^- with the metal cation. On the contrary, late transition metals have higher ionization potentials and thus, although there is also an important charge transfer to CO_2, the bonding for those systems is not as ionic as for the alkali or early transition metals. Moreover, late transition metals have an almost filled d-shell and, consequently, metal-ligand repulsion is larger for those systems, which plays an important role in determining the relative stability of the different coordination modes. One of the adsorbed CO_2 structures mentioned in the study of Habas *et al.* [46] was the one in our work for which C and O atoms of the adsorbed CO_2 are bonded to surface Pt and Sn atoms, respectively.

Pt_3Sn surface is an important candidate in CO oxidation as CO and O does not compete for the same sites and, thus, no blocking occurs. In case of CO_2 existence, we tried to investigate the site preference of CO_2 and find out whether it interferes with CO adsorption and, if so, the type of interference. As reported in the literature by Gülmen *et al.* CO prefers to adsorb on Pt sites and avoids sites that include Sn atom [41]. On the $Pt_3Sn(111)$ surface, CO adsorption was a favorable process as observed from the adsorption energies. The bridge Pt–Sn structure was not chosen as a possible site; it is clear that we cannot compare the adsorption property but it is known that the adsorption energy of CO on hollow hcp Pt_3 on Sn was exothermic, and this suggests that CO would be adsorbed in a competitive situation. All the other sites investigated by Gülmen *et al.* resulted in structures that are thermodynamically stable.

4.3.2. $Pt_3Sn(110)$ surface

On $Pt_3Sn(110)$ surface with mixed termination, CO_2–atop adsorption at site A was studied firstly. The binding energy was calculated from Equation 3.1 and found as -0.07 eV. This negative change in enthalpy could indicate exothermic adsorption but, as the value is too close to zero, it is not clear whether CO_2 adsorption is stable or not. Thus, the geometry of the resulting structure is examined. The CO_2 molecule on site A did not change its configuration after geometry optimization and laid at a distance of 3.31 Å perpendicular to surface. The resulting molecule's molecular bond lengths were both 1.17 Å, and the bond angle was 179.07 °, same as gaseous phase CO_2. Apart from the geometry check, LDOS graphs for free CO_2, Pt atom of the bare $Pt_3Sn(110)$ surface with mixed terminations as well as those of adsorbed CO_2 and Pt at the site upon adsorption are given in Figure 4.8. The shifts in the LDOS peaks are examined to decide whether the process ended with a bonded CO_2 at the site. The energy levels of the free CO_2 and that of placed on the atop the Pt for every point below Fermi level (0 eV). There were slight changes in electron density of CO_2 which can be attributed to presence of neighboring CO_2 molecules due to slab calculation and the adsorbent surface. Geometry and electron density analyses point out that the molecule was not adsorbed though the adsorption energy was exothermic.

The second site in consideration for this surface was the bridge site formed through C atom of CO_2 interacting with Pt and a Sn atom of the site. The binding energy calculated for this structure expressed that energy of the CO_2–Pt_3Sn complex lies at a slightly higher energy level than the sum of the energies of free CO_2 molecule and the slab; thus, the binding energy being equal to 0.03 eV. This value is also close to zero, which forces us to analyze the geometry and LDOS profiles for the free states and the adsorption complex after optimization. The position of the molecule assumes an equilibrium structure such that C attached to Pt atom and one O atom attached to Sn. The bond that was formed between Pt–C was 2.06 Å and Sn–O was 2.09 Å, with the molecule laying at a distance of 1.88 Å from the surface. The bond length between Pt-bonded C and Sn-bonded O was 1.29 Å, and 1.20 Å between Pt-bonded C and nonbonded O. These values show a significant deviation from those of free CO_2. Also,

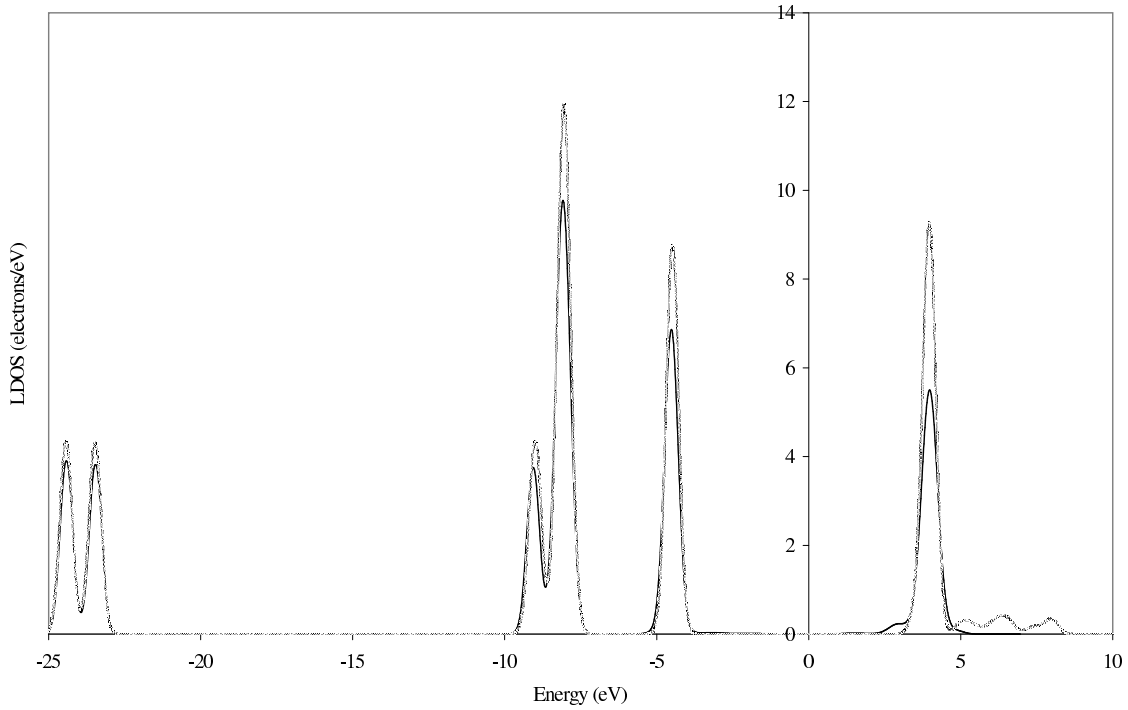

(a)

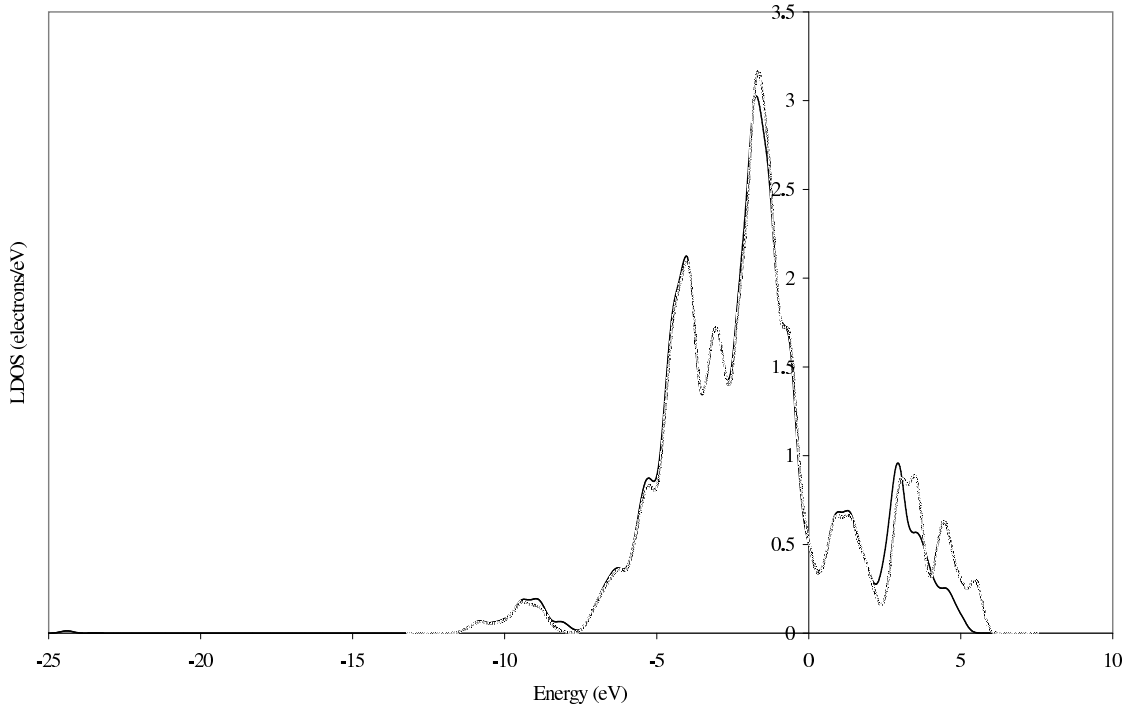

(b)

Figure 4.8. LDOS for site A of $Pt_3Sn(110)$ surface with mixed termination (a)CO_2 molecule (b)surface Pt atom (black: bonded cases, gray: free cases)

the O–C–O angle was 130.43 °. It is obvious that the final geometry of the molecule offers that there has been a process that changes the basic configuration. The electron density charts would offer insight to this electronic process. The Pt LDOS curve is of the highest intensity just below the Fermi level, in the region between −5 and 0 eV. In the Sn LDOS curve, no specific region that electron density is condensed is present. The LDOS profile of CO_2 is given in Figure 4.9 (a). This profile highly resembles the profile of CO_2 on bridge Pt–Sn site of Pt_3Sn (111), the site given in Figure 4.6 (a), with an important difference; the LUMO band orbital has moved significantly below Fermi level for site I of Pt_3Sn (111) surface, whereas in Figure 4.9 (a), a small peak is present above the Fermi level for site B of Pt_3Sn (110) surface with mixed termination. A portion of the peak at 5.77 eV has shifted to 4.18 eV and the remaining peak has showed up at −3.00 eV, below the Fermi level. The peak at 4.18 eV for site B on Pt_3Sn (110) surface was not present for the same site on Pt_3Sn (111) surface. The coverage of the Pt_3Sn (111) surface was 0.5 ML but that of the Pt_3Sn (110) surface with mixed atom termination was 0.25 ML. As the number of CO_2 molecules per monolayer on Pt_3Sn (110) surface is twice the number of molecules per monolayer on Pt_3Sn (111) surface, this peak above the Fermi level could imply CO_2–CO_2 interaction. Also, when the orbitals are analyzed based on the positions of the peaks, it is seen that some orbitals that are formed at the end of the optimization are common for all three profiles, ie. the profiles of CO_2 molecule, Pt atom and Sn atom. The shoulder seen at about −9.70 eV from the LDOS profile of CO_2 molecule upon adsorption has reflections at the same energies for Pt atom and Sn atom upon adsorption. The peaks at about −8.85 eV, −7.62 eV, and −6.45 are also common for the three profiles. All these common peaks signify the existence of a mixed orbital that are formed by CO_2 molecule, Pt atom, and Sn atom. Thus, along with geometric proof of bonding, LDOS profiles suggest that CO_2 molecule placed at site B of the Pt_3Sn (110) surface with mixed termination was adsorbed on the surface at the end of the optimization, though the calculated adsorption energy was slightly endothermic.

Site C on Pt_3Sn (110) surface was atop Sn site. The CO_2 was bonded to surface through the interaction between surface Sn and C atom of CO_2. The adsorption energy was calculated as 0.06 eV. The CO_2 molecule had a O–C–O bond angle of 179.41 ° and

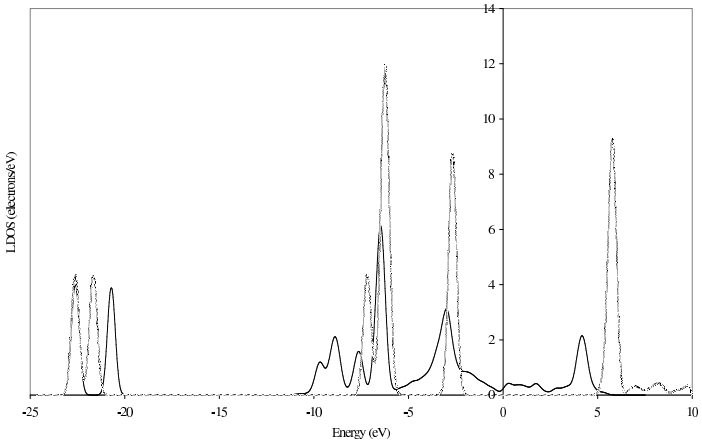

(a)

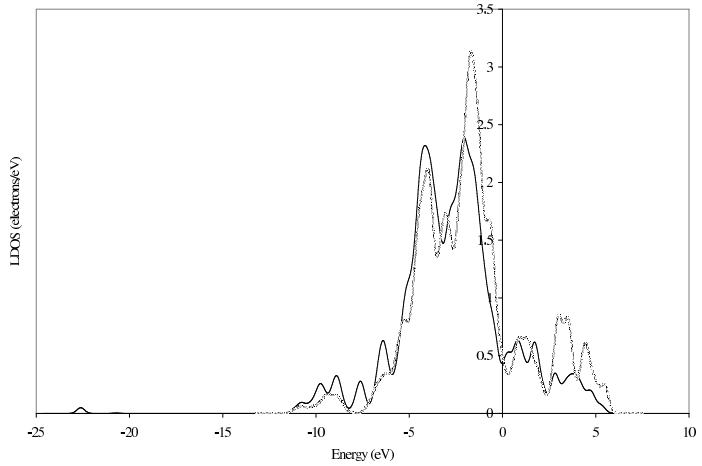

(b)

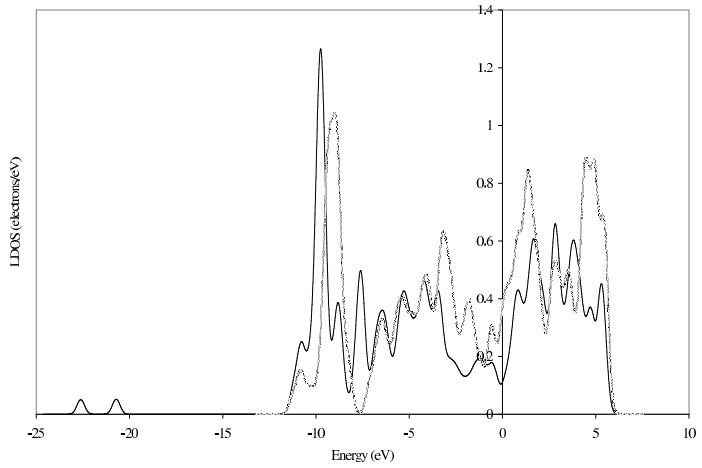

(c)

Figure 4.9. LDOS for site B of $Pt_3Sn(110)$ surface with mixed termination (a)CO_2 molecule (b)surface Pt atom (c)surface Sn atom (black: bonded cases, gray: free cases)

C–O bond lengths of 1.17Å at the end. The molecule was placed at a distance of 3.44 Å from the surface. The geometry of the optimized molecule suggests that no adsorption has taken place and the molecule is either physisorbed or in gaseous state. The results obtained from the electron density data also supports this conclusion. Figure 4.10 shows the LDOS graphs of both CO_2 molecule and Sn atom of the surface. The line that represents free CO_2 molecule matches with the line that represents CO_2 at site C that have peaks at the same energy level, and although there are slight differences in their amplitudes, no new orbital energy levels are present.

The optimized CO_2 molecule was also tested when the it is bonded to two Pt atoms from C atom, site D. The enthalpy change was -0.22 eV. The Pt–C bond lengths were both 3.56 Å and the distance of the molecule from the surface was 2.94 Å. The C–O bond lengths were 1.17 Å and the bond angle was 178.64 °. Here, again, the resulting structure resembles the gaseous phase CO_2, and this assumption can be analyzed by LDOS profiles, Figure 4.11. The minor changes in the peak intensities from the LDOS of free CO_2 to LDOS of CO_2 at the site upon adsorption could be due to the presence of adsorbent layer along with the CO_2 molecule.

The last CO_2 adsorption site on Pt_3Sn (110) surface with mixed termination was site E, where CO_2 molecule is bonded to two Sn atoms.The CO_2 adsorption site was also analyzed in terms of geometry and LDOS profiles. Similar to sites A, C and D, the CO_2 adsorption site E is an unstable site with an exothermic energy of adsorption. Figure 4.12 shows the corresponding LDOS profiles of free CO_2 and the Pt atom of the bare surface Pt_3Sn(110) surface with mixed termination in comparison with CO_2 and Pt at the site, respectively.

On Pt_3Sn (110) surface with pure termination, only two CO_2 adsorption sites were present. The CO_2–atop adsorption site F was studied firstly. The binding energy calculated for site F was 0.20 eV. The CO_2 molecule was bonded to the Pt atom of the surface at a distance of 2.17 Å. The equilibrium structure assumes a highly bent CO_2 molecule with both O atoms pointing away from the surface. The O–C–O angle for the adsorbed molecule was 148.08 °, and the C–O bond lengths were 1.21 Å and 1.22

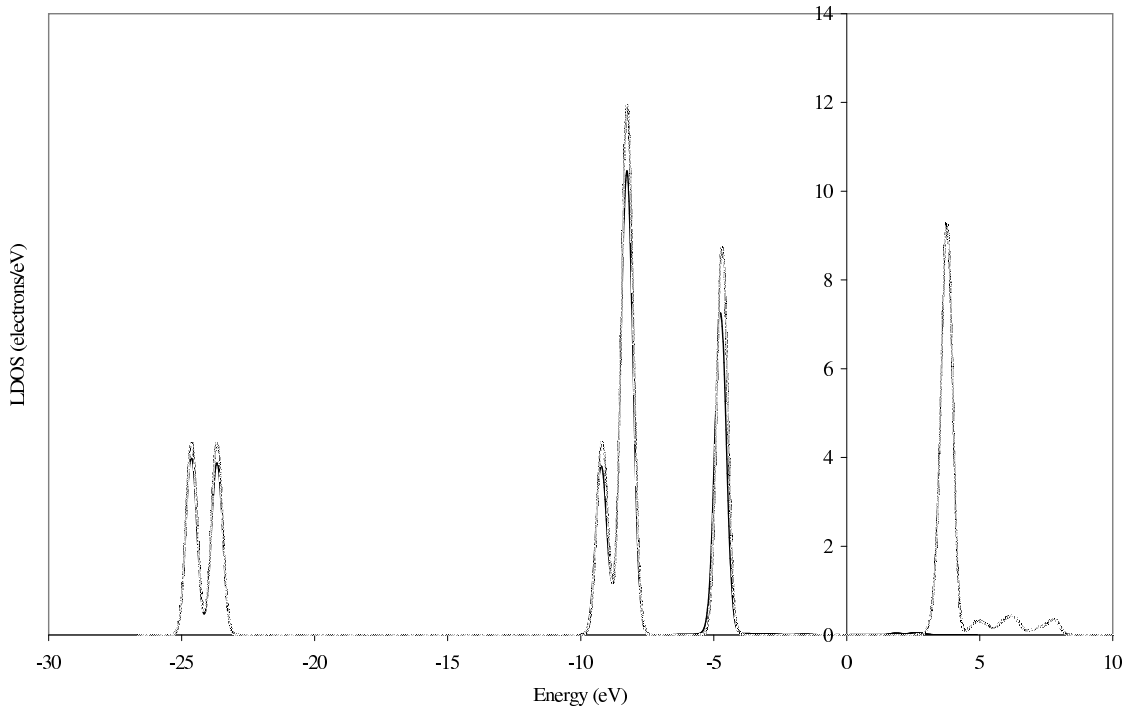

(a)

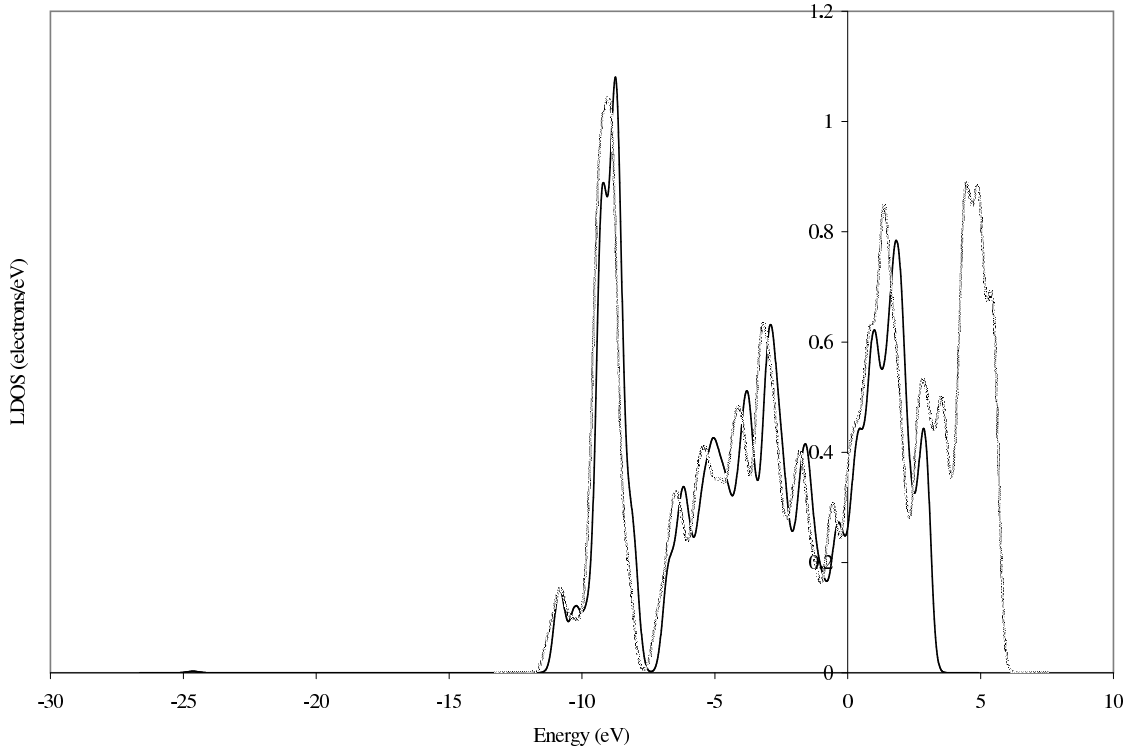

(b)

Figure 4.10. LDOS for site C of $Pt_3Sn(110)$ surface with mixed termination (a)CO_2 molecule (b)surface Pt atom (black: bonded cases, gray: free cases)

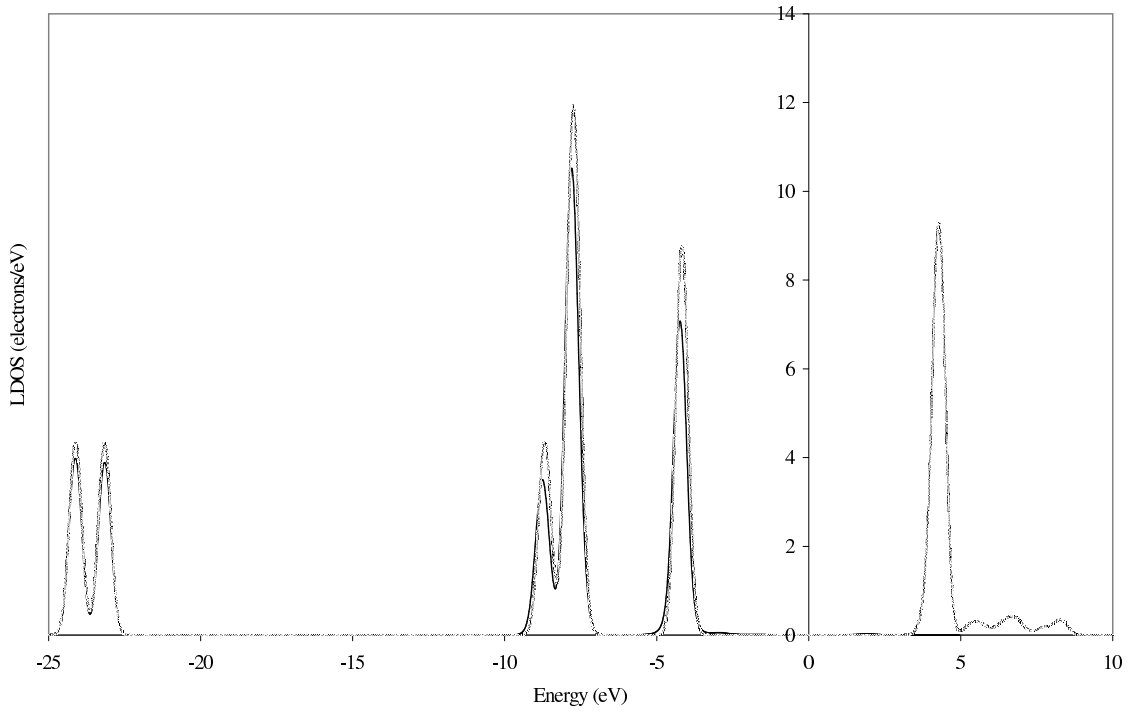

(a)

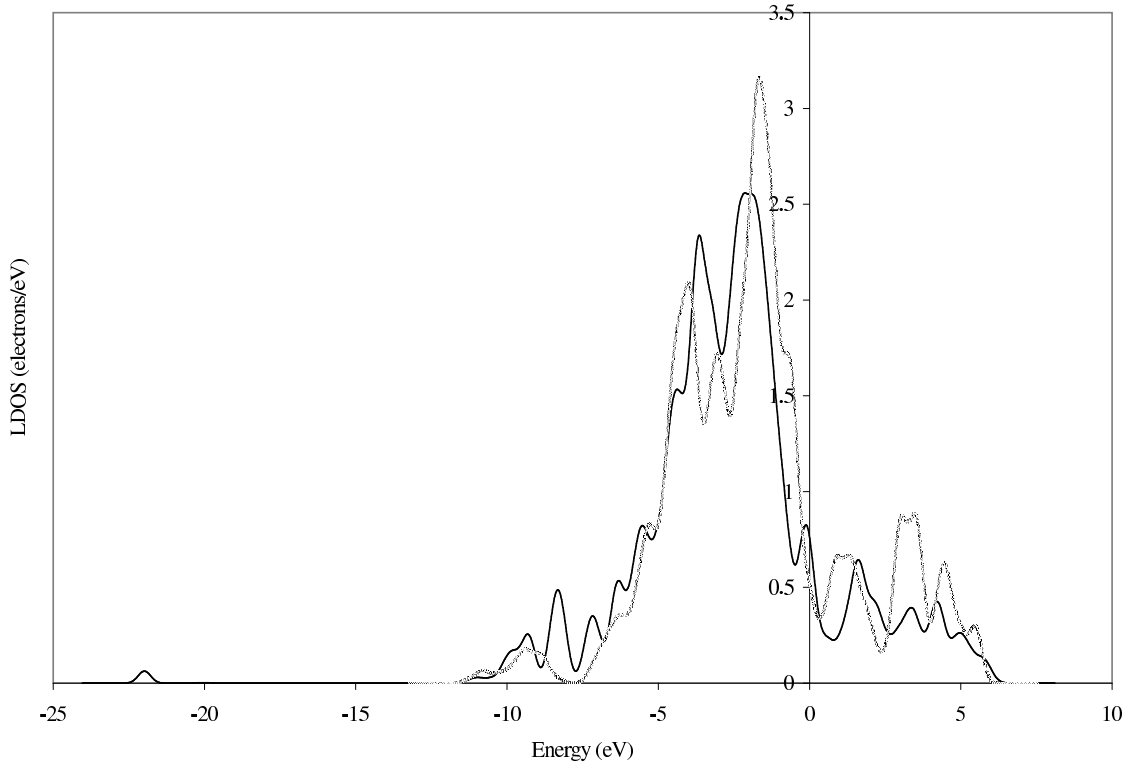

(b)

Figure 4.11. LDOS for site D of $Pt_3Sn(110)$ surface with mixed termination (a)CO_2 molecule (b)surface Pt atom (black: bonded cases, gray: free cases)

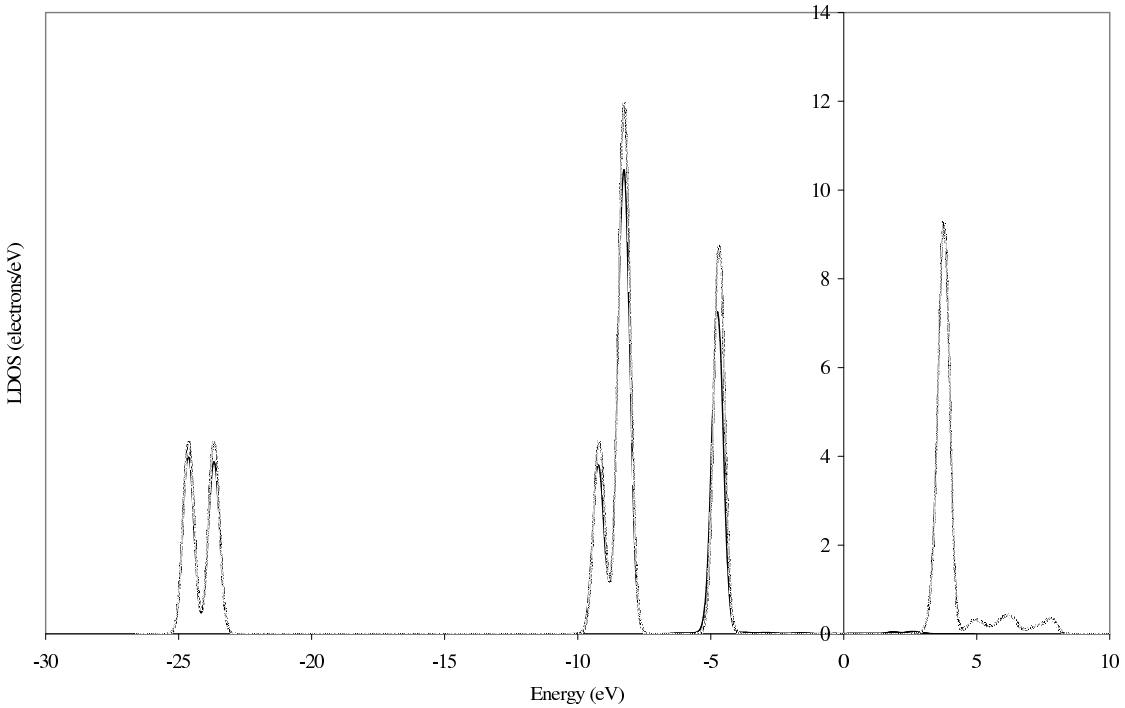

(a)

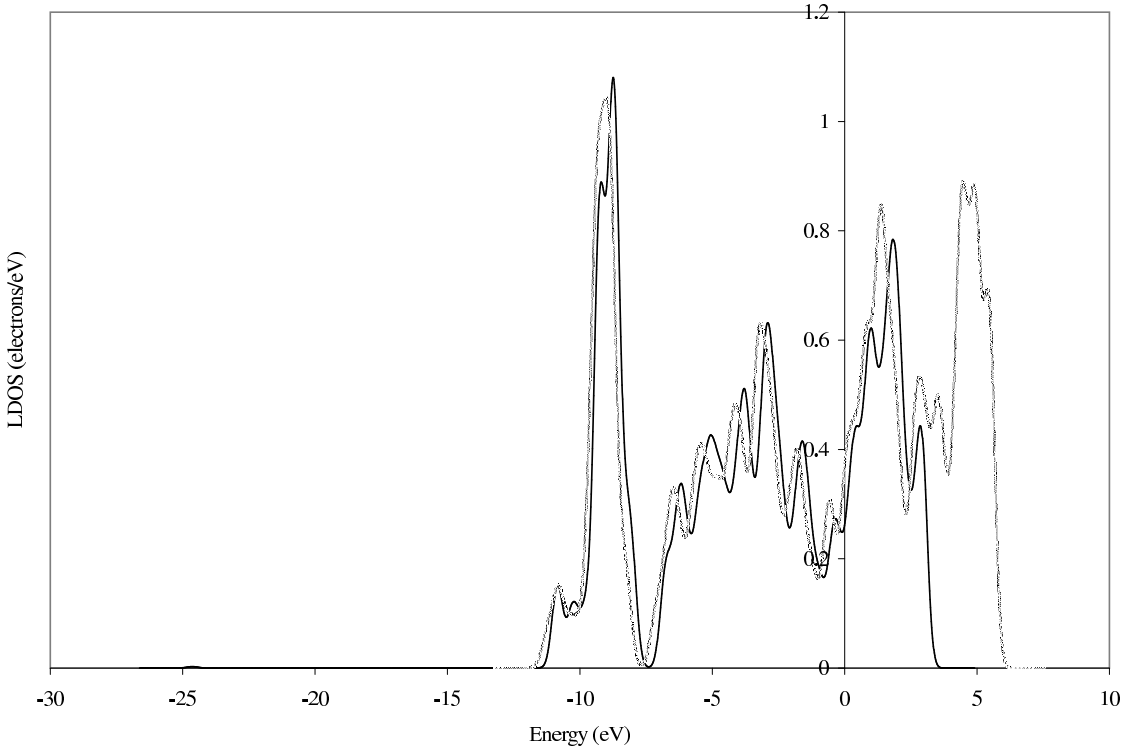

(b)

Figure 4.12. LDOS for site E of $Pt_3Sn(110)$ surface with mixed termination (a)CO_2 molecule (b)surface Sn atom (black: bonded cases, gray: free cases)

Å. Both the bond angle and the bond lengths of the CO_2 molecule are different from those of free CO_2, more likely resembling those of CO_2^- anion (see Table 4.3). Apart from the geometric analysis, the comparison of electron density profiles of the free CO_2 molecule, bare Pt atom at the site and the profiles of the corresponding phases of CO_2–Pt_3Sn complex upon adsorption were also compared. Figure 4.13 (a) and (b) gives the LDOS profiles of CO_2 molecule at its free form compared with the LDOS profile at the end of the optimization and Pt atom of the bare Pt_3Sn (110) surface with pure Pt termination compared with the LDOS profile at the end of the optimization, respectively. The peak representing the LUMO band has partly shifted in energy below the Fermi level and its intensity has decreased considerably. A shoulder has formed at -1.64 eV in the electron density profile of the CO_2 molecule that is reflected in the LDOS profile of the Pt atom of the surface upon adsorption. Also, the peak at -8.18 eV of the Pt LDOS curve represents a newly formed mixed orbital between the CO_2 molecule and the surface alloy, as the peak is also present in the CO_2 LDOS profile, which is formed by the downwards shift of the CO_2 molecular orbital that has a peak at -7.07 eV.

Another CO_2 adsorption site on the Pt_3Sn (110) surface with pure termination is the bridge Pt–Pt site, G. The binding energy was 0.09 eV; it is endothermic though too close to zero. The CO_2 molecule on site G assumed an equilibrium structure such that CO_2 molecule takes a bent geometry, the O–C–O angle is 143.96 °, and at a distance of 1.91 Å from the surface. The molecular bond lengths of the CO_2 molecule at the end of the optimization were both 1.22 Å. Though the bond calculation tool of Materials Visualizer could not detect a bond formation between CO_2 molecule placed at site G and the surface, the resulting CO_2 molecule's geometry suggests that the molecule is in strong interaction with the surface. Analysis of LDOS profiles will give an idea about the electronic changes in CO_2 molecule as well as at Pt_3Sn surface. Figure 4.14 gives LDOS graphs for free CO_2 and Pt atom of the bare Pt_3Sn surface with pure Pt termination as well as CO_2 and Pt at the site upon adsorption. Only one Pt graph is given for this bridge Pt–Pt site as both Pt atoms have the same LDOS graphs. We're guaranteed that adsorption has taken place since the electron density at Fermi level for Pt atom of the Pt_3Sn (110) surface with pure termination

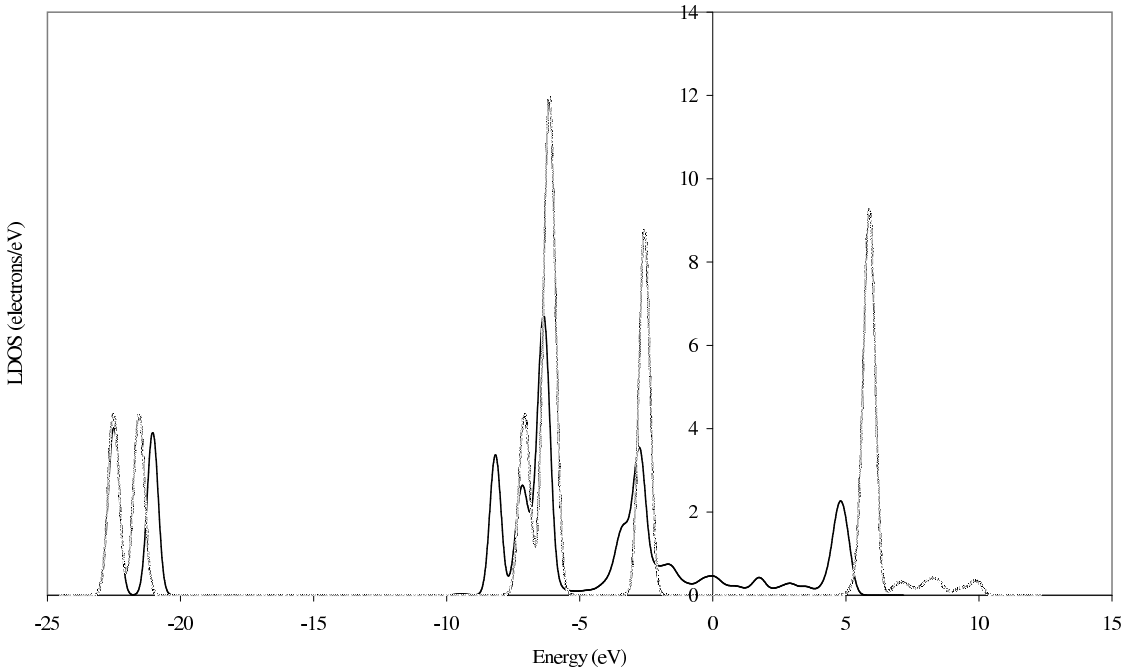

(a)

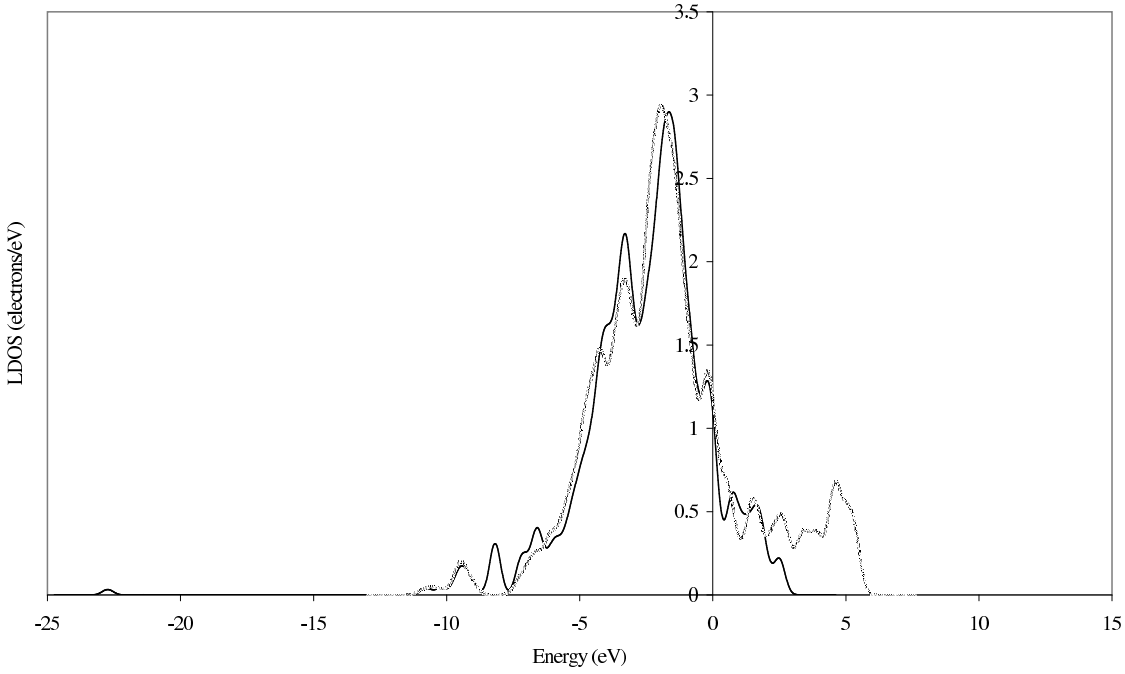

(b)

Figure 4.13. LDOS for site F of $Pt_3Sn(110)$ surface with pure termination (a)CO_2 molecule (b)surface Pt atom (black: bonded cases, gray: free cases)

has decreased significantly for the case of the optimized CO_2–Pt_3Sn complex. Here, in the LDOS profile of the CO_2 molecule, the peak above the Fermi level for the CO_2 molecule at the site upon adsorption is still present. Therefore, for this adsorption site on Pt_3Sn (110) surface with pure Pt termination, 0.5 ML coverage is too high if one wants to perform QM calculation without any effect coming from adsorbate-adsorbate interaction. The broadening of the bands in the region between -5 and 0 eV also imply the mixing-backmixing with the metal's d-band, thus bonding to the surface.

The remaining CO_2 adsorption sites on Pt_3Sn (110) surface with pure Pt termination all resulted in unstable structures. The properties of CO_2 adsorbate at long bridge Pt–Pt site, four-fold hollow site with Pt at bottom, and the four-fold hollow site with Sn at bottom, at sites H, I, and J, respectively, are not different from the gaseous phase CO_2. The geometry and LDOS analyses also confirm that these sites could not adsorb CO_2 stably.

4.3.3. $Pt_3Sn(001)$ surface

From the two terminations of the Pt_3Sn surface, the one with Pt and Sn present at the upper layer, namely mixed termination surface, was studied firstly. The studies start with site A of the mixed surface for which CO_2 is adsorbed atop. The binding energy calculated from Equation 3.1 was found as 2.05 eV. This energy suggests a highly endothermic process in comparison to other adsorption sites. The distance of the optimized CO_2 molecule to the surface was 2.05 Å. In the final structure of the CO_2–Pt_3Sn complex, the bond lengths of the CO_2 molecule were both 1.24 Å and the O–C–O bond angle was 112.29 °. This angle is the acutest angle encountered over the whole CO_2 adsorption sites. Thus, the highly endothermic adsorption energy of this structure can stem from the energy needed to bend the molecule. The electron density profiles of free CO_2 in comparison with CO_2 of the CO_2–Pt_3Sn complex, and Pt atom of the bare surface in comparison with Pt atom at the site upon adsorption are given in Figures 4.15 (a) and (b), respectively. The electron density of the CO_2 molecule has changed extensively upon adsorption. The entire electron density profile within the region -10 and 0 eV have shifted downward, decreased in intensity and broadened. The

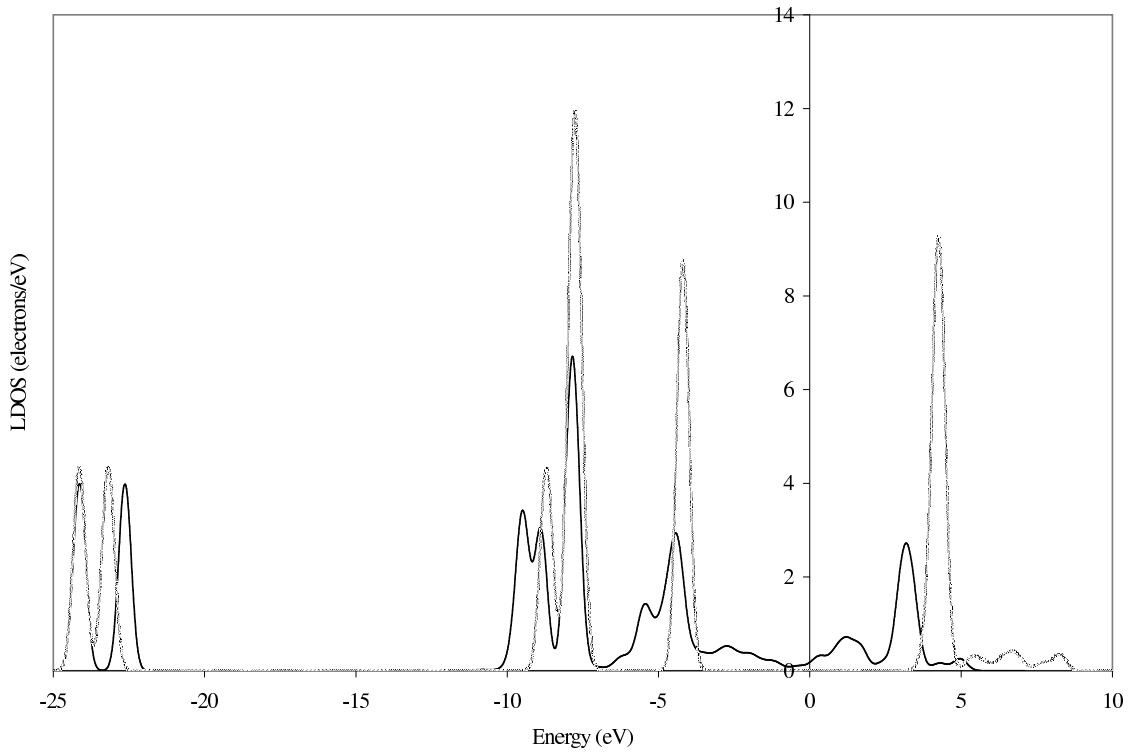

(a)

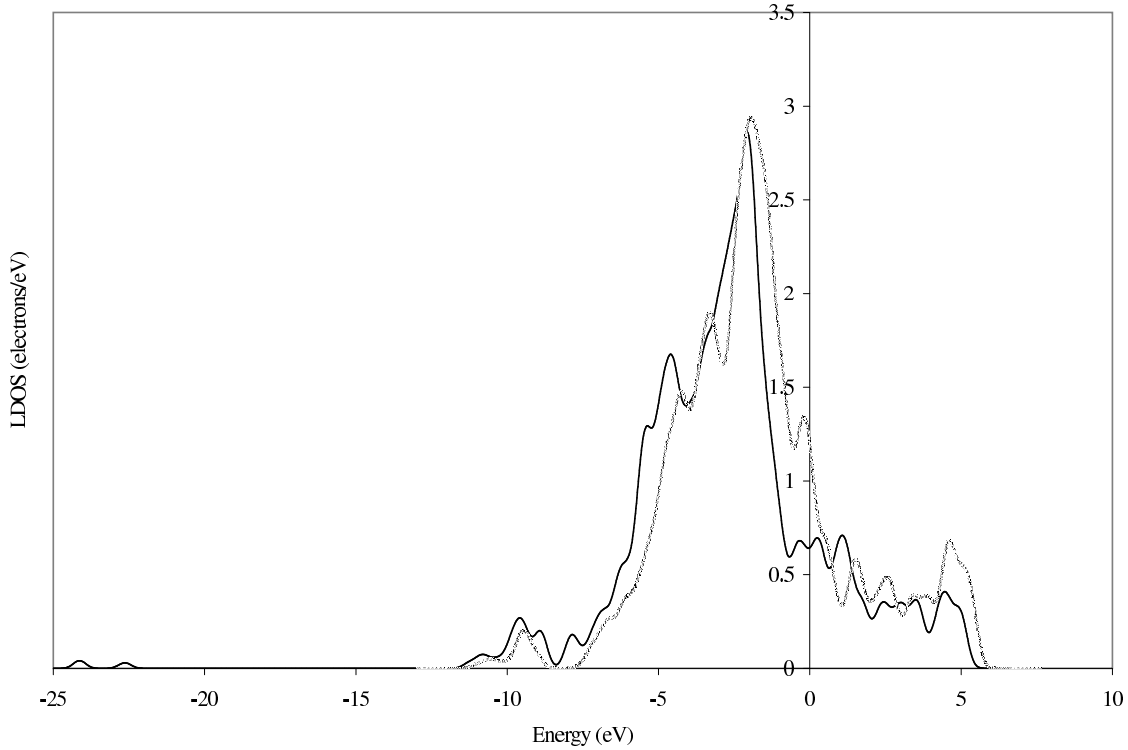

(b)

Figure 4.14. LDOS for site G of $Pt_3Sn(110)$ surface with pure termination (a)CO_2 molecule (b)surface Pt atom (black: bonded cases, gray: free cases)

local density of the Pt atom of the surface was also affected by that decrease in energy as the band for the clean Pt surface atom has also shifted downwards upon adsorption. The CO_2 molecular orbitals with the lowest energies, at -22.21 eV and at -21.25 eV, are so low in energy that they can not mix with the metallic d-states. Therefore, the states derived from the mentioned molecular orbitals have shifted upwards in energy upon chemisorption probably only because of the proximity of the neighboring atoms of the alloy surface. This destabilization can also be viewed by the elongation of the C–O bonds in the CO_2 molecule.

The second site that was tested for CO_2 adsorption is atop Sn site, site B. The adsorption energy calculated for site B was 2.58 eV and the distance of the CO_2 molecule from the Sn atom of the surface was 3.70 Å. The geometry analysis point out that the optimized CO_2 molecule's bond lengths were 1.12 Å and the O–C–O bond angle was 178.81 °. This site was the single unstable site on the Pt_3Sn (001) surface with mixed termination. The shortened bond lengths of the CO_2 molecule at the end of the optimization are interesting; LDOS profiles of the CO_2 molecule and Sn atom of the Pt_3Sn (001) surface with mixed termination in their free forms and in the CO_2–Pt_3Sn complex upon optimization can offer an explanation to this phenomenon. Figure 4.16 (a) represents the electron density distribution at the CO_2 molecule at its free state and at the site upon optimization, and Figure 4.16 (b) is the LDOS profile of Sn atom of the bare Pt_3Sn (001) surface with mixed termination and that of the Sn atom at the site upon optimization. The LDOS curve representing the CO_2 molecule at the site B upon optimization deviates highly from the profile belonging to the free CO_2 molecule. But those deviations can not be attributed to chemisorption since there are no downward shifts in the peaks, or any broadening which would led by an interaction with the Pt_3Sn (001) surface. Additionally, when the LDOS profiles for Sn atom of the Pt_3Sn (001) surface was analyzed, it is seen that the LDOS profiles representing Sn of the bare site and in CO_2-adsorbed state match, and there is no decrease in intensity of the peak at Fermi level. Thus, the shortening of the bonds for the CO_2 molecule can not be ascribed to adsorption at the site B of the Pt_3Sn (001) surface, but probably can be assigned to pronounced CO_2–CO_2 interaction on this surface.

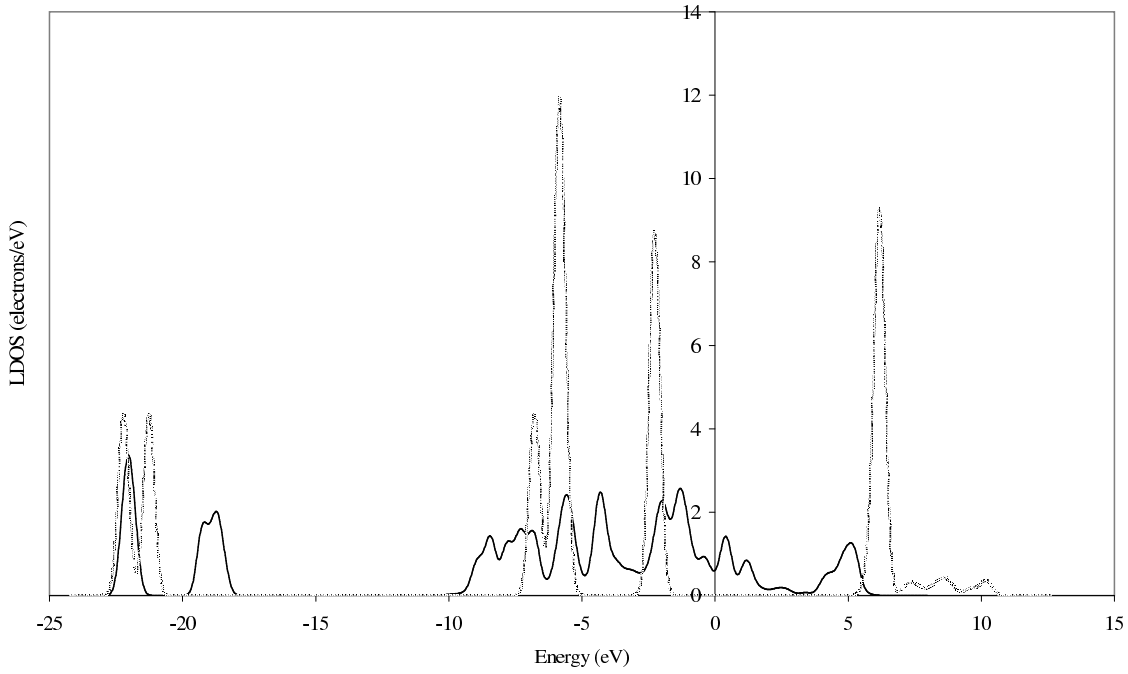

(a)

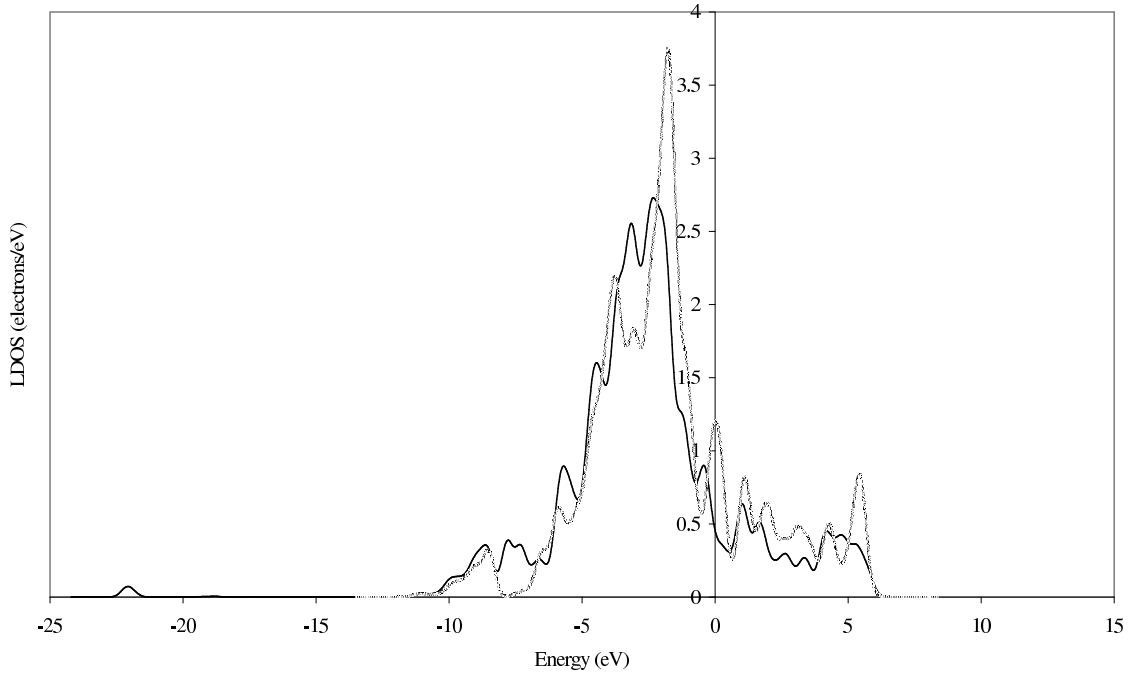

(b)

Figure 4.15. LDOS for site A of $Pt_3Sn(001)$ surface with mixed termination (a)CO_2 molecule (b)surface Pt atom (black: bonded cases, gray: free cases)

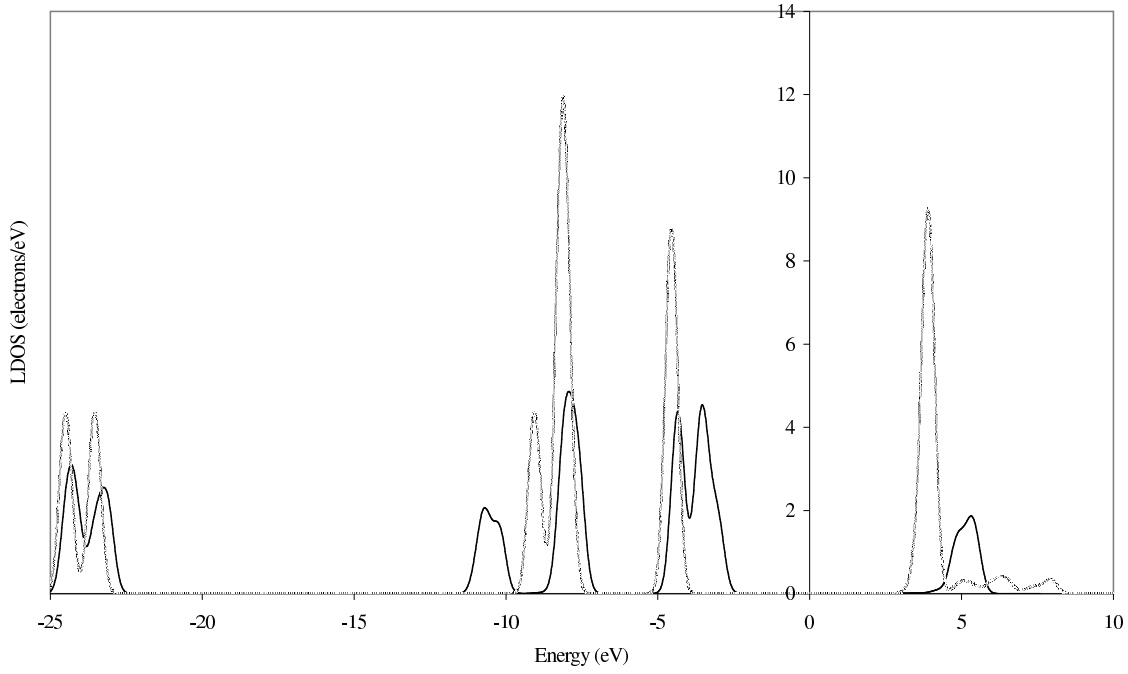

(a)

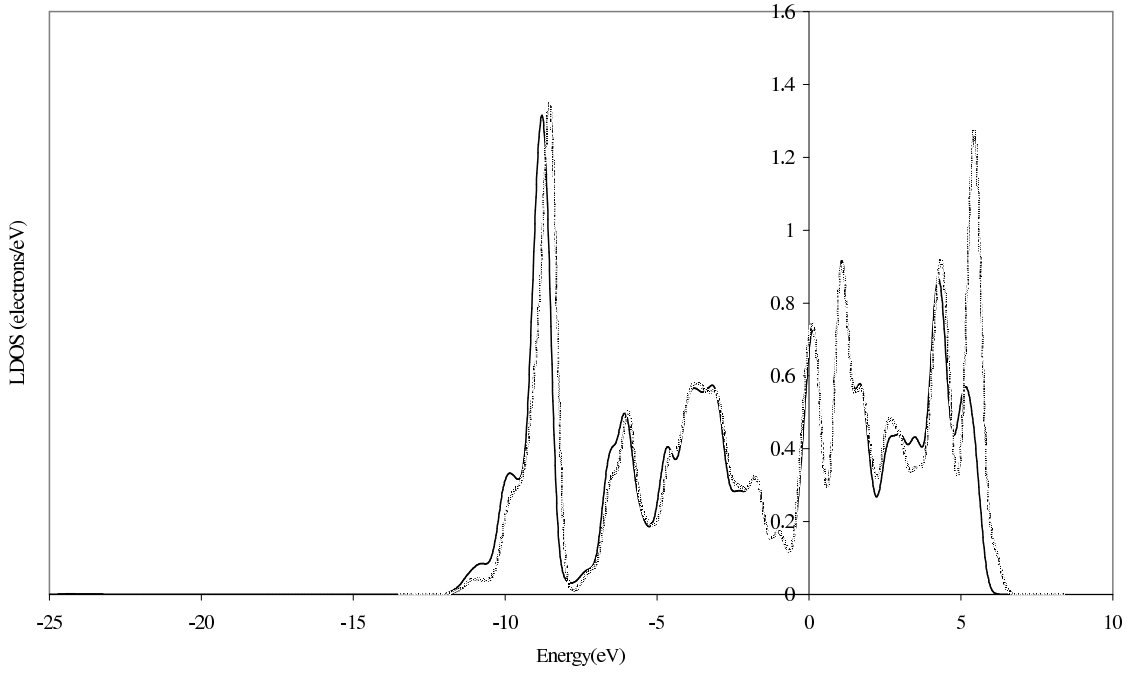

(b)

Figure 4.16. LDOS for site B of $Pt_3Sn(001)$ surface with mixed termination (a)CO_2 molecule (b)surface Sn atom (black: bonded cases, gray: free cases)

The last site that was tested for CO_2 adsorption on Pt_3Sn (001) surface with mixed termination was the bridge site where CO_2 was bonded to a surface Pt and a surface Sn atom, site C. The binding energy calculated at the end of the optimization was 0.11 eV. The geometry of the CO_2 molecule at the end of the optimization process assumes a bent geometry for which one of the O–C bonds parallel to the surface and the other O was tilted 51.45 ° upward from the surface plane. The O and C atoms of the parallel bond were attached to the surface Sn and Pt atoms, respectively. The length of the C–Pt bond was 2.09 Å and O–Sn bond was also 2.09 Å, whereas the distance of the molecule to the surface was 1.96 Å. The length of the C–O bond that was parallel to surface was 1.29 Å, indicating a clear elongation from the free state CO_2. The length of the other C–O bond was 1.21 Å. Since the geometry analysis suggests the CO_2 molecule at site C is in interaction with Pt_3Sn surface, LDOS profiles are analyzed further. Figure 4.17 gives the electron density profiles of the free CO_2, Pt and Sn atoms of the bare Pt_3Sn (001) surface as well as their corresponding LDOS profiles in CO_2–Pt_3Sn complex. In the LDOS of the adsorbed carbon atom, the lowest energy peak has not changed but the following energy peak at -20 eV has shifted upwards in energy relative to the corresponding peak of CO_2 in the free state,which is an indication that the orbital is not involved in bonding of the molecule to the surface. The slight increase in the energy of the $2\sigma_\mu$ peak suggests that the adsorbed CO_2 is destabilized, and this may lead to the elongation of CO_2 molecular bonds. The LDOS of the CO_2 in its adsorbed state has an electron density peak ca. -9.23 eV, which probably induce the formation of peaks in LDOS profiles of the Pt and Sn atoms at the site. This is an acceptable evidence showing the new orbital is not a CO_2 molecular orbital, but a derived orbital of the CO_2–Pt_3Sn complex. The peaks in LDOS profile of the adsorbed CO_2 at -8.28 eV, and -7.17 eV are also present in the LDOS profiles of Pt and Sn at the site upon adsorption. The electron densities at the derived orbitals of the CO_2–Pt_3Sn complex are less than those of the molecular orbitals belonging to free CO_2 molecule, as seen in the Figure 4.17 (a). Thus, both the geometry and LDOS analyses of the CO_2 molecule at site C of Pt_3Sn (001) surface with mixed termination suggest that CO_2 is bonded to the alloy site via forming a bridge structure for which C atom is bonded to Pt atom of the site and one of the O atoms of CO_2 is bonded to Sn atom of the site.

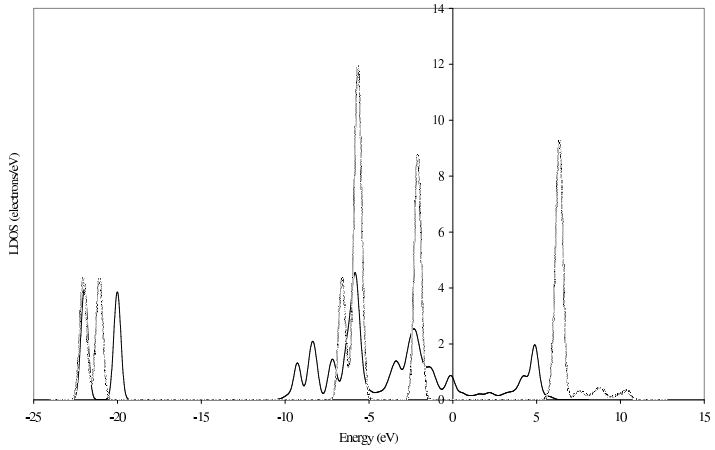

(a)

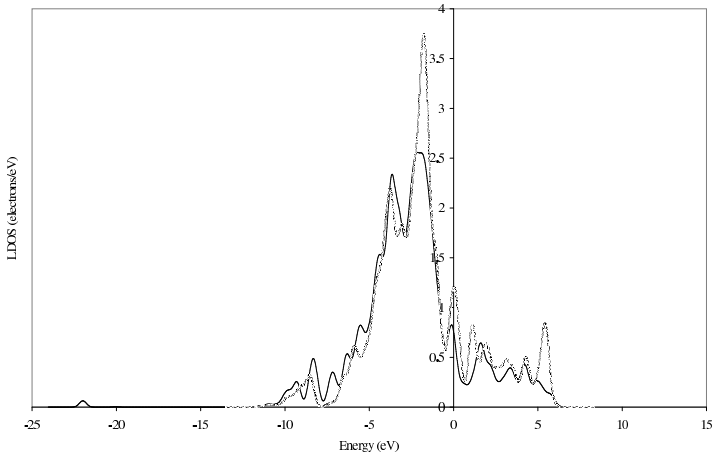

(b)

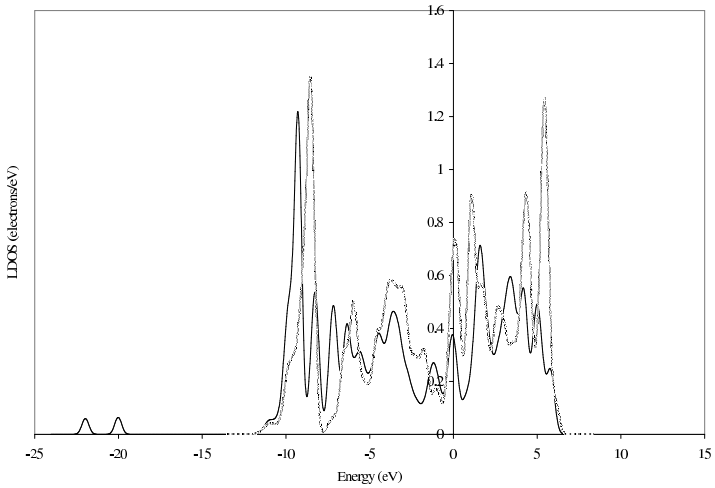

(c)

Figure 4.17. LDOS for site C of $Pt_3Sn(001)$ surface with mixed termination (a)CO_2 molecule (b)surface Pt atom (c)surface Sn atom (black: bonded cases, gray: free cases)

On the Pt_3Sn (001) surface with pure termination, there were two CO_2 adsorption sites. The CO_2–atop Pt adsorption site D was tested firstly. At the end of the optimization process, the CO_2 molecule assumed a position 2.02 Å away from the surface. The CO_2 binding energy of at the site was found to be 2.47 eV, the highest energy among all stable adsorption sites tested on all of the faces of the Pt_3Sn surfaces. The resulting CO_2 molecule's O–C–O bond angle was 114.64 °, highly bent as in the case of CO_2–atop adsorption site on Pt_3Sn (001) surface with mixed termination. The C–O bonds of the CO_2 molecule at the site upon adsorption were elongated to a length of 1.23 Å. LDOS profiles of CO_2 molecule and the surface Pt atom for the CO_2–Pt_3Sn system are given in Figure 4.18 along with the corresponding local density profiles for free CO_2 and for a clean surface Pt atom have been superimposed as reference basis. The shifts and changes in the intensities of the adsorbed CO_2 at site D highly resemble the electron density profile of the CO_2 adsorbed at site A, CO_2–atop adsorption site on Pt_3Sn (110) surface with mixed termination. The pronounced broadening of the peaks indicate strong interaction between those states and the metal d-states. The common peak to CO_2 and Pt atom local density upon adsorption, ca. −7.80 eV, corresponds to an orbital formed by the mixing of a CO_2 molecular orbitals and the d-band of the metal. The two lowest energy peaks present at the CO_2 local density profile are shifted upwards, thus destabilized upon adsorption, as in the case of CO_2–atop adsorption site on Pt_3Sn (110) surface with mixed termination; on the other hand, for CO_2 on site D of pure termination, the shifts in peak energies are more pronounced than the shift seen at the CO_2 LDOS profile adsorbed at site A, with mixed termination. As mentioned before, lengthening of the C–O bonds is directly related with the destabilization of those low energy peaks which do not interact with the alloy's d-states but are affected by the neighboring surface atoms. The higher upwards shift in CO_2 LDOS peak energies for this site is accompanied by the longer bonds of the CO_2 molecule.

The last site tested on Pt_3Sn (001) surface was the bridge Pt–Pt site on pure Pt termination, site E. The binding energy calculated for site E indicates that the energy of the CO_2–Pt_3Sn complex is 0.09 eV lower than the sum of the energies of free CO_2 molecule and the slab. The geometry and electron density profiles are analyzed since the binding energy is too low and does not suggest any information on adsorption

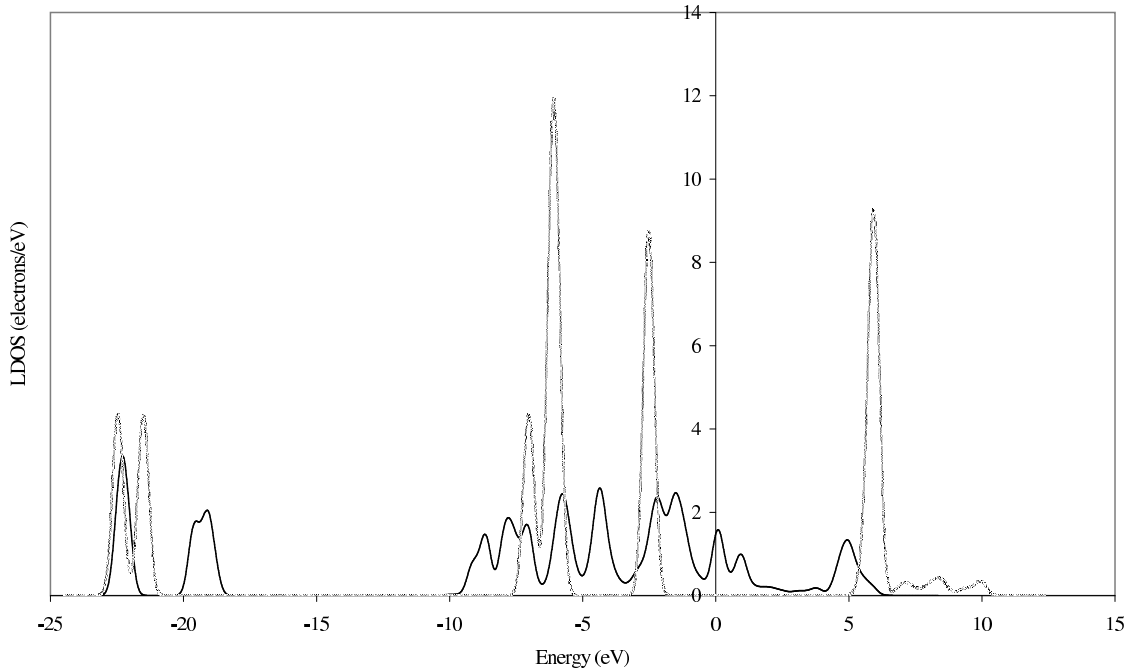

(a)

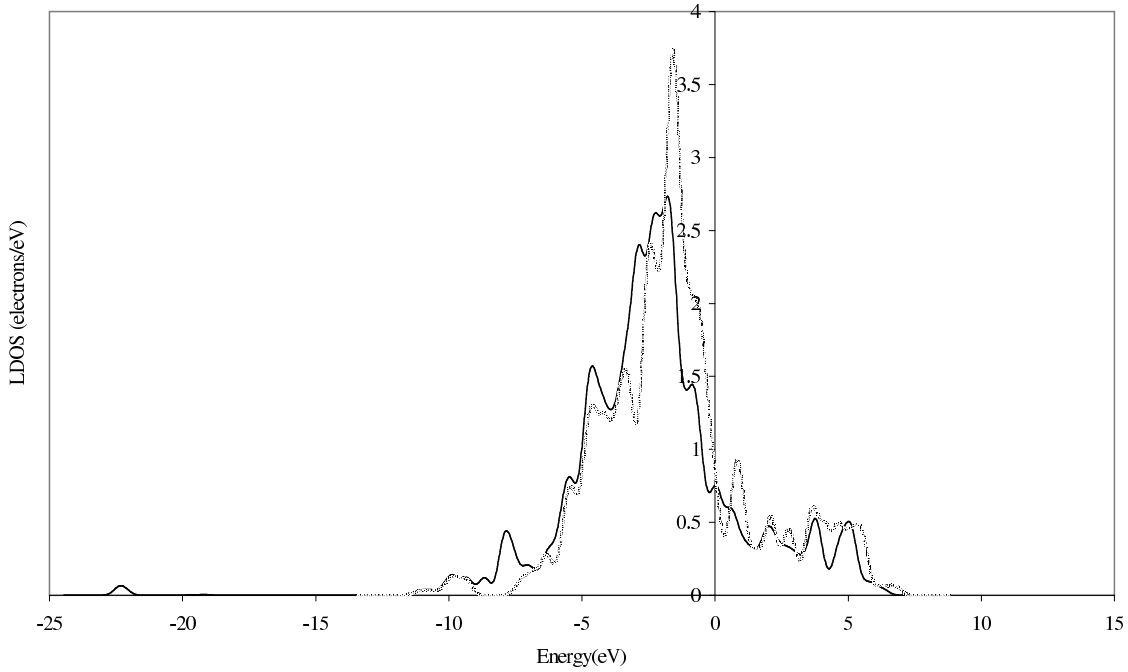

(b)

Figure 4.18. LDOS for site D of $Pt_3Sn(001)$ surface with pure termination (a)CO_2 molecule (b)surface Pt atom (black: bonded cases, gray: free cases)

process. The bond lengths of the CO_2 molecule upon adsorption were 1.17 Å and the O–C–O bond angle was 179.78 °. The resulting CO_2 molecule laid at a distance of 3.64 Å from the surface. Since the CO_2 molecule–Pt_3Sn surface distance is so large, and the geometric data on the CO_2 molecule are too close to gaseous phase CO_2, the geometry analysis concludes that the CO_2 molecule was not adsorbed on site E of the Pt_3Sn (001) surface with pure termination. The corresponding LDOS profiles are given in Figure 4.19; the comparison of LDOS profiles of free and adsorbed CO_2 as well as LDOS of Pt of the bare surface and Pt of the CO_2–Pt_3Sn system clearly show that there is no change in the LDOS profiles of CO_2 and Pt at the site upon adsorption. Thus, the preceding arguments claim that CO_2 is not adsorbed on site E of the Pt_3Sn (001) surface with pure Pt termination are supported by the analysis of LDOS profiles.

4.3.4. Thermodynamical Comments on Adsorption Energies

The calculation of adsorption energy was given in Equation 3.1. It is commonly accepted that adsorption processes are always exothermic. It is known from thermodynamics that the Gibbs free energy must decrease for any spontaneous event, and since adsorption is an event that is accompanied by a decrease of entropy, then from

$$\Delta G = \Delta H - T\Delta S \tag{4.1}$$

ΔH, the enthalpy change accompanying adsorption, must be negative. For the majority of adsorption processes, this argument is valid. But there can be situations where a net gain in the number of degrees of freedom might happen and a positive entropy change, ΔS, would result; and thus, the free energy change associated with this process could be negative although the enthalpy change is positive. One occurrence of positive entropy might be when the structure of the adsorbent altered in adsorption. By this way, even if the entropy of the species adsorbed decreases on adsorption, that decrease may be exceeded by a concomitant increase in the entropy of the adsorbent itself, which would lead to an endothermic process if the $T\Delta S$ term were numerically greater than the ΔG term. Another occurrence is hypothetically explained by the dissociative adsorption of a diatomic gas molecule where the strength of the surface-gas atom bond is equal to

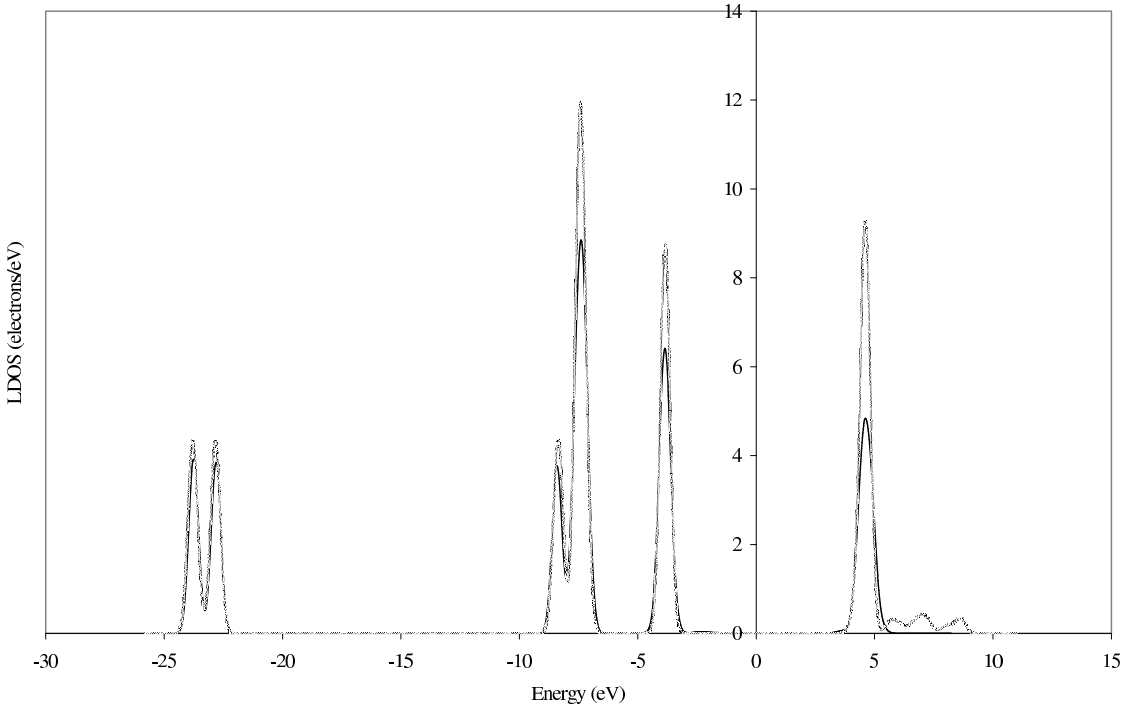

(a)

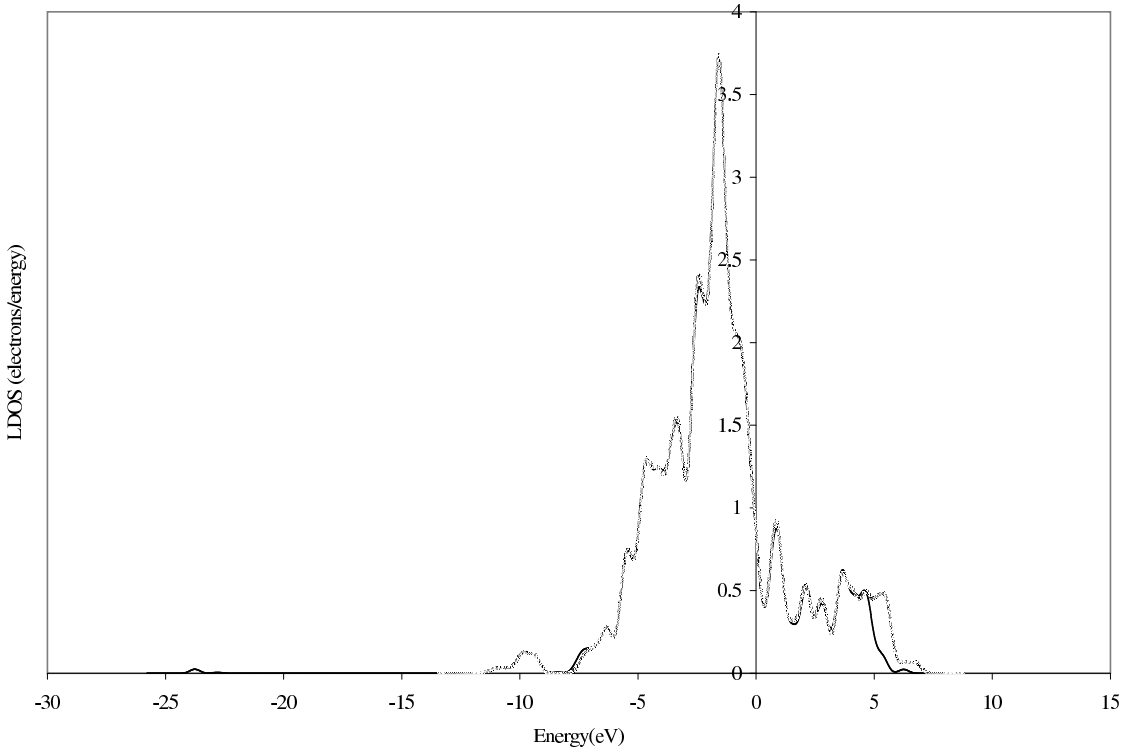

(b)

Figure 4.19. LDOS for site E of $Pt_3Sn(001)$ surface with pure termination (a)CO_2 molecule (b)surface Pt atom (black: bonded cases, gray: free cases)

half the strength of the bond between two atoms. If the adsorbed atoms have complete two-dimensional mobility, it would then follow that a positive entropy change ΔS would result and the free energy change associated with this thermally neutral process ($\Delta H = 0$) would be equal solely to the $T\Delta S$ term [53].

The adsorption energies for the chemisorbed species calculated in this work are all endothermic. As mentioned above, this is not always impossible in terms of thermodynamics. In CO_2–Pt_3Sn case, the structure of the adsorbate alters and this is also a process that requires enthalpy change. Additionally, there are minor changes on the adsorbent surface. There is an energy cost to bend the CO_2 molecule and the quantity of that energy changes, generally increases, as the O–C–O angle becomes more acute. Another point to be mentioned is the Pauli repulsion, which is higher since the molecule is close to surface. All these factors may result in endothermic adsorption energy.

From the results that have been obtained, it is obvious that when the O–C–O angle is $\sim 120\,^\circ$ the adsorption energy is the most endothermic for every surface. On $Pt_3Sn(111)$ surface, the hollow hcp Pt_3 on Sn site resulted in a type that both oxygens are bonded to carbon with an O–C–O angle of $130\,^\circ$, carbon bonded to the surface atom, and that structure was the most endothermic among others. The most endothermic and stable CO_2 on all surfaces was CO_2–atop Pt site on Pt_3Sn (001) surface with pure termination and the angle of the CO_2 molecule was $114\,^\circ$. The acute angles that are encountered in CO_2 geometries, such as the one at site D on the Pt_3Sn (001) surface, require more energy to be bent; thus, the corresponding adsorption energies are more endothermic. The higher endothermic adsorption energies of these structures cause them to be thermodynamically less favorable.

The other structure, the one with both O and C bonding to surface atoms, has obtuser angles. The adsorption energies are less endothermic in this structure. The elongation of C–O bond may be indicative of dissociative adsorption. But as Ren *et al.* had stated, the adsorption processes with high energies result in spontaneous dissociation [54]. So, the case of dissociation remains unclear in the range of calculated adsorption energies, since the values are very low.

5. CONCLUSIONS AND RECOMMENDATIONS

5.1. Conclusions

CO_2 adsorption was studied on flat Pt_3Sn surfaces using semi ab-initio quantum mechanical code, CASTEP, by Accelrys. The findings of this study can be summarized as:

- for CO_2/Pt_3Sn adsorption system, if both Pt atom and Sn atom are present at the adsorption site, CO_2 molecule stabilizes at this site with C atom bonded to Pt atom of the surface and one of the O atoms bonded to Sn atom of the surface,

- for all stable adsorption sites, the adsorption strength is far below the necessary level for dissociative adsorption,

- if the adsorption site is only the Sn atom of the surface, no adsorption occurs. Since O_2 is adsorbed at Sn sites on Pt_3Sn surface, there is no hindrance on O_2 adsorption sites coming from CO_2 adsorption.

5.2. Recommendations

The scope of this study can be widened by:

- considering CO_2 adsorption on monometallic Pt surfaces to see the effect of alloying on adsorption of CO_2 as the positive effect of bimetallic catalysts has been revealed by previous studies,

- studying coadsorption of CO_2 and CO in order to investigate the effect of presence of CO_2 on the adsorption of CO – the active site choices and adsorption strength of CO – ,

- studying coadsorption of CO_2 and O_2 in order to see if adsorption of CO_2 hinders the adsorption of O_2 – whether it blocks the sites that adsorb O_2 or restricts O_2 mobility – ,

- carrying out CO_2 adsorption on stepped, kinked and reconstructed surfaces of Pt_3Sn alloy for a more realistic performance evaluation.

REFERENCES

1. Song, C., "Fuel Processing for Low-Temperature and High-Temperature Fuel Cells: Challenges, and Opportunities for Sustainable Development in the 21^{st} Century", *Catalysis Today*, 77 17–49 (2002).

2. Trimm, D. L. and Z. İ. Önsan, "Onboard Fuel Conversion for Hydrogen-Fuel-Cell-Driven Vehicles", *Catalysis Reviews*, 43 (1–2) 31–84 (2001).

3. Jhalani, A. and L. D. Schmidt, "Preferential CO Oxidation in the Presence of H_2,H_2O, and CO_2 at Short Contact-Times", *Catalysis Letters*, 104 (3–4) 103–110 (2005).

4. Özkara, Ş. and A. E. Aksoylu, "Selective Low Temperature Carbon Monoxide Oxidation in H_2-Rich Streams over Activated Carbon Supported Catalysts", *Applied Catalysis A: General*, 251 75–83 (2003).

5. Roh, H. S., H. S. Potdar, K. W. Jun, S. Y. Han, and J. W. Kim, "Low Temperature Selective CO Oxidation in Excess of H_2 over Pt/Ce–ZrO_2 Catalysts", *Catalysis Letters*, 93 (3–4) 203–207 (2004).

6. Manasilp, A. and E. Gulari, "Selective CO Oxidation over Pt/Alumina Catalysts for Fuel Cell Applications", *Applied Catalysis B: Environmental*, 37 (1) 17–25 (2002).

7. Avgouropoulos, R., T. Ioannides, Ch. Papadopoulou, J. Batista, S. Hocevar and H. K. Matralis, "A Comparative Study of Pt/γ–Al_2O_3, Au/α–Fe_2O_3 and CuO–CeO_2 Catalysts for the Selective Oxidation of Carbon Monoxide in Excess Hydrogen", *Catalysis Today*, 75 157–167 (2002).

8. Teschner, D., A. Wootsch, O. Pozdnyakova, H. Sauer, A. Knop-Gericke and R. Schlogl, "Surface and Structural Properties of Pt/CeO_2 Catalyst under Preferential CO Oxidation in Hydrogen (PROX)", *Reaction Kinetics and Catalysis Letters*, 87 (2) 235–247 (2006).

9. Hoflund, G. B., S. D. Gardner, D. R. Schryer, B. T. Upchurch and E. J. Kielin, "Effect of CO_2 on the Performance of Au/MnO_x and Pt/SnO_x Low Temperature CO Oxidation Catalysts", *Langmuir*, 11 (9) 3431–3434 (1995).

10. Korotkikh, O. and R. Farrauto, "Selective Catalytic Oxidation of CO in H_2: Fuel Cell Applications", *Catalysis Today*, 62 (2–3) 249–254 (2000).

11. Haruta, M., N. Yamada, T. Kobayashi and S. Iijima, "Gold Catalysts Prepared by Coprecipitation for Low-Temperature Oxidation of Hydrogen and of Carbon Monoxide", *Journal of Catalysis*, 115 (2) 301–309 (1989).

12. Schubert, M. M., A. Venugopal, M. J. Kahlich, V. Plzak and R. J. Behm, "Influence of H_2O and CO_2 on the Selective CO Oxidation in H_2–Rich Gases over Au/α–Fe_2O_3", *Journal of Catalysis*, 222 (1) 32–40 (2004).

13. Aksoylu, A. E., M. Madalena, A. Freitas and J. L. Figueiredo, "Bimetallic Pt–Sn Catalysts Supported on Activated Carbon I. The Effects of Support Modification and Impregnation Strategy", *Applied Catalysis A: General*, 192 (1) 29–42 (2000).

14. Aksoylu, A. E., M. Madalena, A. Freitas and J. L. Figueiredo, "Bimetallic Pt–Sn Catalysts Supported on Activated Carbon II. CO Oxidation", *Catalysis Today*, 62 (4) 337–346 (2000).

15. Aksoylu, A. E., M. Madalena, A. Freitas, M. F. R. Pereira and J. L. Figueiredo, "The Effects of Different Activated Carbon Supports and Support Modifications on the Properties of Pt/AC Catalysts", *Carbon*, 39 (2) 175–185 (2001).

16. Rajasree, R., J. H. B. J. Hoebink and J. C. Schouten, "Transient Kinetics of Carbon Monoxide Oxidation by Oxygen over Supported Palladium/Ceria/Zirconia Three-Way Catalysts in the Absence and Presence of Water and Carbon Dioxide", *Journal of Catalysis*, 223 (1) 36–43 (2004).

17. Şimşek, E., Ş., Özkara, A. E. Aksoylu, Z. İ. Önsan, "Preferential CO Oxidation over Activated Carbon Supported Catalysts in H_2-rich gas streams containing CO_2 and H_2O", *Applied Catalysis A: General*, 316 (2) 169–174 (2007).

18. Ricart, J. M., M. P. Habas, A. Cloftet, D. Curulla and F. Illas, "Theoretical Study of CO_2 Activation on Pt(111) Induced by Coadsorbed K Atoms", *Surface Science*, 460 (1–3) 170–181 (2000).

19. Ralph, T. R. and G. A. Hards, "Fuel Cells: Clean Energy Production for the New Millennium", *Chemistry & Industry* (9) 334–335 (1998).

20. Avcı, A. K., Z. İ. Önsan and D. L. Trimm, "On-Board Fuel Conversion for Hydrogen Fuel Cells: Comparison of Different Fuels by Computer Simulations", *Applied Catalysis A: General*, 216 (1–2) 243–256 (2001).

21. Oh, S. H. and R. M. Sinkevitch, "Carbon–Monoxide Removal from Hydrogen-Rich Fuel-Cell Feedstreams by Selective Catalytic Oxidation", *Journal of Catalysis*, 142 (1) 254–262 (1993).

22. Kahlich, M. J., H. A.Gasteiger and R. J. Behm, "Kinetics of the selective CO oxidation in H_2-rich gas on Pt/Al_2O_3", *Journal of Catalysis*, 171 (1) 93–105 (1997).

23. Kim, D. H. and M. S. Lim, "Kinetics of Selective CO oxidation in Hydrogen–rich Mixtures on Pt/Alumina Catalysts", *Applied Catalysis A: General*, 224 27–38 (2002).

24. Akın, A. N., G. Kılaz, A. İ. İşli and Z. İ. Önsan, "Development and Characterization of Pt–SnO_2/Al_2O_3 Catalysts", *Chemical Engineering Science*, 56 881–888 (2001).

25. Shubina, T. E. and M. T. M. Koper, "Quantum Chemical Calculations of CO and OH Interacting with Bimetallic Surfaces", *Electrochimica Acta*, 47 3621–3628 (2002).

26. Stamenković, V. R., M. Arenz, C. A. Lucas, M. E. Gallagher, P. N. Ross and N. M. Marković, "Surface Chemistry on Bimetallic Alloy Surfaces: Adsorption of Anions and Oxidation of CO on $Pt_3Sn(111)$", *Journal of American Chemical Society*, 125 (9) 2736–3745 (2003).

27. Stamenković, V. R., M. Arenz, B. B. Blizanac, K. J. J. Mayrhofer, P. N. Ross and N. M. Marković, "In Situ CO Oxidation on Well Characterized $Pt_3Sn(hkl)$ Surfaces: A Selective Review", *Surface Science*, 576 145–157 (2005).

28. Avgouropoulos, G. and T. Ioannides, "Selective CO Oxidation over CuO–CeO_2 Catalysts Prepared via the Urea-Nitrate Combustion Method", *Applied Catalysis A: General*, 244 155–167 (2003).

29. Marino, F., C. Descorme and D. Dupreza, "Supported Base Metal Catalysts for the Preferential Oxidation of Carbon Monoxide in the Presence of Excess Hydrogen (PROX)", *Applied Catalysis B: Environmental*, 58 175–183 (2005).

30. Panzera, G., V. Modafferi, S. Candamanoa, A. Donato, F. Frusteri and P.L. Antonucci, "CO Selective Oxidation on Ceria-Supported Au Catalysts for Fuel Cell Application", *Journal of Power Sources*, 135 177–183 (2004).

31. Luengnaruemitchai, A., D. T. K. Thoa, S. Osuwan and E. Gulari, "A Comparative Study of Au/MnO_x and Au/FeO_x Catalysts for the Catalytic Oxidation of CO in Hydrogen Rich Stream", *International Journal of Hydrogen Energy*, 30 (9) 981–987 (2005).

32. Maier, W. F. and J. Saalfrank, "Discovery, Combinatorial Chemistry and a New Selective CO-Oxidation Catalyst", *Chemical Engineering Science*, 59 4673–4678 (2004).

33. Gajdoš, M, A. Eichler and J. Hafner, "CO Adsorption on Close-Packed Transition and Noble Metal Surfaces: Trends From Ab Initio Calculations", *Journal of Physics: Condensed Matter*, 16 (8) 1141–1164 (2004).

34. Blackman, G. S., C. T. Kao, B. E . Bent, C. M. Mate, M. A. Vanhove and G. A. Somorjai, "LEED and HREELS Studies of the Coadsorbed CO + ethylidyne and NO + ethylidyne systems on the (111) Crystal-Surface", *Surface Science*, 207 (1) 66–88 (1988).

35. Lynch, M. and P. Hu, "A Density Functional Theory Study of CO and Atomic Oxygen Chemisorption on Pt(111)", *Surface Science*, 458 1–14 (2000).

36. Hammer, B., O. H. Nielsen and J. K. Norskov, "Structure Sensitivity in Adsorption: CO Interaction with Stepped and Reconstructed Pt Surfaces", *Catalysis Letters*, 46 31–35 (1997).

37. Alavi, A., P. Hu, T. Deutsch, P. L. Silvestrelli and J. Hutter, "CO Oxidation on Pt(111): An Ab Initio Density Functional Theory Study", *Physical Review Letters*, 80 (16) 3650–3653 (1998).

38. Zhang, C. J., R. J. Baxter, P. Hu, A. Alavi and M. H. Lee, "A Density Functional Theory Study of Carbon Monoxide Oxidation on the $Cu_3Pt(111)$ Alloy Surface: Comparison with the Reactions on Pt(111) and Cu(111)", *Journal of Chemical Physics*, 115 (11) 5272–5277 (2001).

39. Ji, Z. and J. Q. Li, "Density Functional Study of CO Oxidation on Pt and PtMo", *Chemical Physics Letters*, 424 (1–3) 111–114 (2006).

40. Koper, M. T. M., T. E. Shubina and R. A. van Santen, "Periodic Density Functional Theory of CO and OH Adsorption on Pt-Ru Alloy Surfaces: Implications for CO Tolerant Fuel Cell Catalysts", *Journal of Physical Chemistry B*, 106 686–692 (2002).

41. Gülmen, M. A., A. Sümer and A. E. Aksoylu, "Adsorption Properties of CO on Low-Index Pt_3Sn Surfaces", *Surface Science*, 600 (21) 4909-4921 (2006).

42. Hu, P., D. A. King, S. Crampin, M. H. Lee and M. C. Payne, "Ab Initio Diffusional Potential Energy Surface for CO chemisorption on Transitional Metal Surfaces", *Chemical Physics Letters*, 246 73–78 (1995).

43. Sümer, A., M. A. Gülmen and A. E. Aksoylu, "A Theoretical Investigation on $Pt_3Sn(102)$ Surface Alloy and $Pt_3Sn(102)$ System", *Surface Science*, 600 (10) 2026–2039 (2006).

44. Freund, H. J. and M. W. Roberts, "Surface Chemistry of Carbon Dioxide", *Surface Science Reports*, 25 (8) 225–273 (1996).

45. Solymosi, F., "The Bonding, Structure and Reactions of CO_2 Adsorbed on Clean Promoted Metal-Surfaces", *Journal of Molecular Catalysis*, 65 (3) 337–358 (1991).

46. Habas, M. P., F. Mele, M. Sodupe and F. Illas, "Density Functional Cluster Model Study of Bonding and Coordination Modes of CO_2 on Pd(111)", *Surface Science*, 431 (1–3) 208–219 (1999).

47. Wang, G. C., L. Jiang, Y. Morikawa, J. Nakamura, Z. S. Cai, Y. M. Pan and X. Z. Zhao, "Cluster and Periodic DFT Calculations of Adsorption and Activation of CO_2 on the Cu(*hkl*) Surfaces", *Surface Science*, 570 (3) 205–217 (2004).

48. Wang, S. G., D. B. Cao, Y. W. Li, J. G. Wang and H. J. Jiao, "Chemisorption of CO_2 on Nickel Surfaces", *Journal of Physical Chemistry B*, 109 (40) 18956–18963 (2005).

49. Segall, M. D., P. L. D. Lindan, M. J. Probert, C. J. Pickard, P. J. Hasnip, S. J. Clark, M. C. Payne,"First-Principles Simulation: Ideas, Illustrations and the CASTEP Code", *Journal of Physics: Condensed Matter* 14 (11) 2717-2744 (2002).

50. Nijhuis, A., M. Makkee, A. D. van Langeveld and J. A. Moulijn, "New insight in the platinum-catalyzed CO oxidation kinetic mechanism by using an advanced TAP reactor system", *Applied Catalysis A: General*, 164 (1–2) 237–249 (1997).

51. Hoheisel, M., S. Speller, J. Kuntze, A. Atrei, U. Bardi and W. Heiland, "Structure of $Pt_3Sn(110)$ Studied by Scanning Tunneling Microscopy", *Physical Review B*, 63 245403/1–7 (2001).

52. Downs, R. T. and M. S. Somayazulu, "Carbon Dioxide at 1.0 GPa", *Acta Crystallographica: Section C, Crystal Structure Communications*, C54 897–898 (1998).

53. Thomas, J. M. and W. J. Thomas, *Principles and Practice of Heterogeneous Catalysis*, VCH, New York, 1997.

54. Ren, J., C. F. Huo, J. Wang, Z. Cao, Y. W. Li and H. Jiao,"Density Functional Theory Study into the Adsorption of CO_2, H and CH_x (x= 0- 3) as well as C_2H_4 on α–$Mo_2C(0001)$", *Surface Science*, 600 (11) 2329–2337 (2006).